SCUOLA DI DOTTORATO
UNIVERSITÀ DEGLI STUDI DI MILANO-BICOCCA

Department of Medicine and Surgery

PHD PROGRAM IN TRANSLATIONAL AND MOLECULAR MEDICINE
Cycle XXVIII

MULTI-OMICS APPROACHES IN B CELL HEMATOLOGICAL DISORDERS: TOWARDS A COMPUTATIONAL MODEL

Fabiola Guerra

Registration numbers 896497/ 6782668

Tutor: Prof.ssa Marta Serafini/ Dr. Matteo Barberis

Co-tutor: Dr. Francesco Saettini

Coordinator: Prof. Francesco Mantegazza

ACADEMIC YEAR 2024/2025

Table Of Contents

CHAPTER 1

INTRODUCTION, HYPOTHESIS AND RATIONALE OF THE DOCTORAL PROJECT

1. General Context

1.1 Inborn Errors of Immunity (IEI)

Inborn errors of immunity (IEI), historically known as primary immunodeficiencies (PID), represent a heterogeneous group of rare, monogenic disorders that compromise immune development or regulation. Although individual IEI are rare, IEIs as a group are not, and they represent a significant health burden [1]. Indeed, a recent study reported that the incidence of IEIs in the USA was 6 per 10,000 people [2]. They encompass not only susceptibility to infections but also autoimmunity, autoinflammation, allergy, and malignancy. Advances in next-generation sequencing have revolutionized their identification, while functional assays and multi-omics approaches are essential to delineate pathogenic mechanisms. IEI highlight essential pathways of immune homeostasis, from cytokine signaling to metabolic regulation, and serve as natural experiments that inform our understanding of immunity. Genetic variants underlie IEI by altering the encoded gene product, such as abolition (null) or reduction (hypomorphic) of protein expression, titration of the intrinsic function of the protein (gain- or loss-of-function, GOF or LOF), or acquiring

[1] Zhang Q, Frange P, Blanche S, Casanova JL. Pathogenesis of infections in HIV-infected individuals: insights from primary immunodeficiencies. Curr Opin Immunol. Oct 2017;48:122-133. doi:10.1016/j.coi.2017.09.002

[2] Rider NL, Truxton A, Ohrt T, et al. Validating inborn error of immunity prevalence and risk with nationally representative electronic health record data. J Allergy Clin Immunol. Jun 2024;153(6):1704-1710. doi:10.1016/j.jaci.2024.01.011

novel functions (neomorphic) [3,4]. Mechanisms of disease in IEI depend on the nature of the variant and the mode of inheritance. Most IEI arise from germline gene variants affecting immune development or function, though acquired forms, known as "phenocopies of IEI," also occur [5].

1.2 Syndromic Disorders with Multi-Organ Involvement A significant subset of IEI occur as part of syndromic disorders where immune dysfunction is accompanied by neurological, gastrointestinal, or developmental abnormalities, or of other organs or system. Such conditions include for example mitochondrial disorders, congenital disorders of glycosylation, and metabolic syndromes that affect multiple organ systems. Syndromic immunodeficiencies are conditions in which immunological defects may be present only in a subset of patients [6]. Syndromic IEI may also be diagnosed by Next-Generation Sequencing even in patients presenting predominant immune dysfunction and only mild organ involvement.

In recent years, there has been growing interest not only in identifying novel syndromic immunodeficiencies [7,8,9,] but

[3] Bousfiha A, Jeddane L, Picard C, et al. Human Inborn Errors of Immunity: 2019 Update of the IUIS Phenotypical Classification. J Clin Immunol. Jan 2020;40(1):66-81.

[4] Tangye SG, Al-Herz W, Bousfiha A, Cunningham-Rundles C, Franco JL, Holland SM, Klein C, Morio T, Oksenhendler E, Picard C, Puel A, Puck J, Seppänen MRJ, Somech R, Su HC, Sullivan KE, Torgerson TR, Meyts I. Human Inborn Errors of Immunity: 2022 Update on the Classification from the International Union of Immunological Societies Expert Committee. J Clin Immunol. 2022 Oct;42(7):1473-1507.

[5] Sun R, Wang Y, Abolhassani H. Cellular mechanisms and clinical applications for phenocopies of inborn errors of immunity: infectious susceptibility due to cytokine autoantibodies. *Expert Rev Clin Immunol*. 2023;19(7):771-784.

[6] Aghamohammadi A, Notarangelo L, editors. Primary immunodeficiency diseases.Springer, Berlin, Heidelberg (2017)

[7] Verdura E, Rodríguez-Palmero A, Vélez-Santamaria V, Planas-Serra L, de la Calle I, Raspall-Chaure M, et al. Biallelic PI4KA variants cause a novel neurodevelopmental syndrome with hypomyelinating leukodystrophy. Brain. (2021) . 144:2659–69. doi: 10.1093/brain/awab124

[8] Saettini F, Guerra F, Mauri M, Salter CG, Adam MP, Adams D, et al. Biallelic PI4KA mutations disrupt B-cell metabolism and cause B-cell lymphopenia and hypogammaglobulinemia. J Clin Immunol. (2024) . 45:15.

also in reassessing known syndromic conditions to determine whether immunological defects have been previously overlooked [10,11,12,13,14]. In these cases, immune phenotypes may be subtle or context-dependent, complicating diagnosis. Multi-omics approaches are especially powerful in such disorders, as they enable the dissection of metabolic and signaling perturbations across multiple cellular compartments.

1.3 Clinical Relevance and Social Impact

IEI, including syndromic immunodeficiencies, have profound clinical, psychological, and societal implications. The additional extra-immunological manifestations often complicate diagnosis, leading to delays that can reduce opportunities for early interventions and worsen long-term outcomes. A detailed understanding of the immune dimension in syndromic disorders is crucial for optimal patient care. Recognition of specific signaling or metabolic defects in these syndromes allows for targeted interventions, including small- molecule modulators, metabolic support, or enzyme replacement therapies, which can improve both immunologic function and systemic manifestations. Early identification also facilitates preventive strategies, such as prophylactic

[9] Saettini F, Poli C, Vengoechea J, Bonanomi S, Orellana JC, Fazio G, et al. Absent B cells, agammaglobulinemia, and hypertrophic cardiomyopathy in folliculin interacting protein 1 deficiency. Blood. (2021) 137:493–9. doi: 10.1182/blood.2020006441

[10] Lacombe D, Bloch-Zupan A, Bredrup C, Cooper EB, Houge SD, Garcıá - Miñaúr S, et al. Diagnosis and management in Rubinstein-Taybi syndrome: first international consensus statement. J Med Genet. (2024) 61:503–19. doi: 10.1136/jmg-2023-109438

[11] Saettini F, Herriot R, Prada E, Nizon M, Zama D, Marzollo A, et al. Prevalence of immunological defects in a cohort of 97 rubinstein-taybi syndrome patients. J Clin Immunol. (2020) 40:851–60,

[12] Rossini L, Ricci S, Montin D, Azzari C, Gambineri E, Tellini M, et al. Immunological aspects of kabuki syndrome: A retrospective multicenter study of the Italian primary immunodeficiency network (IPINet). J Clin Immunol. (2024) 44:105. doi: 10.1007/s10875-024-01676-y;

[13] Baronio M, Saettini F, Gazzurelli L, Rossi S, Marzollo A, Ricci S, et al.Immunological evaluation of patients affected with jacobsen syndrome reveals profound not age-related lymphocyte alterations. J Clin Immunol. (2022)

[14] Saettini F, Guerra F, Fazio G, Bugarin C, McMillan HJ, Ohtake A, et al. Antibody deficiency in patients with biallelic KARS1 mutations. J Clin Immunol. (2023) 43:2115–25. doi: 10.1007/s10875-023-01584-7

antibiotics, immunoglobulin replacement, or tailored vaccination schedules, reducing infection-related morbidity. Awareness of these syndromes highlights the importance of integrating immunologic evaluation into broader clinical assessments for patients with multi-system involvement. From a societal perspective, timely diagnosis and precision therapy in syndromic immunodeficiencies can reduce healthcare costs by minimizing hospitalizations, invasive procedures, and long-term complications, while improving quality of life. Multidisciplinary care, involving immunology, genetics, hematology, endocrinology, and rehabilitation services, is essential to address both the immune and systemic aspects of these complex disorders. Ultimately, syndromic IEI emphasize the need for early, precise, and personalized approaches to diagnosis, therapy, and ongoing patient management.

2. B Cell Metabolism—Fundamentals and Flexibility

2.1 Metabolism and Lymphocyte Function

Lymphocytes face major metabolic challenges upon activation. They must meet the bioenergetic and biosynthetic demands of increased cell proliferation and adapt to changing environmental conditions, in which nutrients and oxygen may be limiting. An emerging theme in immunology is that metabolic reprogramming and lymphocyte activation are intricately linked.[15] Naïve lymphocytes are relatively quiescent, relying on oxidative phosphorylation. Upon activation, they reprogram metabolism, shifting toward glycolysis and increased mitochondrial activity. T-cell fates are metabolically programmed: effector T cells depend on glycolysis, while regulatory and memory T cells rely on fatty acid oxidation. B cells similarly undergo metabolic remodeling upon activation, including glucose and glutamine utilization and mitochondrial

[15] Pearce EL, Poffenberger MC, Chang CH, Jones RG. Fueling immunity: insights into metabolism and lymphocyte function. Science. 2013;342(6155):1242454. doi:10.1126/science.1242454

biogenesis.[16] Germinal center B cells and plasma cells (PCs) are especially sensitive to metabolic stress. Disruption of these processes compromises differentiation and antibody production.

[16] Howie D, Ten Bokum A, Necula AS, Cobbold SP, Waldmann H. The Role of Lipid Metabolism in T Lymphocyte Differentiation and Survival. Front Immunol. 2018;8:1949. Published 2018 Jan 12. doi:10.3389/fimmu.2017.01949

2.2 Crosstalk Between Metabolic Pathways, Cellular Stress, and Immune Response

Immune cell metabolism is tightly interconnected with their activation and function, with distinct metabolic programs shaping the phenotypic and functional outcomes of these cells. This process, known as metabolic reprogramming, enables immune cells to adjust their glycolytic activity, oxidative phosphorylation, lipid metabolism, and amino acid utilization in response to environmental cues and stress signals. Such metabolic flexibility not only fuels energy demands but also directly influences immune signaling pathways, dictating whether cells adopt pro-inflammatory or anti-inflammatory states [17]. The emerging field of immunometabolism highlights how these metabolic adaptations are critical in the pathogenesis of cancers, autoimmune disorders, and metabolic diseases, where dysregulated cellular metabolism contributes to aberrant immune responses. Glycometabolism and lipid metabolism have gained particular attention due to their close association with energy production and immune regulation, while amino acid signaling has been recognized as an additional layer of metabolic control over immune function. The intricate crosstalk between metabolic pathways, cellular stress responses, and immune activity underscores the potential of targeting immune cell metabolism as a therapeutic strategy for modulating disease progression and restoring immune homeostasis.[18,19] We are going to summarize the key metabolic pathways and metabolic reprogramming in B cells.

[17] Pearce EL, Poffenberger MC, Chang CH, Jones RG. Fueling immunity: insights into metabolism and lymphocyte function. *Science*. 2013;342(6155):1242454. doi:10.1126/science.1242454

[18] Hu T, Liu CH, Lei M, et al. Metabolic regulation of the immune system in health and diseases: mechanisms and interventions. Signal Transduct Target Ther. 2024;9(1):268. Published 2024 Oct 9. doi:10.1038/s41392-024-01954-6

[19] Kelly B, O'Neill LA. Metabolic reprogramming in macrophages and dendritic cells in innate immunity. Cell Res. 2015;25(7):771-784. doi:10.1038/cr.2015.68

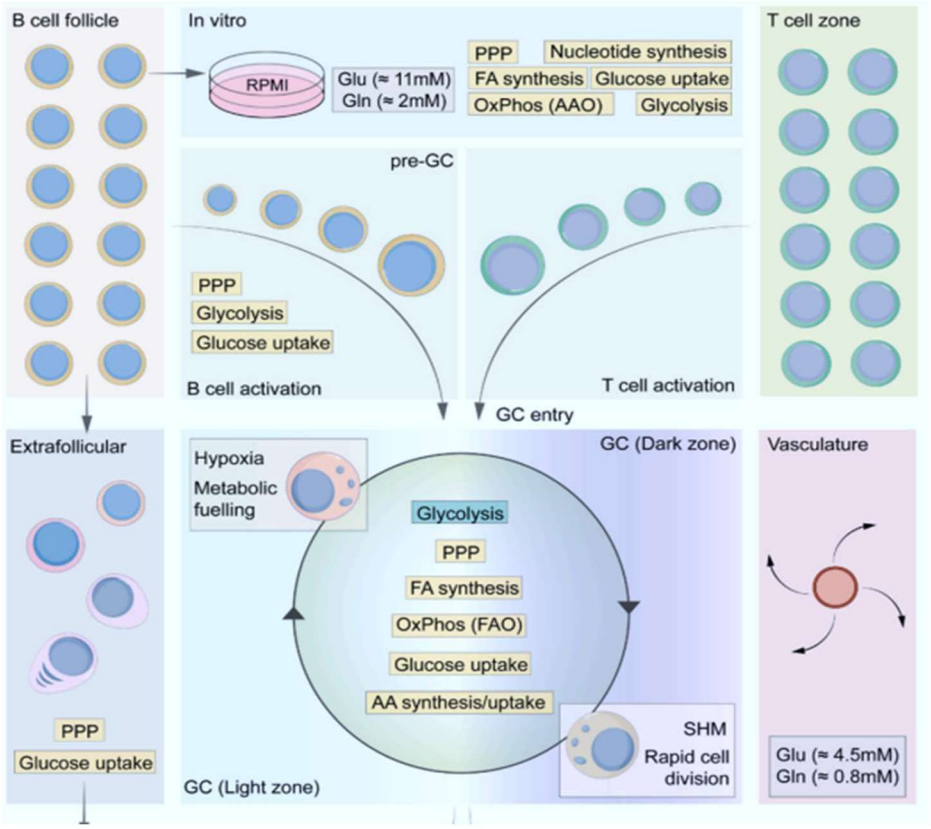

Figure 1. Overview of metabolic remodelling across distinct B cell compartments. During the humoral immune response, B cells undergo dynamic reprogramming of their metabolism to meet metabolic demands and adapt to the distinct metabolic microenvironments in which they reside. Key upregulated metabolic pathways are highlighted in yellow-orange boxes, while downregulated pathways are indicated in blue boxes. FA: fatty acids, AA: amino acids, GO: glucose oxidation, AAO: amino acid oxidation, FAO: fatty acid oxidation, Glu: glucose, Gln: glutamine.

Adapted from Johnstone JC, Yazicioglu YF, Clarke AJ. Fuelling B cells: dynamic regulation of B cell metabolism. Curr Opin Immunol. 2024;91:102484. doi:10.1016/j.coi.2024.102484

2.3 Glucose Metabolism in B Cells

The regulation of glucose uptake and utilization is fundamental throughout the B cell life cycle. Even metabolically quiescent naïve B cells require a fine balance between glycolysis and oxidative phosphorylation (OxPhos) to support proper development. This balance is critically maintained by the von Hippel-Lindau (vHL) protein–hypoxia-inducible factor 1-alpha (HIF1α) axis. Early deletion of vHL during B cell development leads to HIF1α overstabilization, resulting in excessive glycolysis and impaired peripheral B cell homeostasis. [20,21].

Upon antigenic stimulation, B cells increase glucose uptake; however, carbon-tracing experiments ex vivo have shown that glucose is largely diverted into the pentose phosphate pathway (PPP) and nucleotide synthesis, as well as fatty acid synthesis, rather than being fully metabolized through glycolysis. Experimental reduction of glucose availability by ten-fold in culture media did not significantly impair B cell proliferation or differentiation, although class-switch recombination was affected [22].

The role of glycolysis appears particularly crucial during early B cell activation. Targeted deletion of lactate dehydrogenase A (LDHA), a key enzyme in aerobic glycolysis, in naïve B cells caused severe defects in the germinal center (GC) reaction, whereas deletion in already activated B cells had minimal impact. This indicates that early-stage B cells rely more heavily on glycolysis compared with their activated counterparts.

[20] Xu S, Huo J, Huang Y, et al. von Hippel-Lindau Protein Maintains Metabolic Balance to Regulate the Survival of Naive B Lymphocytes. iScience. 2019;17:379-392. doi:10.1016/j.isci.2019.07.002

[21] Burrows, N., Bashford-Rogers, R.J.M., Bhute, V.J. et al. Dynamic regulation of hypoxia-inducible factor-1α activity is essential for normal B cell development. Nat Immunol 21, 1408–1420 (2020). https://doi.org/10.1038/s41590-020-0772-8

[22] Sharma, R., Smolkin, R.M., Chowdhury, P. et al. Distinct metabolic requirements regulate B cell activation and germinal center responses. Nat Immunol 24, 1358–1369 (2023). https://doi.org/10.1038/s41590-023-01540-y

Additional ex vivo studies have confirmed that activated precursors of GC B cells display high glucose dependence and enhanced glycolytic capacity [23].

Glucose transport is mediated by the GLUT1 transporter, encoded by *Slc2a1*. Deletion of *Slc2a1* in mature B cells resulted in reduced GC B cell numbers, impaired GC reactions, decreased PCs differentiation, and reduced production of high-affinity antibodies. Interestingly, light zone (LZ) GC B cells exhibited higher glucose uptake and glycolytic enzyme expression compared with dark zone (DZ) GC B cells, yet DZ B cells were more sensitive to *Slc2a1* deletion, likely due to their higher proliferation rate [24,25]. Mechanistically, inhibition of glucose uptake led to a modest reduction in extracellular acidification rate (ECAR), reflecting lactate production through glycolysis, but had a more pronounced effect on the PPP, particularly in GC B cells and PCs. The PPP is essential for providing biosynthetic intermediates for ribonucleotide synthesis and for generating nicotinamide adenine dinucleotide phosphate (NADPH), which maintains redox homeostasis [26]. Consistent with this, B cells lacking GLUT1 exhibited elevated reactive oxygen species (ROS) levels compared with wild-type controls [21]. In contrast to GC B cells, stable isotope tracing studies in PCs revealed that most glucose is redirected toward antibody glycosylation. In conditions of glucose deprivation, supplementation with mannose restored the capacity of PCs to produce glycosylated antibodies [21]. Furthermore, the conversion of glucose to pyruvate and its subsequent import into mitochondria is critical

[23] Weisel, F.J., Mullett, S.J., Elsner, R.A. et al. Germinal center B cells selectively oxidize fatty acids for energy while conducting minimal glycolysis. Nat Immunol 21, 331–342 (2020). https://doi.org/10.1038/s41590-020-0598-4

[24] Brookens SK, Cho SH, Paik Y, et al. Plasma Cell Differentiation, Antibody Quality, and Initial Germinal Center B Cell Population Depend on Glucose Influx Rate. J Immunol. 2024;212(1):43-56. doi:10.4049/jimmunol.2200756

[25] Bierling TEH, Gumann A, Ottmann SR, et al. GLUT1-mediated glucose import in B cells is critical for anaplerotic balance and humoral immunity. *Cell Rep*. 2024;43(2):113739. doi:10.1016/j.celrep.2024.113739

[26] Stincone A, Prigione A, Cramer T, et al. The return of metabolism: biochemistry and physiology of the pentose phosphate pathway. Biol Rev Camb Philos Soc. 2015;90(3):927-963. doi:10.1111/brv.12140

for the prolonged survival of long-lived PCs, but not for short-lived PCs. Inhibiting mitochondrial pyruvate import did not affect short-lived PCs, highlighting a key metabolic distinction between these subsets that could be exploited to enhance long-term antibody responses following vaccination [27].

2.4 Amino acid metabolism in B cells

In vitro, B lymphocytes display enhanced Krebs cycle and oxidative phosphorylation activity, which does not appear to rely primarily on glucose, suggesting the use of alternative energy sources [28]. Glutamine is essential for proliferation, differentiation, class switching, DNA replication, and biomass increase, partly sustaining mitochondrial metabolism. It is also crucial for glutathione synthesis, a key component of the redox system: lack of glutathione disrupts the respiratory chain in follicular B cells, elevates reactive oxygen species, and reduces both activation and antibody production by derived plasmablasts. Glutathione synthesis via Gclc is also required for marginal zone B cell development [29,30].

PCs express high levels of glutamine transporters. During malaria infection, the rapid expansion of plasmablasts consumes large amounts of glutamine, reducing GC B cells and humoral responses; glutamine supplementation restores long-lived PCs and memory B cells [31]. B cells are not only nutrient consumers but also metabolite producers: conversion of

[27] Lam WY, Becker AM, Kennerly KM, et al. Mitochondrial Pyruvate Import Promotes Long-Term Survival of Antibody-Secreting Plasma Cells. *Immunity*. 2016;45(1):60-73. doi:10.1016/j.immuni.2016.06.011

[28] Waters LR, Ahsan FM, Wolf DM, Shirihai O, Teitell MA. Initial B Cell Activation Induces Metabolic Reprogramming and Mitochondrial Remodeling. *iScience*. 2018;5:99-109. doi:10.1016/j.isci.2018.07.005

[29] Muri J, Kopf M. Redox regulation of immunometabolism. *Nat Rev Immunol*. 2021;21(6):363-381. doi:10.1038/s41577-020-00478-8

[30] Franchina DG, Kurniawan H, Grusdat M, et al. Glutathione-dependent redox balance characterizes the distinct metabolic properties of follicular and marginal zone B cells. *Nat Commun*. 2022;13(1):1789. Published 2022 Apr 4. doi:10.1038/s41467-022-29426-x

[31] Vijay R, Guthmiller JJ, Sturtz AJ, et al. Infection-induced plasmablasts are a nutrient sink that impairs humoral immunity to malaria. *Nat Immunol*. 2020;21(7):790-801. doi:10.1038/s41590-020-0678-5

glutamate into GABA promotes the polarization of anti-inflammatory macrophages, whereas inhibition of this pathway enhances antitumor immunity [32]. Altered glutamine metabolism has also been reported in murine lupus models, and its inhibition alleviates disease severity [33].

Beyond glutamine, other amino acids play important roles [34]. L-leucine uptake through SLC7A5 is critical for CpG-induced activation, cytokine and antibody production, and PCs differentiation [35].

Serine synthesis, via PHGDH, is indispensable for germinal center formation and the generation of high-affinity antibodies. The contribution of other amino acids remains less clear, but for example, tryptophan restriction in mice reduced bone marrow B cell development, with minimal effects on T cells [36].

2.5 Lipid metabolism in B cells

Lipid metabolism has emerged as a central regulator of B cell function. Unlike most rapidly proliferating lymphocytes that

[32] Zhang B, Vogelzang A, Miyajima M, et al. B cell-derived GABA elicits IL- 10^{+} macrophages to limit anti-tumour immunity. *Nature*. 2021;599(7885):471-476. doi:10.1038/s41586-021-04082-1

[33] Zhang X, Wang G, Bi Y, Jiang Z, Wang X. Inhibition of glutaminolysis ameliorates lupus by regulating T and B cell subsets and downregulating the mTOR/P70S6K/4EBP1 and NLRP3/caspase-1/IL-1β pathways in MRL/lpr mice. *Int Immunopharmacol*. 2022;112:109133. doi:10.1016/j.intimp.2022.109133

[34] Cantor J, Browne CD, Ruppert R, et al. CD98hc facilitates B cell proliferation and adaptive humoral immunity. *Nat Immunol*. 2009;10(4):412-419. doi:10.1038/ni.1712

[35] Yang L, Chu Z, Liu M, et al. Amino acid metabolism in immune cells: essential regulators of the effector functions, and promising opportunities to enhance cancer immunotherapy. *J Hematol Oncol*. 2023;16(1):59. Published 2023 Jun 5. doi:10.1186/s13045-023-01453-1

[36] van Beek AA, Hugenholtz F, Meijer B, et al. Frontline Science: Tryptophan restriction arrests B cell development and enhances microbial diversity in WT and prematurely aging *Ercc1-/Δ7* mice. *J Leukoc Biol*. 2017;101(4):811-821. doi:10.1189/jlb.1HI0216-062RR

rely heavily on aerobic glycolysis, GC B cells preferentially engage fatty acid oxidation (FAO) and OxPhos, while displaying minimal glycolysis, even under hypoxic conditions [37]. The relative contribution of glycolysis versus FAO, however, remains debated [38]. OxPhos is directly linked to antibody affinity maturation: its pharmacological enhancement increases high-affinity antibody production, whereas inhibition with oligomycin weakens GC responses [39]. Silencing of carnitine palmitoyltransferase 2 (Cpt2), which shuttles fatty acids into mitochondria, also impaired B cell participation in GC reactions [20], although other studies suggest Cpt2 loss does not necessarily disrupt GC formation, indicating that the role of FAO requires further clarification [40].

Additional evidence supports the importance of lipid metabolism. Sterol regulatory element-binding protein (SREBP) signaling, which drives fatty acid synthesis, is required for antigen-specific PCs and memory generation after vaccination [41]. GC B cells lacking SREBP activity showed reduced lipid raft content and impaired proliferation and differentiation. Glucose also contributes indirectly by fueling the synthesis of monounsaturated fatty acids (MUFA) through stearoyl-CoA desaturase (SCD) upregulation. Blocking SCD prevents proliferation and class switching in vitro, while MUFAs help

[37] Cho SH, Raybuck AL, Stengel K, et al. Germinal centre hypoxia and regulation of antibody qualities by a hypoxia response system. Nature. 2016;537(7619):234-238. doi:10.1038/nature19334

[38] Choi SC, Morel L. Immune metabolism regulation of the germinal center response. Exp Mol Med. 2020;52(3):348-355. doi:10.1038/s12276-020-0392-2

[39] Haniuda K, Fukao S, Kitamura D. Metabolic Reprogramming Induces Germinal Center B Cell Differentiation through Bcl6 Locus Remodeling. *Cell Rep*. 2020;33(5):108333. doi:10.1016/j.celrep.2020.108333

[20] Weisel, F.J., Mullett, S.J., Elsner, R.A. et al. Germinal center B cells selectively oxidize fatty acids for energy while conducting minimal glycolysis. Nat Immunol 21, 331–342 (2020). https://doi.org/10.1038/s41590-020-0598-4

[40] Li M, Zhou X, Zhu X, et al. CPT2 mediated fatty acid oxidation is dispensable for humoral immunity. Preprint. *bioRxiv*. 2024;2024.05.15.594133. Published 2024 May 18. doi:10.1101/2024.05.15.594133

[41] Luo W, Adamska JZ, Li C, et al. SREBP signaling is essential for effective B cell responses. *Nat Immunol*. 2023;24(2):337-348. doi:10.1038/s41590-022-01376-y

protect against ER stress and autophagy. Pharmacological SCD inhibition dampens mTORC1 activity, an effect reversible with exogenous MUFAs. Interestingly, intrinsic SCD activity is not strictly required in vivo, suggesting extracellular MUFA sources may compensate [42].

Short-chain fatty acids (SCFAs) influence B cell responses through epigenetic regulation: they suppress Aicda and Prdm1 expression, thereby reducing class switch recombination, somatic hypermutation, and PCs differentiation. This may help preserve tolerance in the gut, preventing Ig production against commensals [43]. In autoimmune models, SCFA administration reduced inflammation and promoted regulatory B cells [44].

Finally, peroxisomes—organelles central to β-oxidation and redox balance—are gaining attention in immune cell metabolism [45]. In B cells, peroxisomal activity appears important for marginal zone and B1 B cell expansion and antibody production [46], though this area remains understudied.

2.6 Checkpoint of B cell metabolism

[42] Zhou X, Zhu X, Li C, et al. Stearoyl-CoA Desaturase-Mediated Monounsaturated Fatty Acid Availability Supports Humoral Immunity. *Cell Rep*. 2021;34(1):108601. doi:10.1016/j.celrep.2020.108601

[43] Sanchez HN, Moroney JB, Gan H, et al. B cell-intrinsic epigenetic modulation of antibody responses by dietary fiber-derived short-chain fatty acids. *Nat Commun*. 2020;11(1):60. Published 2020 Jan 2. doi:10.1038/s41467-019-13603-6

[44] Yao Y, Cai X, Zheng Y, et al. Short-chain fatty acids regulate B cells differentiation via the FFA2 receptor to alleviate rheumatoid arthritis. *Br J Pharmacol*. 2022;179(17):4315-4329. doi:10.1111/bph.15852

[45] Kim DS, Woo JS, Min HK, et al. Short-chain fatty acid butyrate induces IL-10-producing B cells by regulating circadian-clock-related genes to ameliorate Sjögren's syndrome. *J Autoimmun*. 2021;119:102611. doi:10.1016/j.jaut.2021.102611

[46] Muri J, Corak B, Matsushita M, Baes M, Kopf M. Peroxisomes Are Critical for the Development and Maintenance of B1 and Marginal Zone B Cells but Dispensable for Follicular B Cells and T Cells. *J Immunol*. 2022;208(4):839-850. doi:10.4049/jimmunol.2100518

B cell growth and activity are tightly linked to external cues [47] and nutrient status [48]. To adapt, these cells rely on metabolic sensors that adjust pathway usage accordingly, with mTORC1 acting as a major regulator [49]. Upon B cell activation, mTORC1 promotes mitochondrial biogenesis and remodeling, processes essential for GC reactions [50]. Mitochondrial DNA replication and respiration sustain mTORC1 activity [51], and its levels influence fate decisions: reduced activity favors memory B cell development [52], while stronger activation drives PCs differentiation [53]. mTORC1 also controls autophagy, a lysosomal degradation process important for B cell homeostasis [54]. In subsets such as B1a cells, defective autophagy leads to metabolic stress and impaired self-renewal [55]. It is also critical for sustaining PCs and long-lived antibody

[47] Jellusova J. Cross-talk between signal transduction and metabolism in B cells. *Immunol Lett*. 2018;201:1-13. doi:10.1016/j.imlet.2018.11.003
[48] Young C, Brink R. The unique biology of germinal center B cells. Immunity. 2021;54(8):1652-1664. doi:10.1016/j.immuni.2021.07.015
[49] Goul C, Peruzzo R, Zoncu R. The molecular basis of nutrient sensing and signalling by mTORC1 in metabolism regulation and disease. Nat Rev Mol Cell Biol. 2023;24(12):857-875. doi:10.1038/s41580-023-00641-8
[50] Iborra-Pernichi M, Ruiz García J, Velasco de la Esperanza M, et al. Defective mitochondria remodelling in B cells leads to an aged immune response. *Nat Commun*. 2024;15(1):2569. Published 2024 Mar 22. doi:10.1038/s41467-024-46763-1
[51] Urbanczyk S, Baris OR, Hofmann J, et al. Mitochondrial respiration in B lymphocytes is essential for humoral immunity by controlling the flux of the TCA cycle. *Cell Rep*. 2022;39(10):110912. doi:10.1016/j.celrep.2022.110912
[52] Inoue T, Shinnakasu R, Kawai C, et al. Exit from germinal center to become quiescent memory B cells depends on metabolic reprograming and provision of a survival signal. J Exp Med. 2021;218(1):e20200866. doi:10.1084/jem.20200866
[53] Benhamron S, Pattanayak SP, Berger M, Tirosh B. mTOR activation promotes plasma cell differentiation and bypasses XBP-1 for immunoglobulin secretion. Mol Cell Biol. 2015;35(1):153-166. doi:10.1128/MCB.01187-14
[54] Arnold J, Murera D, Arbogast F, Fauny JD, Muller S, Gros F. Autophagy is dispensable for B-cell development but essential for humoral autoimmune responses. Cell Death Differ. 2016;23(5):853-864. doi:10.1038/cdd.2015.149
[55] Clarke AJ, Riffelmacher T, Braas D, Cornall RJ, Simon AK. B1a B cells require autophagy for metabolic homeostasis and self-renewal. J Exp Med. 2018;215(2):399-413. doi:10.1084/jem.20170771

responses [56]. Regulation of autophagy through Rubicon isoforms (RUBCN100 and RUBCN130) shapes memory B cell versus plasmablast differentiation, with RUBCN130 loss enhancing autophagy and promoting memory formation [57]. Nutrient scarcity suppresses mTORC1 through AMPK activation [58]. Loss of AMPK regulators like LKB1 or Fnip1 disrupts B cell development, as cells fail to downregulate mTORC1 and undergo metabolic stress [59]. Interestingly, AMPK seems dispensable for proliferation in mature B cells [60], though it supports memory responses by preserving mitochondrial balance and limiting ROS [61]. AMPK has also been linked to IgD expression, suggesting a possible role in early B cell activation [62].

[56] Pengo N, Scolari M, Oliva L, et al. Plasma cells require autophagy for sustainable immunoglobulin production. Nat Immunol. 2013;14(3):298-305. doi:10.1038/ni.2524

[57] Tsai CY, Sakakibara S, Kuan YD, et al. Opposing roles of RUBCN isoforms in autophagy and memory B cell generation. Sci Signal. 2023;16(803):eade3599. doi:10.1126/scisignal.ade3599

[58] González A, Hall MN, Lin SC, Hardie DG. AMPK and TOR: The Yin and Yang of Cellular Nutrient Sensing and Growth Control. *Cell Metab*. 2020;31(3):472-492. doi:10.1016/j.cmet.2020.01.015

[59] Park H, Staehling K, Tsang M, et al. Disruption of Fnip1 reveals a metabolic checkpoint controlling B lymphocyte development. Immunity. 2012;36(5):769-781. doi:10.1016/j.immuni.2012.02.019

[60] Müschen M. Metabolic gatekeepers to safeguard against autoimmunity and oncogenic B cell transformation. Nat Rev Immunol. 2019;19(5):337-348. doi:10.1038/s41577-019-0154-3

[61] Brookens SK, Cho SH, Basso PJ, Boothby MR. AMPKα1 in B Cells Dampens Primary Antibody Responses yet Promotes Mitochondrial Homeostasis and Persistence of B Cell Memory. J Immunol. 2020;205(11):3011-3022. doi:10.4049/jimmunol.1901474

[62] Waters LR, Ahsan FM, Ten Hoeve J, et al. Ampk regulates IgD expression but not energy stress with B cell activation. Sci Rep. 2019;9(1):8176. Published 2019 Jun 3. doi:10.1038/s41598-019-43985-y

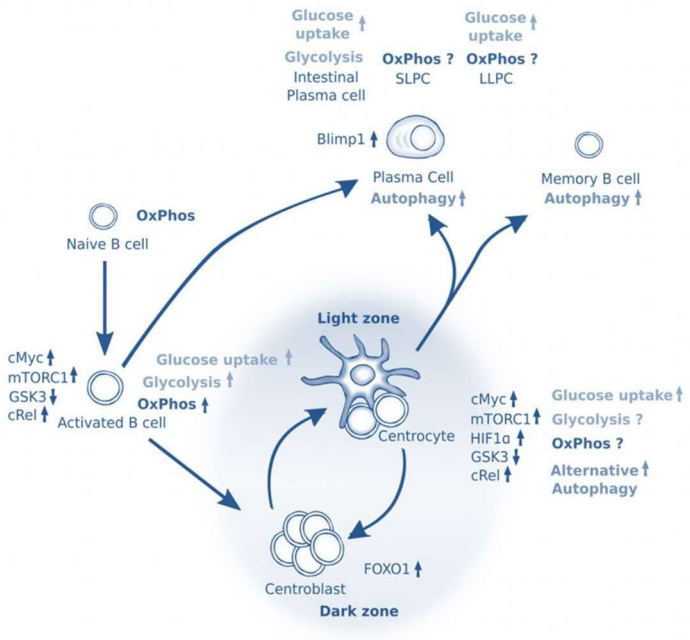

Figure 2. Summary of the metabolic profile in different B cell subsets
Adapted from Jellusova J. Cross-talk between signal transduction and metabolism in B cells. Immunol Lett. 2018;201:1-13. doi:10.1016/j.imlet.2018.11.003

Because of their high proliferative and mutational rates, B cells are prone to malignant transformation, requiring metabolic safeguards [63]. Transcription factors such as PAX5 and IKZF1 restrict glucose metabolism to reduce oncogenic risk [64]. Additionally, GSK3 restrains cell size, ROS levels, and metabolism [65]. Its absence skews GC B cells toward plasmablasts in vitro but impairs antibody responses in vivo [66].

[63] Chan LN, Chen Z, Braas D, et al. Metabolic gatekeeper function of B-lymphoid transcription factors. Nature. 2017;542(7642):479-483. doi:10.1038/nature21076
[64] Xiao G, Chan LN, Klemm L, et al. B-Cell-Specific Diversion of Glucose Carbon Utilization Reveals a Unique Vulnerability in B Cell Malignancies. Cell. 2018;173(2):470-484.e18. doi:10.1016/j.cell.2018.02.048
[65] Jellusova J, Cato MH, Apgar JR, et al. Gsk3 is a metabolic checkpoint regulator in B cells. *Nat Immunol*. 2017;18(3):303-312. doi:10.1038/ni.3664
[66] Lee J, Park H, Lim J, et al. GSK3 Restrains Germinal Center B Cells to Form Plasma Cells. *J Immunol*. 2021;206(3):481-493. doi:10.4049/jimmunol.2000908

A deeper understanding of how B cells integrate metabolic and signaling pathways may open therapeutic opportunities in cancer, autoimmunity, and aging.

3. Introduction to Multi-Omics

3.1 Multi-Omics Approaches in the Study of Immunodeficiencies

Achieving a comprehensive understanding of the human immune system presents a significant scientific challenge due to its inherent complexity and dynamic nature. Immune responses are orchestrated through an intricate network of interactions involving diverse immune cell populations and a wide array of biomolecules, including cytokines, immunoglobulins, and metabolites. This immunological network exhibits substantial plasticity, adapting to the specific characteristics of various pathogens and environmental stimuli. Furthermore, considerable inter-individual variability exists in immune responses, contributing to heterogeneity across populations. Such variation arises from multiple molecular and environmental factors, highlighting both the necessity and complexity of employing multi-omics strategies to investigate immune function [67]. Multi-omics approaches enable the identification of immunological mediators and facilitate the characterization of immune phenotypes through the integration of diverse molecular and cellular layers, including the genome, transcriptome, proteome, metabolome, lipidome. While single-omics analyses—such as transcriptomic profiling—can yield valuable insights into specific biological processes, they are inherently limited to regulatory levels. In contrast, multi-omics integration provides a systems-level perspective that is essential for elucidating the full scope of immune regulation. The following sections introduces the principal omic layers relevant to immunological research, with emphasis on

[67] Chu X, Zhang B, Koeken VACM, Gupta MK, Li Y. Multi-Omics Approaches in Immunological Research. *Front Immunol*. 2021;12:668045. Published 2021 Jun 11. doi:10.3389/fimmu.2021.668045

transcriptomic, proteomic, lipidomic, and metabolomic data. The subsequent section discusses analytical and computational strategies for multi-omics data integration. [68]

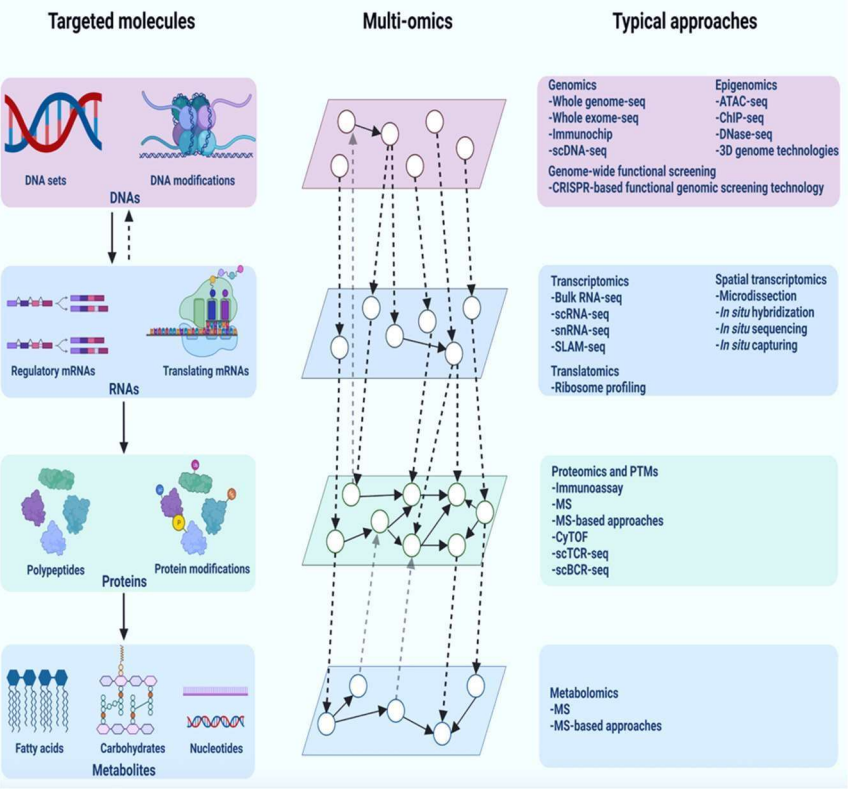

Figure 3. Overview of multi-omics layers, targeted molecular entities, and associated analytical approaches in immunological research

Adapted from Wang X, Fan D, Yang Y, Gimple RC, Zhou S. Integrative multi-omics approaches to explore immune cell functions: Challenges and opportunities. iScience. 2023;26(4):106359. Published 2023 Mar 9. doi:10.1016/j.isci.2023.106359

3.2 Transcriptomics

Transcriptomics, the comprehensive analysis of RNA molecules transcribed from the genome, provides a quantitative view of gene activity and regulatory dynamics underpinning cellular function, differentiation, and disease. By capturing the full range of expressed transcripts, transcriptomic profiling enables

[68] Wang X, Fan D, Yang Y, Gimple RC, Zhou S. Integrative multi-omics approaches to explore immune cell functions: Challenges and opportunities. iScience. 2023;26(4):106359. Published 2023 Mar 9. doi:10.1016/j.isci.2023.106359

the identification of molecular pathways, biomarkers, and gene regulatory networks that drive phenotypic diversity and pathological states [69]. Among its various modalities, bulk transcriptomics remains the most widely applied approach for assessing gene expression in tissues or cell populations, yielding an averaged representation of the transcriptome that integrates signals from multiple cell types. While this averaging limits cellular resolution, it provides valuable insights into overall biological processes, environmental responses, and disease progression when analyzed appropriately [70]. Bulk RNA sequencing (RNA-seq) has largely replaced microarrays due to its higher sensitivity, broader dynamic range, and capacity to detect novel transcripts and isoforms [71]. In a typical workflow, RNA is extracted from homogenized tissue, converted to cDNA, and sequenced to generate millions of short reads that represent transcript abundance. These reads undergo quality control and alignment or pseudoalignment to a reference genome or transcriptome (e.g., using STAR, HISAT2, or Salmon) before quantification and normalization steps that correct for library size, sequencing depth, and compositional biases [72]. Downstream statistical models such as those implemented in DESeq2 or edgeR apply negative binomial frameworks to identify differentially expressed genes across conditions, while functional enrichment analyses (e.g., Gene Ontology or GSEA) contextualize these changes in biological pathways. Recent methodological advances have extended bulk transcriptomics beyond traditional analyses through meta-analytic integration and computational deconvolution, which estimate cell-type proportions using single-cell reference data to address

[69] Lowe R, Shirley N, Bleackley M, Dolan S, Shafee T. Transcriptomics technologies. PLoS Comput Biol. 2017;13(5):e1005457. Published 2017 May 18. doi:10.1371/journal.pcbi.1005457

[70] Luo J, Fu J, Lu Z, Tu J. Deep learning in integrating spatial transcriptomics with other modalities. Brief Bioinform. 2024;26(1):bbae719. doi:10.1093/bib/bbae719

[71] Zhao S, Fung-Leung WP, Bittner A, Ngo K, Liu X. Comparison of RNA-Seq and microarray in transcriptome profiling of activated T cells. PLoS One. 2014;9(1):e78644. Published 2014 Jan 16. doi:10.1371/journal.pone.0078644

[72] Deshpande D, Chhugani K, Chang Y, et al. RNA-seq data science: From raw data to effective interpretation. Front Genet. 2023;14:997383. Published 2023 Mar 13. doi:10.3389/fgene.2023.997383

heterogeneity and enhance interpretability [73]. Despite the growing prominence of single-cell approaches, bulk transcriptomics continues to serve as a cost-effective and robust tool for exploring gene expression at the tissue level, particularly when coupled with careful experimental design, quality control, and bioinformatic standardization [74].

3.3 Proteomics

Proteomics, the large-scale study of the entire complement of proteins expressed by a genome, cell, tissue, or organism, provides a dynamic and functional perspective of biology that extends beyond what transcriptomic data alone can reveal. Because proteins represent the main executors of cellular processes—including enzymatic catalysis, signal transduction, and structural organization—proteomic profiling is fundamental for understanding phenotype, post-transcriptional regulation, and disease mechanisms [75]. Unlike the relatively static nature of the genome, the proteome is highly context-dependent, reflecting changes in environmental conditions, developmental stages, and pathological states [76]. Advances in mass spectrometry (MS)–based technologies have enabled comprehensive and quantitative characterization of thousands of proteins in complex biological samples, transforming proteomics into a core discipline of systems biology [77]. Two major approaches dominate the field: discovery proteomics, which identifies and quantifies proteins globally

[73] Liu S, Wang Z, Zhu R, Wang F, Cheng Y, Liu Y. Three Differential Expression Analysis Methods for RNA Sequencing: limma, EdgeR, DESeq2. *J Vis Exp*. 2021;(175):10.3791/62528. Published 2021 Sep 18. doi:10.3791/62528

[74] Hegenbarth JC, Lezzoche G, De Windt LJ, Stoll M. Perspectives on Bulk-Tissue RNA Sequencing and Single-Cell RNA Sequencing for Cardiac Transcriptomics. Front Mol Med. 2022;2:839338. Published 2022 Feb 22. doi:10.3389/fmmed.2022.839338

[75] Al-Amrani S, Al-Jabri Z, Al-Zaabi A, Alshekaili J, Al-Khabori M. Proteomics: Concepts and applications in human medicine. World J Biol Chem. 2021;12(5):57-69. doi:10.4331/wjbc.v12.i5.57

[76] Sun BB, Suhre K, Gibson BW. Promises and Challenges of populational Proteomics in Health and Disease. Mol Cell Proteomics. 2024;23(7):100786. doi:10.1016/j.mcpro.2024.100786

[77] Vitorino R. Transforming Clinical Research: The Power of High-Throughput Omics Integration. Proteomes. 2024;12(3):25. Published 2024 Sep 6. doi:10.3390/proteomes12030025

through data-dependent or data-independent acquisition (DDA/DIA), and targeted proteomics, which employs methods such as selected or parallel reaction monitoring (SRM/PRM) to measure predefined protein sets with high precision. Quantitative strategies include label-free spectral counting, chemical labeling (e.g., TMT, iTRAQ), and metabolic labeling (e.g., SILAC), each optimized for specific experimental needs and sample types [78]. Downstream bioinformatic analyses integrate protein identification, quantification, and functional annotation using databases such as UniProt, Gene Ontology, and STRING to elucidate molecular interactions and pathway perturbations. Despite challenges in dynamic range, sample complexity, and post-translational modification analysis, recent innovations in single-cell proteomics, machine learning–based spectra interpretation, and multi-omics integration are expanding the analytical power and biological relevance of proteomic research [79]. Thus, proteomics represents a crucial bridge between genotype and phenotype, offering a mechanistic layer of understanding that complements genomics and transcriptomics in modern molecular biology.

3.4 Lipidomics

Lipidomics, a branch of metabolomics, is dedicated to the comprehensive analysis of lipids within cells, tissues, or organisms, offering critical insights into the structural, energetic, and signaling functions of these biomolecules in health and disease. Lipids are fundamental components of cellular membranes, energy storage systems, and signaling cascades, and their dynamic regulation reflects both physiological states and pathological alterations such as

[78] Li J, Smith LS, Zhu HJ. Data-independent acquisition (DIA): An emerging proteomics technology for analysis of drug-metabolizing enzymes and transporters. Drug Discov Today Technol. 2021;39:49-56. doi:10.1016/j.ddtec.2021.06.006

[79] Haider S, Pal R. Integrated analysis of transcriptomic and proteomic data. Curr Genomics. 2013;14(2):91-110. doi:10.2174/1389202911314020003

inflammation, metabolic disorders, and neurodegeneration [80]. By profiling diverse lipid classes —including glycerophospholipids, sphingolipids, sterols, and triglycerides— lipidomics provides a molecular snapshot of cellular homeostasis and metabolic adaptation [81]. Because lipids exhibit vast structural diversity and subtle chemical variations, lipidomic research relies heavily on high-resolution analytical techniques capable of resolving complex mixtures with high sensitivity and specificity. The field has been revolutionized by advances in MS coupled with chromatographic separation, such as liquid chromatography–mass spectrometry (LC–MS), gas chromatography–mass spectrometry (GC–MS), and shotgun lipidomics, which allow precise identification and quantification of hundreds to thousands of lipid species in a single experiment [82]. Sample preparation methods, including extraction protocols like Bligh-Dyer and Folch, play a crucial role in minimizing oxidation and ensuring reproducibility [83]. Data processing and interpretation typically involve software pipelines for peak detection, lipid annotation, and quantification (e.g., LipidSearch, MS-DIAL), followed by statistical and pathway analyses to reveal lipid alterations associated with biological conditions. Despite challenges such as ion suppression, isomeric overlap, and the need for standardized quantification, ongoing developments in high-resolution MS, ion mobility spectrometry, and bioinformatics are significantly enhancing lipidome coverage and accuracy. As such, lipidomics has emerged as a key pillar of systems biology, bridging metabolism

[80] Belhaj MR, Lawler NG, Hoffman NJ. Metabolomics and Lipidomics: Expanding the Molecular Landscape of Exercise Biology. Metabolites. 2021;11(3):151. Published 2021 Mar 7. doi:10.3390/metabo11030151

[81] Quehenberger O, Armando AM, Brown AH, et al. Lipidomics reveals a remarkable diversity of lipids in human plasma. J Lipid Res. 2010;51(11):3299-3305. doi:10.1194/jlr.M009449

[82] Lu G, Xu S, Huang P, Li L. Enhancing Lipidomics With High-Resolution Ion Mobility-Mass Spectrometry. Proteomics. Published online August 13, 2025. doi:10.1002/pmic.70026

[83] Omar AM, Zhang Q. Evaluation of Lipid Extraction Protocols for Untargeted Analysis of Mouse Tissue Lipidome. Metabolites. 2023;13(9):1002. Published 2023 Sep 9. doi:10.3390/metabo13091002

and cell signaling, and providing mechanistic insights into the molecular basis of physiology and disease [84].

3.5 Metabolomics

Metabolomics, the comprehensive study of small-molecule metabolites within biological systems, provides a direct snapshot of cellular metabolism and physiological state, reflecting the dynamic interplay between genetic regulation, environmental influences, and biochemical activity. By simultaneously profiling thousands of low-molecular-weight compounds, metabolomics captures both polar metabolites—such as amino acids, organic acids, nucleotides, and carbohydrates that participate in central carbon metabolism—and nonpolar metabolites, including lipids, sterols, and fatty acids that contribute to membrane structure, energy storage, and signaling [85]. This dual focus allows metabolomics to bridge cellular energetics and structural biology, offering insights into processes like oxidative stress, mitochondrial function, and lipid remodeling that are often invisible to transcriptomic or proteomic analyses [86]. Analytical approaches for metabolomics broadly divide into targeted and untargeted strategies, each employing advanced instrumentation such as nuclear magnetic resonance (NMR) spectroscopy and MS, frequently coupled to chromatographic separation. For polar metabolites, hydrophilic interaction liquid chromatography (HILIC)–MS and gas chromatography–MS (GC–MS) are commonly used to resolve highly soluble compounds of central metabolism, while nonpolar metabolites are best analyzed using reversed-phase

[84] Lee ICH, Tumanov S, Wong JWH, Stocker R, Ho JWK. Integrative processing of untargeted metabolomic and lipidomic data using MultiABLER. iScience. 2023;26(6):106881. Published 2023 May 13. doi:10.1016/j.isci.2023.106881

[85] Qiu S, Cai Y, Yao H, et al. Small molecule metabolites: discovery of biomarkers and therapeutic targets. Signal Transduct Target Ther. 2023;8(1):132. Published 2023 Mar 20. doi:10.1038/s41392-023-01399-3

[86] Cardillo M, Katam K, Suravajhala P. Advancements in multi-omics research to address challenges in Alzheimer's disease: a systems biology approach utilizing molecular biomarkers and innovative strategies. Front Aging Neurosci. 2025;17:1591796. Published 2025 Jul 23. doi:10.3389/fnagi.2025.1591796

liquid chromatography (RP–LC) or direct-infusion MS techniques [87]. Sample preparation protocols often employ dual-phase extraction methods (e.g., methanol–chloroform or MTBE systems) to efficiently separate aqueous and organic fractions, preserving metabolite integrity and minimizing matrix effects [88]. Subsequent data processing involves peak detection, feature alignment, and annotation using curated spectral libraries (e.g., HMDB, METLIN), followed by statistical modeling and pathway enrichment analysis to interpret metabolic perturbations. Despite challenges in compound identification, dynamic range, and standardization, advances in high- resolution MS, stable isotope tracing, and machine learning– based metabolite annotation are rapidly enhancing both sensitivity and interpretability. Consequently, metabolomics— spanning both polar and nonpolar metabolic spaces—has become an essential component of systems biology, elucidating the biochemical underpinnings of physiology, disease, and environmental adaptation [89].

3.6 Computational modelling

Computational modeling that integrates metabolomics, transcriptomics, lipidomics, and proteomics data—often referred to as multi-omics modeling—aims to capture the complex, interconnected nature of biological systems by linking molecular layers into coherent, predictive frameworks. This systems biology approach transcends single-omic analyses by contextualizing gene expression, protein abundance, lipid composition, and metabolite fluxes within dynamic regulatory and metabolic networks, thereby elucidating how molecular

[87] Wang JH, Byun J, Pennathur S. Analytical approaches to metabolomics and applications to systems biology. Semin Nephrol. 2010;30(5):500-511. doi:10.1016/j.semnephrol.2010.07.007

[88] Lee HJ, Kremer DM, Sajjakulnukit P, Zhang L, Lyssiotis CA. A large-scale analysis of targeted metabolomics data from heterogeneous biological samples provides insights into metabolite dynamics. Metabolomics. 2019;15(7):103. Published 2019 Jul 9. doi:10.1007/s11306-019-1564-8

[89] Chen Y, Li EM, Xu LY. Guide to Metabolomics Analysis: A Bioinformatics Workflow. Metabolites. 2022;12(4):357. Published 2022 Apr 15. doi:10.3390/metabo12040357

perturbations propagate across cellular processes [90]. Integrative computational models provide mechanistic insights into disease progression, metabolic reprogramming, and cellular adaptation, offering quantitative predictions that can guide therapeutic target identification and metabolic engineering [91]. Conceptually, these models bridge genotype to phenotype by combining high-throughput molecular data with mathematical and statistical representations of biological systems—ranging from correlation-based and Bayesian network models to constraint-based stoichiometric frameworks such as genome-scale metabolic models (GEMs) and flux balance analysis (FBA) [92]. In such frameworks, transcriptomic and proteomic data often define enzyme capacities or reaction constraints, while metabolomic and lipidomic profiles inform flux distributions and metabolite pool sizes, yielding a multiscale view of metabolism that reflects both regulation and function [93]. Methodologically, multi-omics integration employs diverse computational pipelines, including network reconstruction, machine learning, matrix factorization, and probabilistic graphical models, implemented through platforms such as COBRApy, OmicsIntegrator, and MixOmics [94]. Data preprocessing steps—normalization, batch correction, and feature alignment—are critical to harmonize heterogeneous

[90] Cortassa S, Villon P, Sollott SJ, Aon MA. Integrated Multiomics, Bioinformatics, and Computational Modeling Approaches to Central Metabolism in Organs. Methods Mol Biol. 2022;2399:151-170. doi:10.1007/978-1-0716-1831-8_7

[91] Nafie MS, Abu-Elsaoud AM, Diab MK. A comprehensive review on computational metabolomics: Advancing multiscale analysis through in-silico approaches. Comput Struct Biotechnol J. 2025;27:3191-3215. Published 2025 Jul 13. doi:10.1016/j.csbj.2025.07.016

[92] Zampieri G, Vijayakumar S, Yaneske E, Angione C. Machine and deep learning meet genome-scale metabolic modeling. PLoS Comput Biol. 2019;15(7):e1007084. Published 2019 Jul 11. doi:10.1371/journal.pcbi.1007084

[93] Uematsu S, Ohno S, Tanaka KY, et al. Multi-omics-based label-free metabolic flux inference reveals obesity-associated dysregulatory mechanisms in liver glucose metabolism. iScience. 2022;25(2):103787. Published 2022 Feb 4. doi:10.1016/j.isci.2022.103787

[94] Bessell B, Loecker J, Zhao Z, et al. COMO: a pipeline for multi-omics data integration in metabolic modeling and drug discovery. Brief Bioinform. 2023;24(6):bbad387. doi:10.1093/bib/bbad387

datasets prior to integration. Despite challenges in data dimensionality, scale compatibility, and causal inference, recent advances in AI-assisted modeling, dynamic flux simulations, and cross-modal network inference have substantially improved biological interpretability and predictive accuracy. Thus, computational modeling of integrated multi-omics data stands as a cornerstone of modern systems biology, enabling the transition from descriptive molecular profiling to quantitative, hypothesis-driven understanding of cellular function and disease mechanisms [95].

[95] Ren F, Wei J, Chen Q, et al. Artificial intelligence-driven multi-omics approaches in Alzheimer's disease: Progress, challenges, and future directions. Acta Pharm Sin B. 2025;15(9):4327-4385. doi:10.1016/j.apsb.2025.07.030

4. The PI4KA Complex

Role of Phosphoinositide Metabolism in Cellular Signalling

Phosphoinositides are a family of phosphorylated lipids that play central roles in cellular signaling by modulating membrane dynamics, recruiting effector proteins, and organizing signaling platforms. They are critically involved in regulating diverse cellular processes, including cytoskeletal organization, vesicular trafficking, and signal transduction pathways. Among them, $PI(4,5)P_2$ is particularly important for the regulation of actin filament dynamics, interacting with actin-binding proteins such as gelsolin and cofilin to influence cell shape, motility, and migration. By promoting actin polymerization and inhibiting filament severing, $PI(4,5)P_2$ stabilizes the cytoskeletal network and orchestrates dynamic remodeling in response to cellular cues [96]. Phosphoinositides also function as critical docking sites for proteins involved in vesicular trafficking, regulating endocytosis, exocytosis, and membrane recycling. For example, $PI(3,5)P_2$ is essential for endosome maturation and lysosomal homeostasis [97]. Beyond structural roles, phosphoinositides act as key second messengers in signaling cascades: $PI(3,4,5)P_3$, produced by phosphoinositide 3-kinases (PI3Ks), activates downstream effectors such as Akt, thereby regulating cellular survival, proliferation, and metabolism. These lipids further modulate the function of membrane-associated proteins, including ion channels and G-protein-coupled receptors (GPCRs), affecting their gating and signaling outcomes and shaping the cell's response to external stimuli [98]. Dysregulation of phosphoinositide metabolism, whether through mutations in kinases, phosphatases, or other regulatory enzymes, is implicated in various diseases, including cancer, neurodegenerative disorders, and immune dysfunctions. Collectively, these observations underscore that phosphoinositides are essential coordinators of cellular signaling, capable of integrating structural, trafficking, and biochemical cues to maintain homeostasis, and represent promising targets for therapeutic intervention [99].

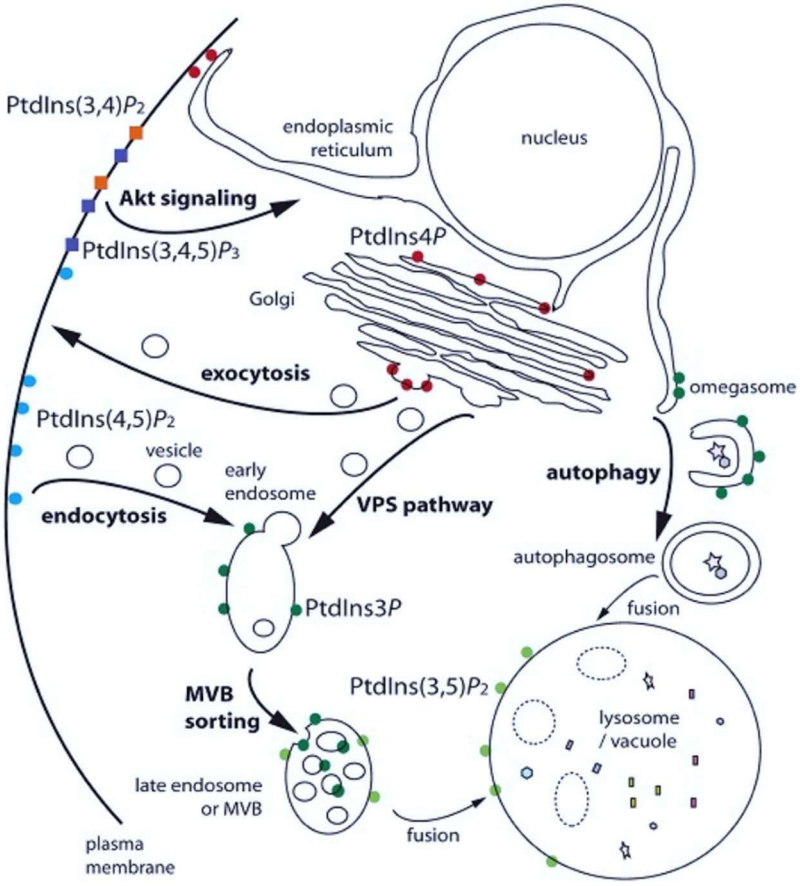

Figure 4. Overview of Phosphoinositide metabolism in Cellular Signalling

Adapted from De Craene JO, Bertazzi DL, Bär S, Friant S. Phosphoinositides, Major Actors in Membrane Trafficking and Lipid Signaling Pathways. Int J Mol Sci. 2017 Mar 15;18(3):634. doi: 10.3390/ijms18030634. PMID: 28294977; PMCID: PMC5372647.

[96] De Craene JO, Bertazzi DL, Bär S, Friant S. Phosphoinositides, Major Actors in Membrane Trafficking and Lipid Signaling Pathways. Int J Mol Sci. 2017 Mar 15;18(3):634. doi: 10.3390/ijms18030634. PMID: 28294977; PMCID: PMC5372647.

[97] Mayinger P. Phosphoinositides and vesicular membrane traffic. Biochim Biophys Acta. 2012;1821(8):1104-1113. doi:10.1016/j.bbalip.2012.01.002

[98] Burke JE, Triscott J, Emerling BM, Hammond GRV. Beyond PI3Ks: targeting phosphoinositide kinases in disease. Nat Rev Drug Discov. 2023;22(5):357-386. doi:10.1038/s41573-022-00582-5

[99] Pendaries C, Tronchère H, Plantavid M, Payrastre B. Phosphoinositide signaling disorders in human diseases. FEBS Lett. 2003 Jul 3;546(1):25-31. doi: 10.1016/s0014-5793(03)00437-x. PMID: 12829232.

4.2 Structure and Function of Phosphatidylinositol 4-Kinase Alpha and Regulatory Components

Phosphatidylinositol 4-kinase alpha (PI4KA, also known as PI4KIIIα) is a lipid kinase that catalyzes the ATP-dependent phosphorylation of phosphatidylinositol (PI) at the D-4 position of its inositol ring, producing phosphatidylinositol 4-phosphate (PI4P)—a central metabolite in the phosphoinositide signaling network. This enzymatic step represents the first committed reaction in the synthesis of polyphosphoinositides, which are key regulators of membrane identity, signal transduction, and intracellular trafficking. PI4P itself serves dual roles: it functions as a precursor for the generation of phosphatidylinositol 4,5-bisphosphate [$PI(4,5)P_2$] and phosphatidylinositol 3,4,5-trisphosphate [$PI(3,4,5)P_3$], and as a signaling lipid that recruits effector proteins with specific PI4P-binding domains (such as PH or OSBP domains) to the plasma membrane [100]. The enzymatic activity and spatial localization of PI4KA are tightly regulated through its assembly into a heterotetrameric complex comprising PI4KA, TTC7 (A/B isoforms), FAM126 (A/B), and EFR3 (A/B). In this structure, EFR3 acts as a membrane- anchoring adaptor, TTC7 and FAM126 provide structural stability and facilitate the correct orientation of the kinase domain toward the membrane surface, while additional regulators such as TMEM150A or ACBD3 can substitute or complement these interactions in specific subcellular contexts (e.g., Golgi vs. plasma membrane). Structural and cryo-EM studies have revealed that this assembly is essential for maintaining both PI4KA activity and membrane specificity [101]. Functionally, the PI4KA-driven generation of PI4P is critical for phosphoinositide turnover and signaling cascades—$PI(4,5)P_2$ serves as a substrate for phospholipase C (PLC) to yield second messengers IP_3 and DAG, or for PI3K to produce $PI(3,4,5)P_3$, a central regulator of the AKT/mTOR signaling axis. These pathways influence processes including cell growth, migration, actin cytoskeleton remodeling, and vesicle trafficking. Dysregulation or mutation of PI4KA complex components has

[7]Verdura E, Rodríguez-Palmero A, Vélez-Santamaria V, et al. Biallelic PI4KA variants cause a novel neurodevelopmental syndrome with hypomyelinating leukodystrophy. Brain. 2021;144(9):2659-2669. doi:10.1093/brain/awab124

[101] Suresh S, Shaw AL, Pemberton JG, et al. Molecular basis for plasma membrane recruitment of PI4KA by EFR3. Sci Adv. 2024;10(51):eadp6660. doi:10.1126/sciadv.adp6660

been linked to neurodevelopmental disorders, immunodeficiencies, viral replication (e.g., HCV, enteroviruses), and cancer, highlighting the enzyme's essential role in coordinating lipid metabolism with cellular signaling [102].

5. PI4KA-Related Disorder

5.1 Clinical Overview and Early Descriptions

PI4KA-related disorder is a recently identified autosomal recessive neurodevelopmental syndrome associated with biallelic pathogenic variants in the *PI4KA* gene. The first clinical descriptions emerged in 2021, highlighting a spectrum of neurological, gastrointestinal, and immunological manifestations. These early reports laid the foundation for subsequent case studies and genetic analyses that have further elucidated the clinical and molecular characteristics of the disorder.[103]

Neurologically, individuals with PI4KA-related disorder often present with limb spasticity, developmental delay, intellectual disability, seizures, ataxia, nystagmus, and dysmetria. Brain imaging typically reveals hypomyelinating leukodystrophy, cerebellar hypoplasia or atrophy, and perisylvian polymicrogyria. Gastrointestinal involvement includes multiple intestinal atresia and early-onset, treatment-refractory inflammatory bowel disease. Immunological features encompass combined immunodeficiency, with varying degrees of leukopenia and immunoglobulin deficiencies. [104]

[102] Stojilkovic SS, Balla T. PI(4,5)P2-dependent and -independent roles of PI4P in the control of hormone secretion by pituitary cells. Front Endocrinol (Lausanne). 2023;14:1118744. Published 2023 Jan 27. doi:10.3389/fendo.2023.1118744

[103] Salter CG, Cai Y, Lo B, et al. Biallelic PI4KA variants cause neurological, intestinal and immunological disease. Brain. 2021;144(12):3597-3610. doi:10.1093/brain/awab313

[104] Baple EL, Salter C, Uhlig H, Wolf NI, Crosby AH. PI4KA-Related Disorder. In: Adam MP, Feldman J, Mirzaa GM, Pagon RA, Wallace SE, Amemiya A, eds. GeneReviews®. Seattle (WA): University of Washington, Seattle; August 11, 2022.

The disorder's phenotypic variability has been attributed to the diverse functional impacts of different *PI4KA* variants. For instance, certain mutations may lead to significant reductions in PI4KA enzyme activity, impairing phosphoinositide signaling and vesicular trafficking. These molecular disruptions are thought to underlie the multi-system involvement observed in affected individuals [104].

The initial clinical descriptions of PI4KA-related disorder were also significantly influenced by the unexpected survival of affected individuals, challenging prior assumptions about the lethality of PI4KA deficiency. Before these reports, biallelic mutations in *PI4KA* were considered incompatible with life, based on findings from murine models in which complete knockout of the *Pi4ka* gene led to early embryonic lethality due to severe intestinal necrosis [105]. However, human cases have demonstrated that certain hypomorphic variants in *PI4KA* can permit survival beyond the neonatal period. In a pivotal 2015 study, three fetuses from a consanguineous family carrying compound heterozygous *PI4KA* mutations were identified. These fetuses exhibited severe neurological anomalies, including perisylvian polymicrogyria, cerebellar hypoplasia, and arthrogryposis, yet survived to varying gestational ages of 16, 24, and 28 weeks. This observation was instrumental in redefining the clinical expectations for PI4KA-related disorder, demonstrating that while complete loss of PI4KA function is lethal, certain mutations allow for fetal development and survival[106]. Subsequent studies have corroborated these findings, identifying additional cases of fetal survival with PI4KA mutations. These cases underscore the critical role of specific PI4KA variants in determining viability and clinical presentation.

[105] Constantin S, Sokanovic SJ, Mochimaru Y, et al. Postnatal Development and Maintenance of Functional Pituitary Gonadotrophs Is Dependent on PI4-Kinase A. Endocrinology. 2023;164(12):bqad168. doi:10.1210/endocr/bqad168

[106] Pagnamenta AT, Howard MF, Wisniewski E, et al. Germline recessive mutations in PI4KA are associated with perisylvian polymicrogyria, cerebellar hypoplasia and arthrogryposis. Hum Mol Genet. 2015;24(13):3732-3741. doi:10.1093/hmg/ddv117

The recognition that some *PI4KA* mutations permit fetal survival has been pivotal in expanding the understanding of the disorder's phenotypic spectrum and informing clinical management strategies [107].

PI4KA-related disorder was first characterized in patients presenting with neurological impairment, intestinal malformations, and variable immunological features. Since the initial description, multiple reports have expanded the phenotypic spectrum[103,108].

5.2 Preliminary Evidence of Immunological Defects

Initial reports described recurrent infections and variable hypogammaglobulinemia, suggesting immune dysfunction. However, systematic immunological characterization was lacking until recent work demonstrated that PI4KA deficiency disrupts B-cell development, metabolism, and function, leading to lymphopenia and hypogammaglobulinemia.

Early clinical reports of individuals with PI4KA-related disorder noted recurrent respiratory and gastrointestinal infections, as well as variable hypogammaglobulinemia, suggesting an underlying immune dysfunction [103, 104].

However, comprehensive immunological characterization was initially limited. Recent studies have provided more systematic evidence, demonstrating that PI4KA deficiency impairs B-cell development, metabolism, and antibody production [100, 103]. Functional analyses revealed that reduced PI4KA activity disrupts phosphoinositide signaling pathways critical for lymphocyte survival and activation, resulting in lymphopenia

[107] Cheng C, Yang F, Chen X, Zhao S. Identifying novel heterozygous PI4KA variants in fetal abnormalities. BMC Med Genomics. 2025;18(1):23. Published 2025 Jan 30. doi:10.1186/s12920-025-02093-9

[7] Verdura E, Rodríguez-Palmero A, Vélez-Santamaria V, Planas-Serra L, de la Calle I, Raspall-Chaure M, et al. Biallelic PI4KA variants cause a novel neurodevelopmental syndrome with hypomyelinating leukodystrophy. Brain. (2021) . 144:2659–69. doi: 10.1093/brain/awab124

[103] Salter CG, Cai Y, Lo B, et al. Biallelic PI4KA variants cause neurological, intestinal and immunological disease. Brain. 2021;144(12):3597-3610. doi:10.1093/brain/awab313

and defective humoral immunity [7,103,109]. These findings have established a mechanistic link between *PI4KA* mutations and immunodeficiency, expanding the clinical spectrum of the disorder beyond its neurological and gastrointestinal manifestations.

[109] Zhang K, Zhang Y, Wang J, et al. A synonymous mutation in PI4KA impacts transcription and splicing, leading to combined immunodeficiency. Front Genet. 2022;13:799. doi:10.3389/fgene.2022.799

CHAPTER 2

BIALLELIC PI4KA MUTATIONS DISRUPT B-CELL METABOLISM AND CAUSE B-CELL LYMPHOPENIA AND HYPOGAMMAGLOBULINEMIA

Francesco Saettini,[1] **Fabiola Guerra**,[1,2,3,4] Mario Mauri,[3] Margaret P Adam,[5] David Adams,[6] Emma Baple E,[7,8] Estibaliz Barredo,[9] Sanil Bhatia,[10] Arndt Borkhardt,[10] Alfredo Brusco,[11,12] Cristina Bugarin,[1] Clizia Chinello,[3] Andrew H Crosby,[7] Precilla D'Souza P,[6] Vanna Denti,[3] Grazia Fazio,[1] Silvia Giuliani,[2,3] Hye Sun Kuehn,[13] Hassan Amel,[14] Asha Elmi,[15] Bernice Lo,[15,16],Federica Malighetti,[3] Giorgia Mandrile,[17] Andrea Martín-Nalda,[18] Heather C Mefford,[5] Daniele Moratto,[19] Fatemeh Emam Mousavi,[4,20] Zoe Nelson,[21] Luis González Gutiérrez-Solana L,[22] Ellen Macnamara,[6] Vincent Michaud,[23] Melanie O'Leary,[24] Lisa Pagani,[3] Lisa Pavinato ,[11,25] Patricia V Velez Santamaria,[26] Laura Planas-Serra,[26,27] Manuel Quadri,[1] Miquel Raspall-Chaure,[28] Stefano Rebellato,[1,3] Sergio D. Rosenzweig,[13] Agathe Roubertie,[29] Claire G Salter,[7,30] Angela Maria Savino,[3] Jennifer L.Stoddard,[13] Holm H Uhlig,[31,21,33] Aurora Pujol,[26,27,34] Fulvio Magni,[3] Giuseppe Paglia,[3] Gianni Cazzaniga,[3] Rocco Piazza,[3] Matteo Barberis,[4,20,35*]Andrea Biondi,[1,2,3*].

AFFILIATIONS

[1]Centro Tettamanti, Fondazione IRCCS San Gerardo dei Tintori, Monza, Italy; [2]Pediatria, Fondazione IRCCS San Gerardo dei Tintori, Monza, Italy; [3]Dipartimento di Medicina e Chirurgia, Università degli Studi Milano-Bicocca, Monza, Italy; [4]Molecular Systems Biology, School of Biosciences, Faculty of Health and Medical Sciences, University of Surrey, Guildford, Surrey, United Kingdom; [5]Genetic Medicine, Department of Pediatrics, University of Washington, Seattle WA, USA; [6]NIH Undiagnosed Diseases Program, NIH, Bethesda, MD, USA; [7]RILD Wellcome Wolfson Centre, University of Exeter Medical School, Exeter, UK; [8]Peninsula Clinical Genetics Service, Royal Devon and Exeter Hospital, Exeter, UK; [9]Neuropediatric Department, Hospital Universitario Gregorio Marañón, Madrid, Spain; [10]Department of Paediatric Oncology, Haematology and Clinical Immunology, Heinrich-Heine University Dusseldorf, Medical Faculty, Düsseldorf, Germany; [11]Department of Neurosciences Rita Levi-

Montalcini, University of Turin, 10126 Turin, Italy; [12]Medical Genetics Unit, Città della Salute e della Scienza University Hospital, 10126 Turin, Italy; [13]Immunology Service, DLM, NIH Clinical Center, Bethesda, MD, USA; [14]Pediatric Allergy and Immunology Department, Sidra Medicine, Doha, Qatar; [15]Research Branch, Sidra Medicine, Doha, Qatar; [16]College of Health and Life Sciences, Hamad Bin Khalifa University, Doha, Qatar; [17]Department of Medical Sciences, University of Turin, 10126, Turin, Italy; [18]Pediatric Infectious Diseases and Immunodeficiencies Unit, Hospital Universitari Vall d'Hebron, Institut de Recerca Vall d'Hebron, Universitat Autònoma de Barcelona, Barcelona, Spain; [19]Flow Cytometry Laboratory, Diagnostic Department, ASST Spedali Civili di Brescia, Brescia, Italy; [20]Centre for Mathematical and Computational Biology, CMCB, University of Surrey, Guildford, Surrey, United Kingdom; [21]Vascular Anomalies Program, Seattle Children's Hospital, Seattle WA, USA; [22]Hospital Infantil Niño Jesús, Madrid, España or Infant Jesus Children's Hospital, Madrid, Spain; [23]Molecular Genetics Laboratory, Bordeaux University Hospital, Bordeaux, Aquitaine, France. INSERM U1211, Rare Diseases Laboratory: Genetics and Metabolism, University of Bordeaux, Talence, Aquitaine, France; [24]Center for Mendelian Genomics, Program in Medical and Population Genetics, Broad Institute of MIT and Harvard, Cambridge, MA, USA; [25]Department of Medical Sciences, University of Turin, 10126 Turin, Italy; [26]Neurometabolic Diseases Laboratory, Bellvitge Biomedical Research Institute (IDIBELL), L'Hospitalet de Llobregat, 08908, Barcelona, Catalonia, Spain; [27]Centre for Biomedical Research in Network on Rare Diseases (CIBERER), Instituto de Salud Carlos III, 28029, Madrid, Spain; [28]Department of Paediatric Neurology, Hospital Universitari Vall d'Hebron, Barcelona, Spain; [29]Département de Neuropédiatrie, CIC, CHU de Montpellier, INM, Univ Montpellier, INSERM U 1298, Montpellier, France; [30]Wessex Clinical Genetics Service, Princess Anne Hospital, Southampton, UK; [31]Translational Gastroenterology Unit, NIHR Oxford Biomedical Research Centre, John Radcliffe Hospital, University of Oxford, Oxfordshire, UK; [32]Department of Paediatrics, University of Oxford, Oxfordshire, UK; [33]Oxford NIHR Biomedical Research Centre, Oxford, UK; [34]Catalan Institution of Research and Advanced Studies (ICREA), Barcelona, Catalonia, Spain; [35]Synthetic Systems Biology and Nuclear Organization, Swammerdam Institute for Life Sciences, University of Amsterdam, Amsterdam, The Netherlands.

*These authors have contributed equally to this work and share senior authorship.

J Clin Immunol. 2024 Sep 23;45(1):15.
doi: 10.1007/s10875-024-01793-8.

2.1 Abstract

Purpose. PI4KA-related disorder is a highly clinically variable condition characterized by neurological (limb spasticity, developmental delay, intellectual disability, seizures, ataxia, nystagmus) and gastrointestinal (inflammatory bowel disease and multiple intestinal atresia) manifestations. Although features consistent with immunodeficiency (autoimmunity/autoinflammation and recurrent infections) have been reported in a subset of patients, the burden of B-cell deficiency and hypogammaglobulinemia has not been extensively investigated. We sought to describe the clinical presentation and manifestations of patients with PI4KA-related disorder and to investigate the metabolic consequences of biallelic PI4KA variants in B cells.

Methods. Clinical data from patients with PI4KA variants were obtained. Multi–omics analyses combining transcriptome, proteome, lipidome and metabolome analyses in conjunction with functional assays were performed in EBV-transformed B cells.

Results. Clinical and laboratory data of 13 patients were collected. Recurrent infections (7/13), autoimmune/autoinflammatory manifestations (5/13), B-cell deficiency (8/13) and hypogammaglobulinemia (8/13) were frequently observed. Patients' B cells frequently showed increased transitional and decreased switched memory B-cell subsets. Pathway analyses based on differentially expressed transcripts and proteins confirmed the central role of PI4KA in B cell differentiation with altered B-cell receptor (BCR) complex and signaling. By altering lipids production and tricarboxylic acid cycle regulation, and causing increased endoplasmic reticulum stress, biallelic PI4KA mutations disrupt B cell metabolism inducing mitochondrial dysfunction. As a result, B cells show hyperactive PI3K/mTOR pathway, increased autophagy and deranged cytoskeleton organization.

Conclusion. By altering lipid metabolism and TCA cycle, impairing mitochondrial activity, hyperactivating mTOR pathway and increasing autophagy, PI4KA-related disorder causes a syndromic inborn error of immunity presenting with B-cell deficiency and hypogammaglobulinemia.

2.2 Introduction

Inborn errors of immunity (IEI) are heterogeneous conditions that share increased susceptibility to infections, autoimmunity, allergy, autoinflammation and predisposition to malignancy [110]. Syndromic immunodeficiencies are a subgroup of IEI characterized by involvement of different organ systems simultaneously [111, 112]. Phosphatidylinositol 4-kinase alpha (PI4KA) encodes PI4KA, a mammalian phosphatidylinositol (PI) 4-kinase that catalyzes the first step of phosphoinositide metabolism, phosphorylating PI to PI-4-phosphate (PI4P) at the plasma membrane (PM) and endoplasmic reticulum (ER). PIs collectively perform fundamental signaling roles at the PM and other organelles [113,114,115,116,] The PI4KA complex comprises a lipid kinase (PI4KA), and two regulatory units, Hyccin (HYCC1/2; formerly FAM126A/B) and TTC7A/B. EFR3 anchors the PI4KA

[110] Tangye SG, Al-Herz W, Bousfiha A, et al. Human Inborn Errors of Immunity: 2022 Update on the Classification from the International Union of Immunological Societies Expert Committee. *J Clin Immunol*. 2022;42(7):1473-1507. doi:10.1007/s10875-022-01289-3

[111] Seidel MG, Kindle G, Gathmann B, et al. The European Society for Immunodeficiencies (ESID) Registry Working Definitions for the Clinical Diagnosis of Inborn Errors of Immunity. J Allergy Clin Immunol Pract. 2019;7(6):1763-1770. doi:10.1016/j.jaip.2019.02.004

[112] Saettini F, Herriot R, Prada E, et al. Prevalence of Immunological Defects in a Cohort of 97 Rubinstein-Taybi Syndrome Patients. J Clin Immunol. 2020;40(6):851-860. doi:10.1007/s10875-020-00808-4

[113] Boura E, Nencka R. Phosphatidylinositol 4-kinases: Function, structure, and inhibition. Exp Cell Res. 2015;337(2):136-145. doi:10.1016/j.yexcr.2015.03.028

[114] Balla A, Tuymetova G, Tsiomenko A, Várnai P, Balla T. A plasma membrane pool of phosphatidylinositol 4-phosphate is generated by phosphatidylinositol 4-kinase type-III alpha: studies with the PH domains of the oxysterol binding protein and FAPP1. Mol Biol Cell. 2005;16(3):1282-1295. doi:10.1091/mbc.e04-07-0578

[115] Nakatsu F, Baskin JM, Chung J, et al. PtdIns4P synthesis by PI4KIIIα at the plasma membrane and its impact on plasma membrane identity. J Cell Biol. 2012;199(6):1003-1016. doi:10.1083/jcb.201206095

[116] JA, Zhang Y, Oh MS, et al. Architecture of the human PI4KIIIα lipid kinase complex. Proc Natl Acad Sci U S A. 2017;114(52):13720-13725. doi:10.1073/pnas.1718471115

complex to the PM [116,117,118,119,120]. HYCC1 variants are associated with a hypomyelinating leukodystrophy, termed hypomyelination and congenital cataracts [121] , while variants in TTC7A cause combined immunodeficiency with multiple intestinal atresia and inflammatory bowel disease (IBD)[122]. First described in 2015 [106], PI4KA-related disorder is caused by biallelic PI4KA mutations and characterized by severe neurological (limb spasticity, developmental delay, intellectual disability, seizures, ataxia, nystagmus) and gastrointestinal (multiple intestinal atresia and IBD) manifestations. Although features consistent with immunodeficiency (lymphopenia, hypogammaglobulinemia, recurrent infections, IBD) have been reported [7,103, 109], the role of - PI4KAmut in B cells remains to be

[117] Wu X, Chi RJ, Baskin JM, et al. Structural insights into assembly and regulation of the plasma membrane phosphatidylinositol 4-kinase complex. Dev Cell. 2014;28(1):19-29. doi:10.1016/j.devcel.2013.11.012

[118] Dornan GL, Dalwadi U, Hamelin DJ, Hoffmann RM, Yip CK, Burke JE. Probing the Architecture, Dynamics, and Inhibition of the PI4KIIIα/TTC7/FAM126 Complex. J Mol Biol. 2018;430(18 Pt B):3129-3142. doi:10.1016/j.jmb.2018.07.020

[119] Bojjireddy N, Botyanszki J, Hammond G, et al. Pharmacological and genetic targeting of the PI4KA enzyme reveals its important role in maintaining plasma membrane phosphatidylinositol 4-phosphate and phosphatidylinositol 4,5-bisphosphate levels. J Biol Chem. 2014;289(9):6120-6132. doi:10.1074/jbc.M113.531426

[120] Lees JA, Zhang Y, Oh MS, et al. Architecture of the human PI4KIIIα lipid kinase complex. Proc Natl Acad Sci U S A. 2017;114(52):13720-13725. doi:10.1073/pnas.1718471115

[121] Traverso M, Yuregir OO, Mimouni-Bloch A, et al. Hypomyelination and congenital cataract: identification of novel mutations in two unrelated families. Eur J Paediatr Neurol. 2013;17(1):108-111. doi:10.1016/j.ejpn.2012.06.004

[122] Chen R, Giliani S, Lanzi G, et al. Whole-exome sequencing identifies tetratricopeptide repeat domain 7A (TTC7A) mutations for combined immunodeficiency with intestinal atresias. J Allergy Clin Immunol. 2013;132(3):656-664.e17. doi:10.1016/j.jaci.2013.06.013

[7] Verdura E, Rodríguez-Palmero A, Vélez-Santamaria V, Planas-Serra L, de la Calle I, Raspall-Chaure M, et al. Biallelic PI4KA variants cause a novel neurodevelopmental syndrome with hypomyelinating leukodystrophy. Brain. (2021) . 144:2659–69. doi: 10.1093/brain/awab124

[103]Salter CG, Cai Y, Lo B, et al. Biallelic PI4KA variants cause neurological, intestinal and immunological disease. Brain. 2021;144(12):3597-3610. doi:10.1093/brain/awab313

[109] Zhang K, Zhang Y, Wang J, et al. A synonymous mutation in PI4KA impacts transcription and splicing, leading to combined immunodeficiency. Front Genet. 2022;13:799. doi:10.3389/fgene.2022.799

elucidated. Here, we report clinical and immunological data on 13 PI4KA- deficient patients. Multi–omics (transcriptome, proteome, lipidome and metabolome) analyses and functional studies unraveled the altered mechanisms in PI4KA-related disorder's B cells. By altering lipid metabolism and tricarboxylic acid cycle (TCA) regulation, biallelic PI4KA mutations disrupt B-cell metabolism causing mitochondrial dysfunction, mTOR hyperactivation, increased autophagy and deranged cytoskeleton organization.

2.3 Methods

This study was approved by the institutional review boards/ethic committee of Comitato Etico Brianza (Monza, Italy; GENPAT-PID). Recruitment of patients and genetic investigations (either whole-exome sequencing or whole-genome sequencing) have been described [7,103]. Biallelic PI4KA-mutant EBV-transformed B cells (LCL) were generated from three patients (P1, P8, and P10; PI4KAmut LCL) and five healthy donors (HD). Full methods are detailed in the Supplementary Materials and Methods.

2.4 Results

Clinical, Immunological and Genetic Features in PI4KA-Related Disorder

Clinical and laboratory data of 13 patients were collected (Table 1, Fig. 1A and Supp. Table 1 in the Electronic Supplementary Material and Methods). All the patients presented with gastrointestinal (P11 and P13) or neurological (P1–P8 and P12) onset in the first 12 months of life, except for P9 and P10 (progressive spastic paraparesis with onset at 17 and 2 years, respectively). The neurological phenotype was heterogeneous, ranging from developmental encephalopathy with hypomyelinating leukodystrophy/delayed myelination and structural brain anomalies to progressive spastic paraplegia [7,103]. Eight individuals had recurrent or severe infections, mostly

[7] Verdura E, Rodríguez-Palmero A, Vélez-Santamaria V, Planas-Serra L, de la Calle I, Raspall-Chaure M, et al. Biallelic PI4KA variants cause a novel neurodevelopmental syndrome with hypomyelinating leukodystrophy. Brain. (2021) . 144:2659–69. doi: 10.1093/brain/awab124

[103]Salter CG, Cai Y, Lo B, et al. Biallelic PI4KA variants cause neurological, intestinal and immunological disease. Brain. 2021;144(12):3597-3610. doi:10.1093/brain/awab313

affecting upper and lower respiratory tract. One individual showed bronchiectasis but did not report any infections. Gastrointestinal (either gastroesophageal reflux disease [n=3], multiple intestinal atresia [n=1] or IBD [n=2]) and genitourinary symptoms (bilateral cryptorchidism) were reported in six and two patients, respectively. Hypothyroidism and juvenile idiopathic arthritis occurred in two and one patient, respectively. Abnormalities in lymphocyte subsets or immunoglobulin levels were found in the whole cohort. Ten patients had B-cell defects (either hypogammaglobulinemia, decreased absolute B-cell numbers or altered B-cell subsets; Table 1). B-cell subsets were investigated in eight patients, showing switched memory B cells (smB) in six, two and four patients, respectively. Six out of eight patients with B-cell lymphopenia had a marked decrease in at least two of the three major immunoglobulin isotypes and two had a decrease in all three isotypes. One individual (P11) with B-cell lymphopenia and decreased IgA and IgM had normal IgG levels, which were considered to be of maternal origin at the time of the investigation (18 days old). Unfortunately, this patient died at three weeks of age, precluding further monitoring of IgG levels. Only three patients had normal findings for absolute number of B cells and the three major immunoglobulin isotypes. Yet, one of them had decreased smB (P7) while B-cell subsets were not tested in the remaining two (P9 and P10). IgG subclasses were tested in five patients, of whom two (P2 and P8) showed IgG1, IgG2, IgG3, IgG4 deficiency, B-cell lymphopenia, hypogammaglobulinemia (both IgG and IgM) and decreased smB. B-cell response to T-independent mitogens was tested in two patients, both of whom showed reduced B-cell proliferation, specifically to IgM and CpG (P5) and pokeweed (P11). T-cell studies showed CD3+ lymphopenia in three out of 13 patients, one of whom had both CD4+ and CD8+ (P11).
One CD4+ (P8) and one CD8+ (P9) lymphopenia. P4 had normal CD3+ absolute count but showed decreased CD8+. CD4:CD8 ratios were normal in all the patients, except for P11 who showed nearly absent CD8+ cells. T-cell subsets showed increased naive cells in five out of eight tested patients. T-cell

Table 1 Clinical and Laboratory Characteristics of 13 Patients with PI4KA-related disorder

Patient No	Protein variants	Clinical manifestations*	Age at onset	Age	Immunoglobulin			B cells				T cells			NK cells	Treatment
					IgG	IgA	IgM	CD19+	Transitional†	Naive†	Switched Memory†	CD3+	CD3+CD4+	CD3+CD8+		
					Mg/dl					%	%					
P1[14]	P876Sf-sTer36/ E1152K	Infections, HT	Newborn	6	931	291	**26**	*995*	NA	NA	NA	*3825*	*2345*	*1213*	*1406*	-
P2[14]	G1925R/ G1925R	Infections, BC	Newborn	6	**503**	85	**<20**	**70**	**93**	71	1	1370	920	400	280	-
P3[14]	H1295R/ M2041T	Infections, GERD	6 months	13	**961‡**	**52**	**57**	**69**	**14**	84	9	1608	1190	413	**58**	IgRT
P4[14]	A1198T/ T2053Sf-sTer4	Infections	1 year	16	NA	146	91	144	NA	NA	NA	1458	1152	**252**	72	-
P5[14]	R618Ter/ D1664N	Infections, JIA	Newborn	8	**395‡**	**34**	**12**	**28**	**32**	88	6	1715	1105	572	259	IgRT, MTX, ASCT
P6[14]	p.?/N1987S	Asymptomatic	Newborn	9	704	77	99	**98**	7	**22**	**8**	1701	919	743	136	-
P7[14]	S472R/ R119W	GERD	4 months	11	821	119	185	591	8	61	**5**	1820	969	812	325	-
P8[14]	D1854N/ D1854N	Infections, BC, GERD	Newborn	5	**231**	97	**6**	**86**	**44**	43	**0**	**1104**	**697**	396	**25**	IgRT
P9[14]	E1820del/ T2053Sf-sTer4	IBD	17 years	40	1075	137	205	95	NA	NA	NA	**776**	558	**199**	**21**	6-MP
P10[14]	V1556M/ T1720I	Asymptomatic	2 years	18	1170	*438*	93	345	NA	NA	NA	1430	816	535	**29**	-
P11[15]	Y1623D/ Y1623D	MIA	Newborn	18d	997	**<2**	**<10**	**67**	NA	NA	NA	**237**	**208**	**5**	**76**	-
P12[15]	D1854N/ D1854N	Bronchiectasis, HyT, NHL, splenomegaly	Newborn	10	**530**	250	**<8**	**27**	**42**	**17**	3	1056	653	337	**31**	RTX
P13[15]	G1925E/ R2022Qf-sTer36	Infections, IBD	1.5 months	7	642	106	**<20**	**106**	**12**	83	8	2107	1188	906	138	IgRT, Adalimumab

The most recent, comprehensive, and representative laboratory data are shown for each patient; complete laboratory data are provided in Table 1 in the Supplemental Appendix. Numbers in italics indicate values above the normal range, and numbers in boldface indicate values below the normal range for age-matched controls in the laboratory in which the study was performed. 6-MP = mercaptopurine. ASCT = autologous stem-cell transplantation. BC = bilateral cryptorchidism. d = days. GERD = gastroesophageal reflux disease. HT = hypothyroidism. HyT = hyperthyroidism. IBD = inflammatory bowel diseases. IgRT = immunoglobulin replacement therapy. JIA = Juvenile idiopathic arthritis, MIA = multiple intestinal atresia. MTX = methotrexate. NA = not available. NHL = non-Hodgkin lymphoma. RTX = rituximab. * Detailed neurological phenotype in Supp. Table 1. † cells are expressed as the percentage among CD19+B cells. ‡ The patient was receiving IgG replacement therapy

naive and decreased to controls in the seven investigated patients. Six out of 13 individuals showed decreased absolute numbers of natural killer (NK) cells (Supp. Table 1). CBC with differential was abnormal in seven patients. Five patients had anemia. Iron-deficiency anemia was diagnosed in P12 and P13. Albeit patient P12 showed also increased fecal calprotectin (829 mcg/g, normal value <50 mcg/g), suggestive of IBD, it was impossible to investigate this further due to her clinical conditions. In the remaining three individuals (P2, P3 and P8), mild normocytic anemia was reported in P3 and P8 and red blood cell transfusions were administered in P2 (neonatal anemia) and P8 (two episodes of severe acute anemia). Regarding the myeloid compartment, monocytosis (P2, P3, P8 and P13), neutropenia (P1, P2 and P12) or mild thrombocytopenia were detected (P6; Supp. Table 1). Immunoglobulin replacement therapy was given in four patients (P3, P5, P8 and P13), in one case after autologous stem cell treatment for cerebral palsy (P5). Immunosuppressive treatment was given in three patients due to juvenile idiopathic arthritis (methotrexate, P5) or IBD (mercaptopurine, P9; adalimumab, P13). Malignancies occurred in one patient (P12), specifically non-Hodgkin lymphoma (follicular lymphoma grade 3A with BCL6 translocation). Considering the overall patient's condition, she was treated with Rituximab monotherapy. Three patients died (unexplained sudden death in P8 at 7 years of age, MIA in P11 at 3 weeks of age and lymphoma in P12 at 14 years of age). Biallelic mutations in *PI4KA* were confirmed in all patients with 20 unique mutations. Plotting *PI4KA* mutations according to protein location, we found that mutations were scattered throughout the gene, although they appeared to concentrate in the catalytic domain (Fig. 1). Counting each allele individually, proportion between missense and other mutations was similar in all the different phenotypes (Supp. Figure 1). As individual mutations cannot account for patients with compound heterozygous mutations, we clustered *PI4KA* mutations into two categories: type A, missense variants; type B, indels, nonsense and splice site variants. Each patient was assigned to one of three groups (AA, n=7; AB, n=5; BB, n=1). Gastrointestinal manifestations and decreased NK cells appeared to be more prominent in the AA group (Fig. 1C).

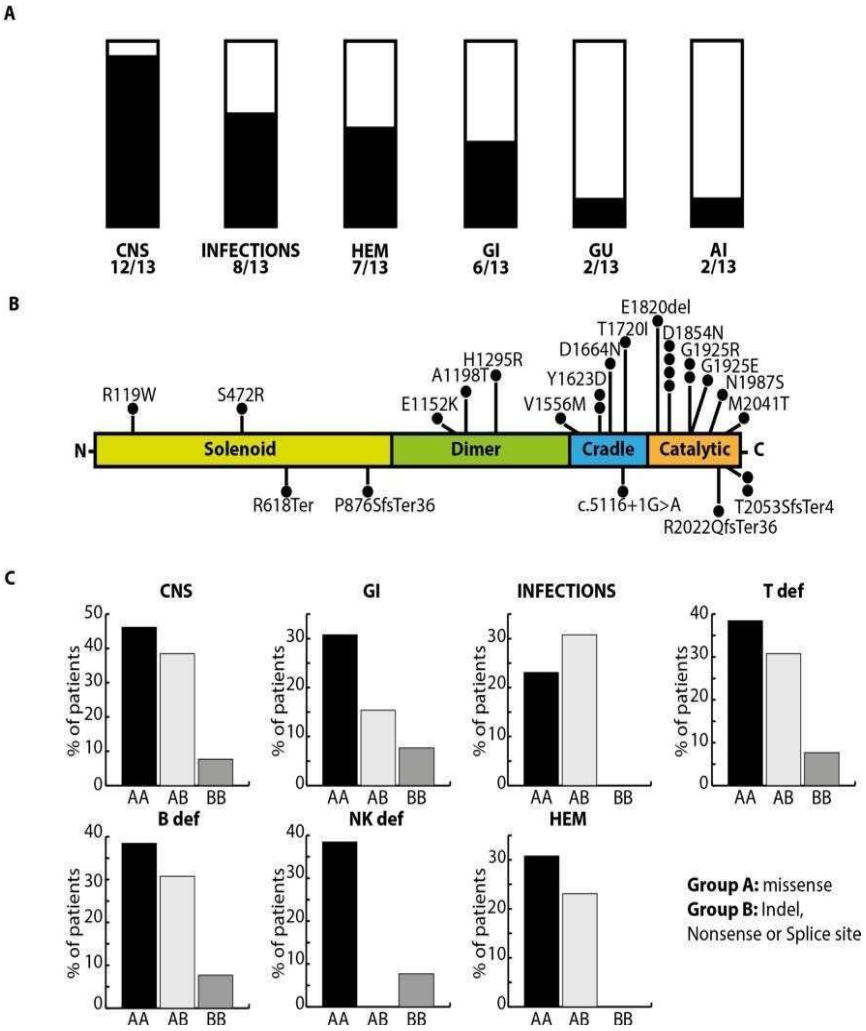

Fig. 1 Clinical phenotype and analysis of PI4KA variants by patient phenotype. **(A)** Main clinical symptoms and complete blood count abnormalities reported in the whole cohort. **(B)** Schematic representation of the PI4KA protein structure illustrating the distribution of the variants identified in this study. **(C)** Genotype-to-phenotype analysis using patient variant configurations. Distribution of patients with different phenotypes in genotype categories assigned on the basis of PI4KA variant type [AI = autoimmune/autoinflammatory manifestations; CNS = central nervous system manifestations; GI = gastrointestinal manifestations; GU = genito-urinary manifestations; HEM = hematological manifestations (anemia, monocytosis, neutropenia or thrombocytopenia); T def = decreased absolute number of T cells (CD3+, CD4+ or CD8+) or altered T-cell subsets; B def = hypogammaglobulinemia, decreased absolute B-cell numbers or altered B-cell subsets; NK def = decreased absolute number of NK cells].

2.4.2 Biallelic *PI4KA* Mutated B Cells Show a Distinct Transcriptional Profile

Whole-transcriptome analysis by next-generation sequencing was performed in three PI4KAmut LCL and four HD (HD1–HD4) and revealed 341 differentially expressed genes (DEGs; Fig. 2A). Principal Component Analysis (PCA) showed that the first (PC1) and second (PC2) principal components explained 43% and 29% of the variance, respectively (Supp. Figure 2). This suggests that the main source of variance in the RNA-Seq experiment is likely due to other factors that are not evident in the first two components of the dimensionality reduction analysis. Gene set enrichment analysis of transcripts.

Identified highly aberrant enrichment of genes involved in B-cell differentiation, suggesting an increase in naive gene sets (Fig. 2B,C). Moreover, enhanced transcription of gene sets involved in the mTOR pathway, autophagy and negative enrichment of fatty acids metabolism and oxidative phosphorylation pathways was noticed (Fig. 2D). Cell cycle arrest was indicated by the decreased transcription of genes related to cell proliferation (E2F targets, G2/M checkpoint). Dysregulated lipid metabolism (sphingolipids and ceramide), mitochondrial dysfunction (electron respiratory chain) and glucocorticoids (including glucocorticoid receptor pathway) emerged. Genes associated with protein secretion, hypoxia, ER stress and the unfolded protein response (UPR) were upregulated (Supp. Table 2). We confirmed that the UPR was activated by analyzing the rate of UPR-sensitive XBP1 splicing. RNA-sequencing data showed significantly higher rates of XBP1 splicing in pediatric PI4KAmut LCL (P1 and P8) compared to age-matched HD (HD1 and HD2; Fig. 2E). To further investigate the pathways affected, we employed CPDB, CTpathway and Reactome Pathway analysis (Supp. Figure 3) [124,125,126]. PI4KAmut LCL showed altered B-cell activation and motility, as well as B-cell receptor (BCR) signalling pathway. Additionally, pathways related to phospholipids metabolism (phospholipases, phospholipase C and D,

[124] Liu H, Yuan M, Mitra R, et al. CTpathway: a CrossTalk-based pathway enrichment analysis method for cancer research. *Genome Med*. 2022;14(1):118. Published 2022 Oct 13. doi:10.1186/s13073-022-01119-6

[125] Fabregat A, Jupe S, Matthews L, et al. The Reactome Pathway Knowledgebase. Nucleic Acids Res. 2018;46(D1):D649-D655. doi:10.1093/nar/gkx1132

[126] Fitzpatrick RB. CPDB: Carcinogenic Potency Database. Med Ref Serv Q. 2008;27(3):303-311. doi:10.1080/02763860802198895

phosphatidylinositol-mediated signalling) were significantly enriched (Supp. Table 2). These results indicated global effects of PI4KA on lymphopoiesis, specifically in B-cell development, differentiation, proliferation and metabolism.

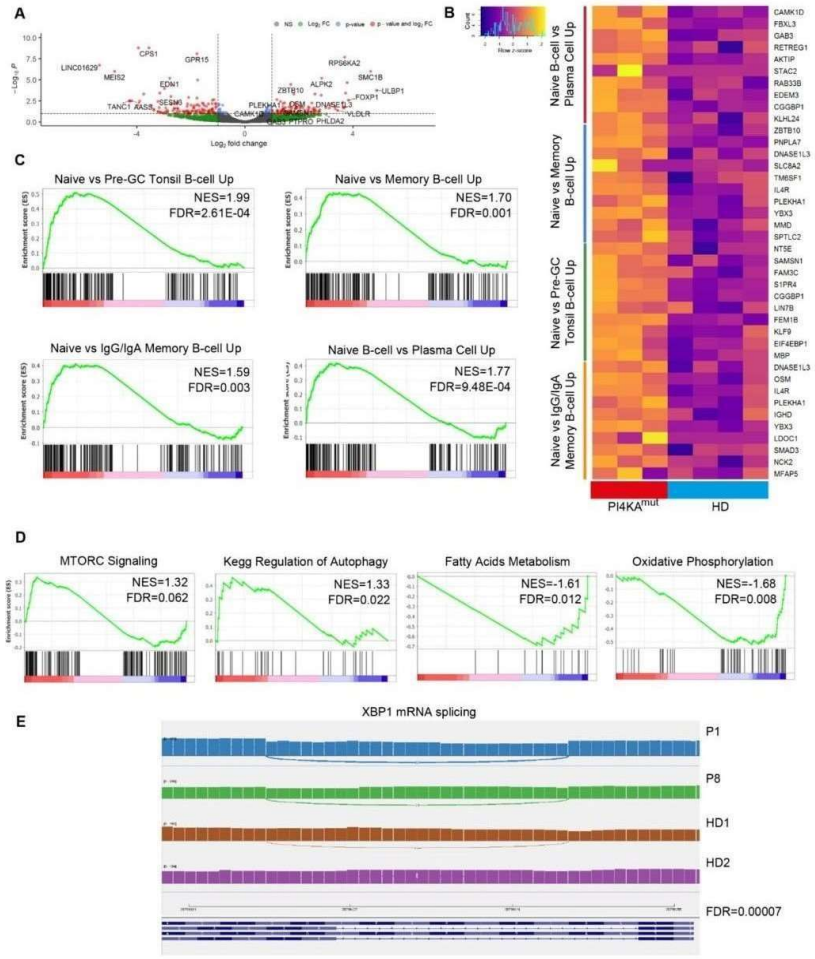

Fig. 2 Differentially expressed genes and pathway analysis in PI4KA-related disorder. (A) Volcano plot showing differentially expressed genes (DEG) in patients with biallelic PI4KA mutations considering a p-value ≤0.05 and a fold change threshold of ±1.5. **(B,C)** Heatmap and gene set enrichment analysis (GSEA) enrichment plots of selected differentially expressed B lineage-related genes involved in B-cell differentiation in PI4KA patients compared with those in healthy donors. Transcript names are shown along the right axis of the heatmap. Violet: increased expression; yellow: decreased expression. **(D)** GSEA enrichment plots of deregulated mTORC1, autophagy, fatty acids and oxidative phosphorylation gene sets. **(E)** Quantification of stress-dependent XBP1 splicing. Data from three patients (P1, P8 and P10) and four healthy donors (HD1–HD4) EBV-transformed B cells [FDRq = false discovery rate q value; NES = normalized enrichment score].

2.4.3 Proteomic Analysis Reveals Enrichment in B Cell Receptor Signalling Pathway

Proteomic analysis was performed in three PI4KAmut LCL and three HD (HD1–HD3). An untargeted and label-free proteomic approach was adopted and, among 7282 identified proteins, 5984 met more stringent quality criteria and were further considered for relative quantification. A volcano plot is shown in Fig. 3A, highlighting the 167 differentially expressed proteins (DEPs; p-value ≤0.05; fold change ≤−1.5 or ≥1.5; false discovery rate 0.05). The top 50 DEPs were used to create a heatmap cluster analysis (Fig. 3B). A defined clusterization consistent with PI4KA-related disorder supported the specificity of the signature. A protein network of DEPs showed potential interactions and functional relationships among the DEPs (Supp. Figure 4) [127]. The PI4KA complex appeared to be dysregulated, with downregulation of either PI4KA (fold change 0.69, p=0.018) or EFR3A (fold change 0.5, p=0.025) in PI4KAmut LCL. To uncover altered biological processes and pathways, we used the Enrichr platform (Fig. 3C–E) [128, 129]. The infectious disease and immune system pathways were significantly affected. Additionally, there was evidence of dysregulation in the adaptive immune response, BCR signalling and CD20-LCK- LYN-FYN-p75/80 pathways. Furthermore, enrichment of second messengers resulting from BCR activation or intracellular signalling was observed. Metabolic dysregulation was noted, particularly in the amino acid and serine metabolism pathways. Finally, lysosome and NF-κB pathways were enriched (Supp. Table 3).

[127] Szklarczyk D, Franceschini A, Wyder S, et al. STRING v10: protein-protein interaction networks, integrated over the tree of life. Nucleic Acids Res. 2015; Database issue: D447–52. https:// doi. org/ 10. 1093/ nar/ gku10 03.

[128] Raudvere U, Kolberg L, Kuzmin I, et al. A web server for functional enrichment analysis and conversions of gene lists (2019 update). Nucleic Acids Res. 2019;47:W191–8.

[129] Kuleshov MV, Jones MR, Rouillard AD, et al. Enrichr: a comprehensive gene set enrichment analysis web server 2016 update. Nucleic Acids Res. 2016;44(W1):W90–7. https:// doi. org/ 10. 1093/ nar/ gkw377.

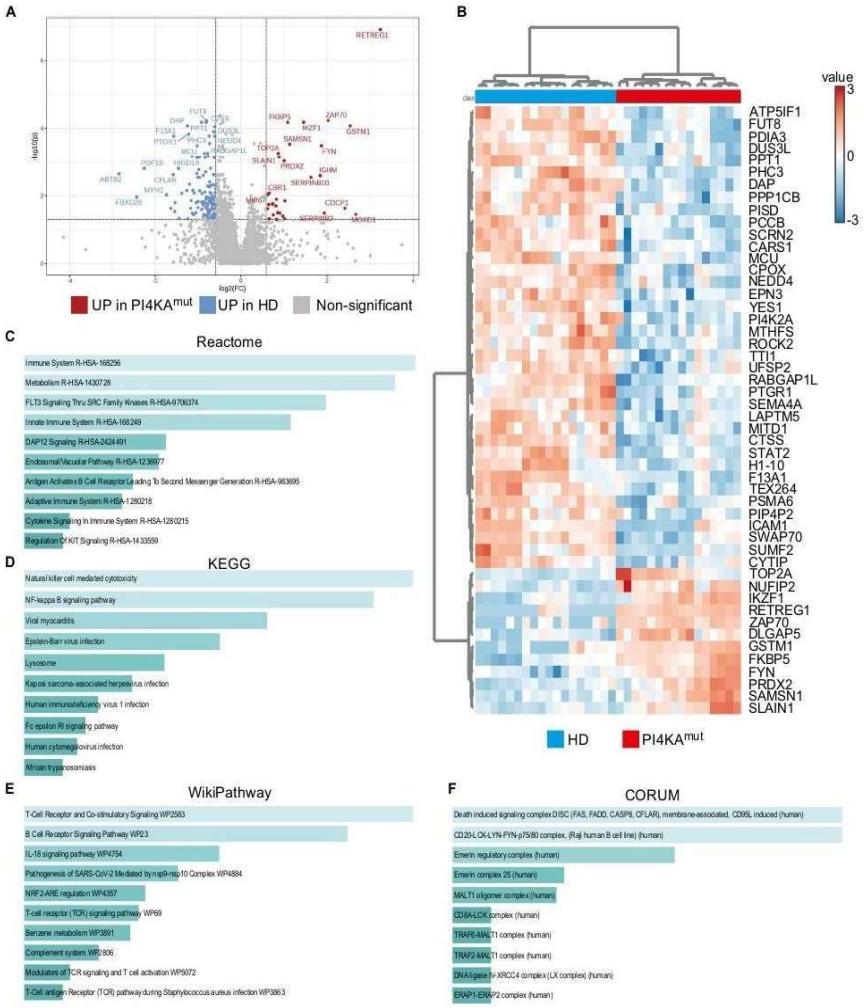

Fig. 3 Differentially expressed proteins and pathway analysis reveal derange B cell receptor activation and signalling. (A) Volcano plot showing differentially expressed proteins between healthy donors and PI4KA patients considering a p- value (p)≤0.05 and a fold change threshold of ± 1.5. Thirty two proteins, in red, are upregulated in PI4KA patients (Fold change≥1.5); while 135 proteins are downreg- ulated (Fold change ≤ -1.5). Proteins are reported as Uniprot_ID. **(B)** Heatmap-cluster analysis. The heatmap shows the different protein expression levels in correlation to each patient (reported as proteomic IDs). The colour scale from red to blue indicates the level of expres- sion of each protein, from a high expression to a low expression. **(C)** Bar chart of top enriched terms from the Reactome_2022 gene set library, KEGG **(D)** WikiPathway_2021_Human gene set library **(E)** and the CORUM gene set library **(F).** The top 10 enriched terms for the input gene set are displayed based on the -log10(p-value). Data from three patients (P1, P8 and P10) and three healthy donors (HD1- HD3) EBV-transformed B-cells. Each experiment was repeated three times (except for P1, two times).

2.4.4 Lipids and Metabolic Alterations in PI4KA-Related Disorder

Untargeted metabolomic and lipidomic workflows were separately applied in three PI4KAmut LCL and three HD (HD1–HD3). Lipidome and metabolome analyses identified 56 and 36 differentially represented lipids or metabolites, respectively (Fig. 4A,B). Among lipids, PI, diacylglycerol and glycerophospholipids appeared the most altered (Fig. 4C). Metabolites such as citric acid, fumaric acid and succinic acid, L-carnitine as well as L-glutamate and glutathione indicated mitochondrial dysfunction. Myo-inositol and cytidine monophosphate suggested impaired phospholipids metabolism (Fig. 4D). Pathway enrichment analysis confirmed impaired glycerophospholipid pathways (phosphatidylethanolamine biosynthesis), showed altered phosphatidylinositol phosphate metabolism and revealed mitochondrial dysfunction, as shown by mitochondrial beta-oxidation of short and long fatty acids, and glutathione metabolism (Supp. Figure 5).

Fig. 4 Biallelic *PI4KA* mutations alter lipid metabolism and result in mitochondrial disruption. A, Volcano plot showing lipids with fold change threshold (x) 1.5 and t-tests threshold (y) 0.05. The red circles represent features above the threshold. Both fold changes and p val- ues are log transformed. The further its position away from the (0,0), the more significant the feature is. **B,** Volcano plot showing metabo- lites with fold change threshold (x) 1.5 and t-tests threshold
(y) 0.05. The red circles represent features above the threshold. Both fold changes and p values are log transformed. The further its position away from the (0,0), the more significant the feature is. **C**, Selected altered lipids in PI4KA patients compared with healthy donors. All results show $p<0.05$ after Benjamini–Hochber test. **D,** Selected altered metabolites in patients compared with healthy donors. All results show $p<0.05$ after Benjamini–Hochberg procedure. **E,** Heat- map showing hierarchical clustering of differentially expressed lipids and metabolites. All results show $p < 0.05$ after Benjamini–Hoch- berg procedure. Data from three patients (P1, P8 and P10) and three healthy donors (HD1-HD3) EBV-transformed B-cells. Each experi- ment was repeated three times [CMP=cytidine monophosphate. DAG = diacylglycerol. HD = healthy donor. PC = phosphatidylcho- line. PE = phosphatidylethanolamine. PI = phosphatydilinositol. PS = phosphatydilcholine]

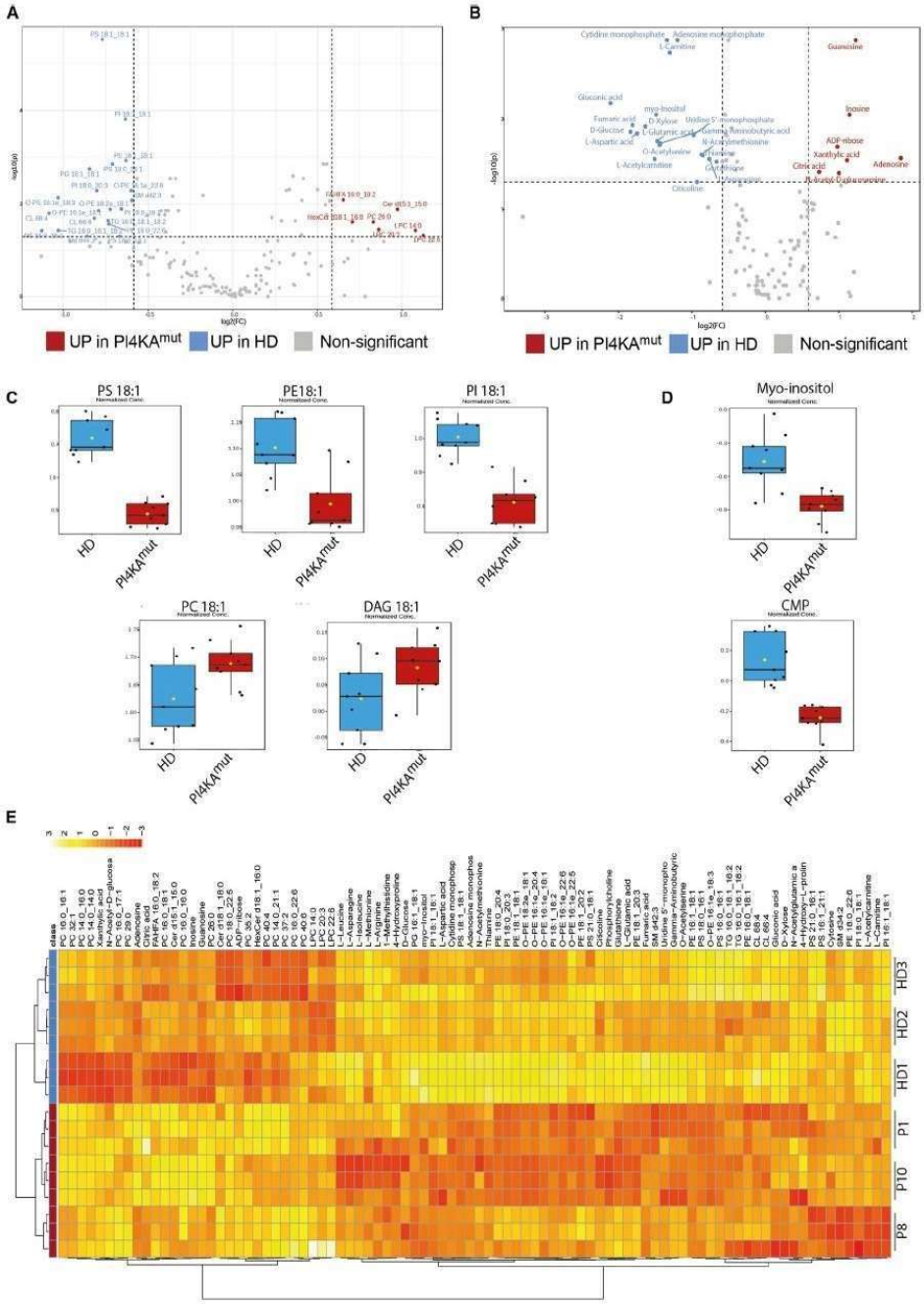

2.4.5 Integration of Proteomic, Lipidomic and Metabolomic

Data Indicates Failure of Mitochondrial Function in PI4KA-Related Disorder. Through integration of proteomic, lipidomic and metabolomic data within the biochemical pathways, we identified the metabolic routes dysregulated in patients with PI4KA mutations (Fig. 5A and Supplemental Methods, Text and

Supp. Figure 6–13). Proteins, lipids and metabolites that were significantly up- or downregulated were mapped in carbon, amino acid and cofactor metabolism (Fig. 5B). Inositol phosphate metabolism is the pathway most proximal to PI4KA. The substrate, phosphatidyl-1D-myo-inositol (PI) and its precursor myo-inositol were significantly downregulated in PI4KA-deficient individuals. Although the enzyme myo-inositol-1-phosphate synthase (ISYN1) was upregulated (Fig. 5Ba-ii), it did not compensate for the reduced levels of myo-inositol and PI. The PI4KA product, 1-phosphatidyl-1D-myo-inositol-4 (PIP), remained unaffected; though it can have a role, through a feedback mechanism, in replenishing PI (Fig. 5Ba-i). These disruptions may be related to altered PI4KA activity and glycerophospholipid metabolism. Indeed, key mitochondrial membrane phospholipids, including PI, cardiolipin, phosphatidyl-L-serine and phosphatidylethanolamine, were significantly downregulated, while 1-Acyl-sn-glycerol-3-phosphocholine was upregulated (Fig. 5Ba-iii). Significant alterations in the TCA cycle were found. Citrate levels were upregulated while fumarate levels were downregulated. The downregulation of L-aspartate, fumarylacetoacetate hydrolase (FAH) domain 1 (FAHD1) and glutathione S-transferase zeta 1 (GSTZ1) (Fig. 5Bc-e), which are involved in fumarate formation, contributed to this imbalance. Additionally, reduced levels of glutathione (GSH) impaired GSTZ1 ability to convert maleylacetoacetate to fumarate (Fig. 5Bb and Supplemental Text). Succinate, precursor of fumarate, was upregulated, yet its regulatory enzyme, succinate semialdehyde dehydrogenase (ALDH5A1), was downregulated (Fig. 5Be), further contributing to TCA cycle dysregulation. Glutathione metabolism also affected the TCA cycle through the downregulation of L-glutamate. Although glutathione transferase mu1 (GSTM1) was upregulated (Fig. 5Bb) and contributed to L-glutamate replenishment, it may not be sufficient to restore its levels. Finally, enzymes involved in cofactors biosynthesis, nicotinate phosphoribosyl transferase (NAPRT) and 3-hydroxyanthranilate 3,4-dioxygenase (HAAO) were downregulated (Fig. 5Bc), affecting NADP+ metabolism. Altogether, integration of –omics data highlights a dysregulation of mitochondrial phospholipids and the TCA cycle. The extensive molecular changes, affecting both lipids and metabolic pathways in an interconnected fashion, point towards defective mitochondrial energy production.

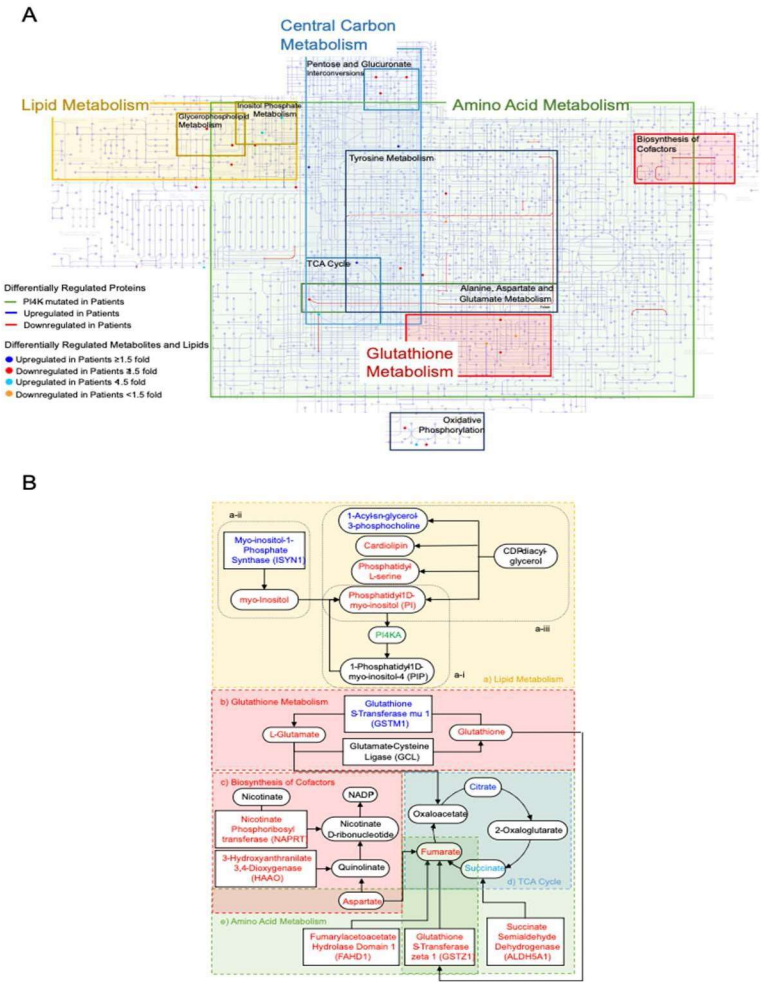

Fig. 5 Integration of proteomic, lipidomic and metabolomic data and biochemical mechanism underlying PI4KA-related disorder. (A) Proteins (lines), metabolites and lipids (dots) significantly upregulated (≥1.5-fold, blue; <1.5-fold, light blue) or downregulated (≥1.5-fold, red; <1.5-fold, orange) in patients with PI4KA mutation (green), relative to control counterparts, mapped on the Metabolic Pathways map of the Kyoto Encyclopedia of Genes and Genomes (KEGG) database. Metabolic pathways within the Metabolic Pathways map are highlighted as follows: lipid metabolism (inositol phosphate metabolism and glycerophospholipid metabolism) in yellow, carbon metabolism (TCA cycle and pentose and glucuronate interconversions) in blue, amino acid metabolism (tyrosine metabolism and alanine, aspartate and glutamate metabolism) in green, glutathione metabolism and biosynthesis of cofactors in red, oxidative phosphorylation in dark blue. **(B)** Biochemical reactions (arrows) integrating differentially regulated proteins (metabolic enzymes, rectangles), metabolites and lipids (ovals); pathways are compartmentalized using dashed boxes and color-coded as in (A). Significantly upregulated or downregulated proteins, lipids and metabolites are derived from bioinformatics analyses conducted on proteomic, lipidomic and metabolomic data, respectively. Connections identified among proteins, lipids and metabolites.

2.4.6. PI4KA-Deficient Patients Show Multiple Defects in B Cell Function

As integrated multi-omics data pointed towards mitochondrial dysfunction, we evaluated by confocal microscopy mitochondria number and membrane potential in three PI4KAmut LCL and three HD (HD1, HD2 and HD5). Although the total number of mitochondria was similar between the groups, PI4KAmut LCL and HD treated with GSK-A1, a PI4KA inhibitor, exhibited a significantly reduced mitochondrial membrane potential (Fig. 6A and Supp. Figure 14). To further explore the functional consequences of mitochondrial dysfunction, we analyzed key metabolic indicators. Treatment with GSK-A1 led to a reduction in all the measured metabolic parameters (basal oxygen consumption rate, ATP production, maximal respiration and spare respiratory capacity) except for extracellular acidification rate (Fig. 6B and Supp. Figure 15). However, in PI4KA mutated cells, a decrease was observed only in ATP production. When analyzing individual patients, P8, who carried the homozygous Asp1854Asn, displayed defects in all the measured parameters (Supp. Figure 15). Transcriptional profiles showed enrichment in PI3K/mTOR pathway with decreased PIK3R3 transcripts, encoding the PI3K regulatory subunit p55γ. Proteomic data also showed an increase of proteins (CD19, PIK3AP1, FYN and PRKCA) that could stimulate the mTOR pathway. We observed constitutive hyperactivation of PI3K upstream and downstream targets by phosphoflow cytometry (Fig. 6C). Specifically, pAKT473, p4EBP1 and pS6 were significantly hyperphosphorylated (median fold change 3.46 ± 0.41 vs 2.24 ± 0.08, p=0.003; 10.84 ± 0.84 vs 5.90 ± 0.57, p=0.003; 6.12 ± 0.78
vs 2.73 ± 0.33, p=0.001), pointing towards either mTORC1 or mTORC2 activation. Omics data indicated that both mTOR-dependent (enriched mTOR-related gene sets and hyperphosphorylation of pAKT/pS6/p4EBP1) and mTOR-independent (enriched AMPK and UPR pathways and decreased levels of phosphatidylethanolamine and phosphatidylserine) regulation of autophagy was deregulated. The upregulation of RAB8B and LAMP3 mRNA with downregulation of RAB24 and the consensual increase of TRIB3 indicated that both

autophagosome formation [130] and autophagosome and lysosome fusion stage [131] could have been affected.
This hypothesis was confirmed by increased LC3, an autophagosome marker, either in the presence or in the absence of chloroquine (an inhibitor of autophagosome degradation; Fig. 6D), implying that biallelic PI4KA mutations enhanced autophagosome formation and/or inhibited its degradation. Transcriptional profile and proteomics analyses highlighted altered BCR complex and signalling pathway. Several dysregulated proteins were noticed. Increased CD19, PIK3AP1 and FYN converge, via PI3K, on Bruton's tyrosine kinase (BTK), which in turn leads to activation of PLCγ. Although decreased levels of PLCγ1/2 were found, increased diacylglycerol was noticed. Reduced CORO1B, ICAM1 and ICAM3 pointed towards impaired cytoskeletal regulation. Analysis of actin structure by confocal microscopy of PI4KAmut LCL showed abnormal actin distribution either in PI4KA-deficient cells or HD treated with GSK-A1 (Fig. 6E and Supp. Figure 16). Although RNA-seq indicated enrichment in STAT5 targets and apoptosis gene sets (Supp. Table 2), both pSTAT5 and apoptosis were similar in patients and HD (Fig. 6F and G). Additionally, we investigated pSTAT5 and apoptosis to determine whether individual patients exhibited distinct behaviours, but no differences were detected (Supp. Figure 17). Finally, we evaluated differential drug sensitivity score [132,133]. We did not observe differences to PI3K/AKT/mTOR targeting drugs.

[130] Ao X, Zou L, Wu Y. Regulation of autophagy by the Rab GTPase network. Cell Death Differ. 2014;21(3):348–58. https:// doi. org/ 10. 1038/ cdd. 2013
[131] Xu J, Gu J, Pei W, et al. The role of lysosomal membrane proteins in autophagy and related diseases. FEBS J. 2023. 10. 1111/ febs. 16820.
[132] Oikonomou A, Valsecchi L, Quadri M, et al. High-throughput screening as a drug repurposing strategy for poor outcome subgroups of pediatric B-cell precursor acute lymphoblastic leukemia. Biochem Pharmacol. 2023;217:115809. https:// doi. org/ 10. 1016/j. bcp. 2023. 115809
[133] Fazio G, Bresolin S, Silvestri D, et al. PAX5 fusion genes are frequent in poor risk childhood acute lymphoblastic leukaemia and can be targeted with BIBF1120. EBioMedicine. 2022;83:104224. https:// doi. org/ 10. 1016/j. ebiom. 2022. 104224.

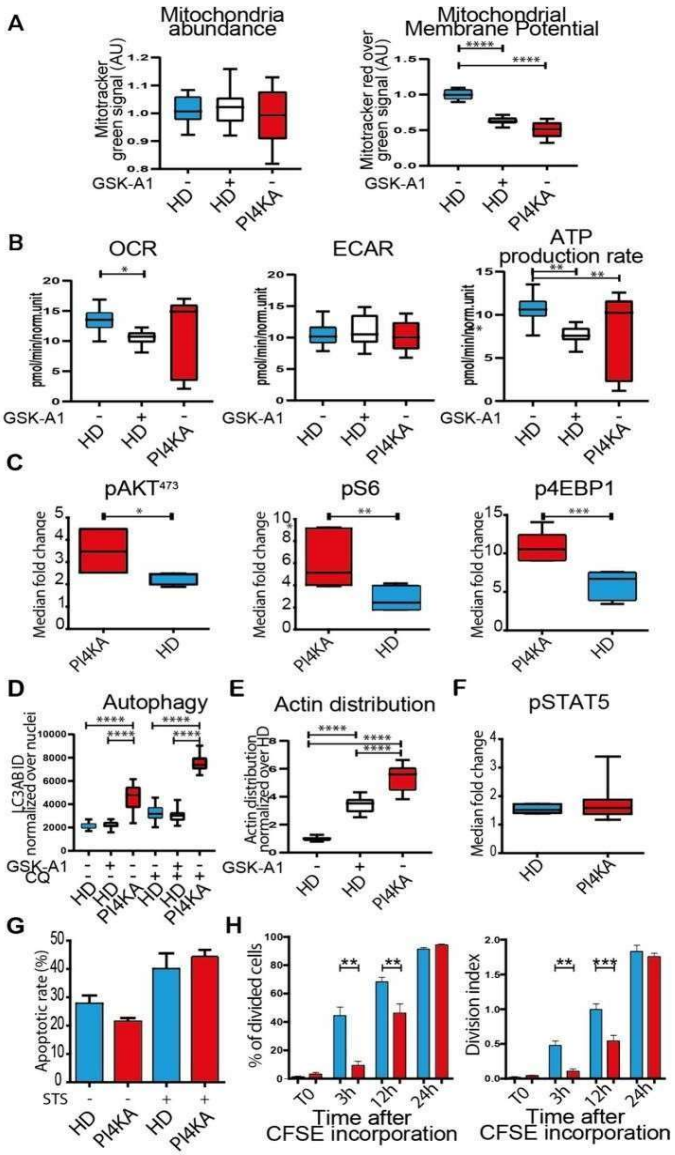

Fig. 6 PI4KA-mutated EBV-transformed B cells from patients exhibit multiple B cell defects. (A) Quantification of total mitochondrial abundance (left) and mitochondrial activity (right). **(B)** Quantification of mitochondrial function analyzing basal respiration, extracellular acidification rate and ATP production. **(C)** Evaluation of pAKT, pS6, p4EBP1 levels. **(D)** LC3 staining in the presence or absence of chloroquine. **(E)** Confocal microscopy studies of F-Actin cytoskeleton levels. **(F)** Evaluation of pSTAT5 levels. **(G)** Cell viability determined as difference from apoptosis and necrosis by Annexin V-PE and 7-AAD staining in the presence or absence of staurosporine. **(H)** Proliferation rates, defined as percentage of divided cells (left) and division index (right), quantified by carboxyfluorescein diacetate succinimidyl ester (CFSE) incorporation. In all graphs, *P < 0.05, **P < 0.01, ***P < 0.001 and ****P < 0.0001 [AU = arbitrary units; CFSE = carboxyfluorescein diacetate succinimidyl ester; ECAR = extracellular acidification rate; h = hours; HD = healthy donors; OCR = oxygen consumption rate; PI4KA = biallelic PI4KA-mutated EBV-transformed B cells].

Biallelic *PI4KA* mutations conferred resistance to drugs targeting cell cycle progression, specifically the G2/M phase (i.e., Paclitaxel, Prexasertib and Teniposide) [134,135,136,137], consistent with downregulation of E2F and G2/M at the transcriptomic level (Supp. Table 2) and defective B-cell proliferation at early time points (Fig. 6H). PI4KAmut LCL were highly resistant to dexamethasone and MEK inhibitors (Trametinib, Mirdametinib and PD184352). Although it did not reach statistical significance (p=0.052), PI4KAmut LCL appeared to be resistant to Ibrutinib, a known BTK inhibitor. PI4KAmut LCL were found to be significantly sensitive to inhibitors of Bromodomain and extra-terminal domain (BET) proteins such as JQ1 (p=0.044; Supp. Table 4).

2.5 Discussion

PI4KA-related disorder is a syndromic IEI presenting with neurological, gastrointestinal, genitourinary and autoimmune/autoinflammatory manifestations. The onset is frequently in the first 12 months of life and the phenotype is wide and variable. By altering lipid metabolism and the TCA cycle, impairing mitochondrial activity, hyperactivating the mTOR pathway and increasing ER stress, UPR and autophagy, PI4KA-related disorder causes B-cell deficiency with decreased smB and hypogammaglobulinemia (Fig. 7). PI4KA mutations are scattered throughout the PI4KA gene and affect all the known PI4KA protein domains. Identifying genotype–phenotype correlations in ultra-rare disease is often not possible. Inference

[134] Li G, Xu D, Sun J, et al. Paclitaxel inhibits proliferation and invasion and promotes apoptosis of breast cancer cells by blocking activation of the PI3K/AKT signaling pathway. Adv Clin Exp Med. 2020;29(11):1337–45. https:// doi. org/ 10. 17219/ acem/ 127681

[135] Nakayama S, Torikoshi Y, Takahashi T, et al. Prediction of paclitaxel sensitivity by CDK1 and CDK2 activity in human breast cancer cells. Breast Cancer Res. 2009;11(1):R12. https:// doi. org/ 10. 1186/ bcr22 31

[136] Ghelli Luserna Di Rorà A, Iacobucci I, Imbrogno E, et al. Prexasertib, a Chk1/Chk2 inhibitor, increases the effectiveness of conventional therapy in B-/T- cell progenitor acute lymphoblastic leukemia. Oncotarget. 2016; 7(33):53377–53391. https:// doi. org/ 10. 18632/ oncot arget. 10535

[137] Hande KR, Topoisomerase II. Inhibitors. Update Cancer Therapeutics. 2008;3:13–26. https:// doi. org/ 10. 1016/j. uct. 2008. 02. 001.

from genotype was complicated by a high prevalence of compound heterozygosity in PI4KA-related disorder. Clinicians should suspect PI4KA-related disorder in non-consanguineous families and in areas with low rates of consanguinity, as in our cohort. Counting each allele individually, half of the mutations occur in the catalytic domain and the only two patients with the previously described homozygous mutations (Asp1854Asn) in the catalytic domain had a severe phenotype (B-cell deficiency with hypogammaglobulinemia, infections, autoimmunity, polyclonal lymphoproliferation or lymphoma) and died. The catalytic domain may therefore represent a hotspot and be associated with severe phenotype, particularly the Asp1854Asn which nearly completely abrogates the PI4KA catalytic activity [106] . Yet, our ability to predict genotype–phenotype correlation remains limited and only speculative with the limited available data.

Immunological features of PI4KA-related disorder are broadly heterogeneous, ranging from asymptomatic patients to subjects with a severe phenotype, including recurrent/severe infections, combined immunodeficiency and lymphoproliferation (either polyclonal or malignant). The alterations observed in the erythroid and myeloid compartment, such as anemia, monocytosis or neutropenia, have been described by in vitro inactivation of Pi4ka and suggest involvement of PI4KA in hematopoiesis [138]. Currently, treatment options are limited to IgRT and immunosuppressive treatments in case of autoimmunity/autoinflammation.

Our work showed hyperactivation of the mTOR pathways and the use of mTOR/PI3K inhibitors is worth investigating. One alternative approach, in case of severe phenotype, could be hematopoietic stem cell transplantation. Although this procedure could correct the immunological defect, restoring immunocompetence may not be sufficient to revert the neurological or the gastrointestinal phenotype, as shown in

[106] Pagnamenta AT, Howard MF, Wisniewski E, et al. Germline recessive mutations in PI4KA are associated with perisylvian polymicrogyria, cerebellar hypoplasia and arthrogryposis. Hum Mol Genet. 2015;24(13):3732-3741. doi:10.1093/hmg/ddv117

[138] Ziyad S, Riordan JD, Cavanaugh AM, et al. A forward genetic screen targeting the endothelium reveals a regulatory role for the lipid kinase Pi4ka in myelo- and erythropoiesis. Cell Rep. 2018;22(5):1211–24. https:// doi. org/ 10. 1016/j. celrep. 2018. 01. 017.

TTC7A deficiency [139]. Considering the very early onset of the neurological symptoms, gene therapy could potentially provide benefits if performed before symptom onset [140]. PI4KA can be found in different organelles [141, 142]In the context of B cells, along with decreased levels of PI4KA, reduced levels of EFR3A may cause defective anchoring of PI4KA to the PM with impaired PI4KA enzymatic activity [7, 103].Impaired mitochondrial functionality in IEI with B-cell lymphopenia and hypogammaglobulinemia has recently emerged [143, 144] .PI4KA plays a critical role in regulating lipid homeostasis (as seen in

[139] Kammermeier J, Lucchini G, Pai SY, Worth A, Rampling D, Amrolia P, Silva J, Chiesa R, Rao K, Noble-Jamieson G, Gasparetto M, Ellershaw D, Uhlig H, Sebire N, Elawad M, Notarangelo L, Shah N, Veys P. Stem cell transplantation for tetratricopeptide repeat domain 7A deficiency: long-term follow-up. Blood. 2016;128(9):1306–8. https:// doi. org/ 10. 1182/blood- 2016- 01- 696385.

[140] Fumagalli F, Calbi V, Natali Sora MG, Sessa M, Baldoli C, Rancoita PMV, Ciotti F, Sarzana M, Fraschini M, Zambon AA, Acquati S, Redaelli D, Attanasio V, Miglietta S, De Mattia F, Barzaghi F, Ferrua F, Migliavacca M, Tucci F, Gallo V, Del Carro U, Canale S, Spiga I, Lorioli L, Recupero S, Fratini ES, Morena F, Silvani P, Calvi MR, Facchini M, Locatelli S, Corti A, Zancan S, Antonioli G, Farinelli G, Gabaldo M, Garcia-Segovia J, Schwab LC, Downey GF, Filippi M, Cicalese MP, Martino S, Di Serio C, Ciceri F, Bernardo ME, Naldini L, Biffi A, Aiuti A. Lentiviral haematopoietic stem-cell gene therapy for early-onset metachromatic leukodystrophy: long-term results from a non- randomised, open-label, phase 1/2 trial and expanded access. Lancet. 2022;399(10322):372–83. https:// doi. org/ 10. 1016/ S0140- 6736(21) 02017-1.

[141] Bura A, Čabrijan S, Đurić I, et al. A plethora of functions condensed into tiny phospholipids: the story of PI4P and PI(4,5)P2. Cells. 2023;12:1411. https:// doi. org/ 10. 3390/ cells 12101 411.

[142] Chung J, Nakatsu F, Baskin JM, De Camilli P. Plasticity of PI4KIIIα interactions at the plasma membrane. EMBO Rep. 2015;16(3):312–20. https:// doi. org/ 10. 15252/ embr. 20143 9151.

[7] Verdura E, Rodríguez-Palmero A, Vélez-Santamaria V, Planas-Serra L, de la Calle I, Raspall-Chaure M, et al. Biallelic PI4KA variants cause a novel neurodevelopmental syndrome with hypomyelinating leukodystrophy. Brain. (2021) . 144:2659–69. doi: 10.1093/brain/awab124

[103]Salter CG, Cai Y, Lo B, et al. Biallelic PI4KA variants cause neurological, intestinal and immunological disease. Brain. 2021;144(12):3597-3610. doi:10.1093/brain/awab313

[143] Saettini F, Poli C, Vengoechea J, et al. Absent B cells, agammaglobulinemia, and hypertrophic cardiomyopathy in folliculin-interacting protein 1 deficiency. Blood. 2021;137(4):493–9. https:// doi. org/ 10. 1182/ blood. 20200 06441.

[144] Saettini F, Guerra F, Fazio G, et al. Antibody deficiency in patients with biallelic KARS1 mutations. J Clin Immunol. 2023. https:// doi. org/ 10. 1007/ s10875- 023- 01584-7.

Schwann cells with Pi4ka deletion) [145,146] and may ultimately impact mitochondrial structural integrity. In PI4KA-related disorder, phospholipid dysregulation may also alter the composition of the mitochondrial membranes, either the outer (phosphatidylcholine, phosphatidylethanolamine, and to a lesser degree PI and phosphatidylserine) [147, 148] or the inner mitochondrial membranes (cardiolipin). Cardiolipin, which constitutes 15% of the inner mitochondrial membrane and is essential for various mitochondrial functions, including protein translocation and oxidative phosphorylation [149], was significantly downregulated. Phosphatidylethanolamine may significantly alter the activity of respiratory chain complexes, in particular cytochrome c oxidase [147], which was downregulated. The integration of multiple –omics suggests dysfunction of metabolic pathways beyond lipids, i.e., TCA cycle, glutathione and amino acid metabolism. Dysregulation of TCA substrates, directly and indirectly, may lead to impaired oxidative phosphorylation, thereby impacting mitochondrial energy production.Biallelic PI4KA mutations skewed the transcriptional profile towards less differentiated B cells. Naïve B cells activate fatty acid oxidation, which is impaired in PI4KA-related disorder, to meet additional energy demand over glycolysis [150,]

[145] Sohn M, Korzeniowski M, Zewe JP, Wills RC, Hammond GRV, Humpolickova J, Vrzal L, Chalupska D, Veverka V, Fairn GD, Boura E, Balla T. PI(4,5)P2 controls plasma membrane PI4P and PS levels via ORP5/8 recruitment to ER-PM contact sites. J Cell Biol. 2018;217(5):1797–813. https:// doi. org/ 10. 1083/ jcb. 20171 0095.

[146] Alvarez-Prats A, Bjelobaba I, Aldworth Z, et al. Schwann-cell- specific deletion of phosphatidylinositol 4-kinase alpha causes aberrant myelination. Cell Rep. 2018;23(10):2881–90. https:// doi.org/ 10. 1016/j. celrep. 2018.05. 019.

[147] Mårtensson CU, Doan KN, Becker T. Effects of lipids on mitochondrial functions. Biochim Biophys Acta Mol Cell Biol Lipids.2017;1862(1):102–13. https:// doi. org/ 10. 1016/j. bbalip. 2016. 06. 015.

[148]van der Veen JN, Kennelly JP, Wan S, et al. The critical role of phosphatidylcholine and phosphatidylethanolamine metabolism in health and disease. Biochim Biophys Acta Biomembr. 2017;1859(9 Pt B):1558–72. https:// doi. org/ 10. 1016/j. bbamem. 2017. 04. 006.

[149] Schenkel LC, Bakovic M. Formation and regulation of mitochondrial membranes. Int J Cell Biol. 2014; 709828. https:// doi. org/ 10.1155/ 2014/ 709828.

[150] Iperi C, Bordron A, Dueymes M, Pers JO, Jamin C. Metabolic program of regulatory B lymphocytes and influence in the control of malignant and autoimmune situations. Front Immunol. 2021;12:735463. https://doi.org/10.3389/fimmu.2021.735463

[151]. B cells also show altered BCR complex, co-stimulatory proteins and signalling, including second messengers, which can be regulated by PIs [152,153]. These modifications could ultimately affect cell proliferation, B-cell development and antigen recognition. PI4P and its metabolite PI(4,5)P2 specifically recruit protein effectors to the PM, are modulated by BTK and control cytoskeletal dynamics [120,154,155,156]. The actin cytoskeleton in turn modulates B-cell signalling and activation [157]. TTC7A deficiency and inhibition of Pi4ka cause migration defects and actin rearrangements [158,159]. Consistently, actin organization was severely altered in PI4KAmut LCL. Additionally, we have also shown decreased levels of CORO1B, which regulates branched actin turnover, directional cell motility, and overall

[151] Weisel FJ, Mullett SJ, Elsner RA, et al. Germinal center B cells selectively oxidize fatty acids for energy while conducting minimal glycolysis. Nat Immunol. 2020;21(3):331–42. https://doi.org/10.1038/s41590-020-0598-4

[152] Xu C, Wan Z, Shaheen S, et al. A PI(4,5)P2-derived "gasoline engine model" for the sustained B cell receptor activation. Immunol Rev. 2019;291(1):75–90. https://doi.org/10.1111/imr.12775

[153] Kapoor I, Li Y, Sharma A, et al. Resistance to BTK inhibition by ibrutinib can be overcome by preventing FOXO3a nuclear export and PI3K/AKT activation in B-cell lymphoid malignancies. Cell Death Dis. 2019;10(12):924. https://doi.org/10.1038/s41419-019-2158-0

[120] Lees JA, Zhang Y, Oh MS, et al. Architecture of the human PI4KIIIα lipid kinase complex. Proc Natl Acad Sci U S A. 2017;114(52):13720-13725. doi:10.1073/pnas.1718471115

[154] Saarikangas J, Zhao H, Lappalainen P. Regulation of the actin cytoskeleton-plasma membrane interplay by phosphoinositides. Physiol Rev. 2010;90(1):259–89. https://doi.org/10.1152/physrev.00036.2009

[155] Tan J, Brill JA. Cinderella story: PI4P goes from precursor to key signaling molecule. Crit Rev Biochem Mol Biol. 2014;49(1):33–58. https://doi.org/10.3109/10409238.2013.853024

[156] Sharma S, Orlowski G, Song W. Btk regulates B cell receptor-mediated antigen processing and presentation by controlling actin cytoskeleton dynamics in B cells. J Immunol. 2009;182(1):329–39. https://doi.org/10.4049/jimmunol.182.1.329

[157] Tolar P. Cytoskeletal control of B cell responses to antigens. Nat Rev Immunol. 2017;17(10):621–34. https:// doi. org/ 10. 1038/ nri. 2017. 67.

[158] Alvarez-Prats A, Bjelobaba I, Aldworth Z, et al. Schwann-cell-specific deletion of phosphatidylinositol 4-kinase alpha causes aberrant myelination. Cell Rep. 2018;23(10):2881–90. https:// doi.org/ 10. 1016/j. celrep. 2018. 05. 019.

[159] Gajardo T, Bernard M, Lô M, et al. Actin dynamics regulation by TTC7A/PI4KIIIα limits DNA damage and cell death under confinement. J Allergy Clin Immunol. 2023;152(4):949–60. https:// doi. org/ 10. 1016/j. jaci. 2023. 06. 016.

cell contractility [159, 160]. The effect of PI4KA on the mTOR pathway is controversial [138, 146,161] . Our data implicate a relevant role for PI4KA in modulating the mTOR pathway, similarly to APDS and other IEI presenting with B-cell defects [140,161], indicating either mTORC1 or mTORC2 activation. mTOR hyperactivation could be secondary to the dysregulated BCR signalling (upregulation of CD19 and PIK3AP1) or subsequent to the overrepresented PRKCA. Autophagy is a highly regulated process that can be modulated by mTOR-dependent and independent pathways [162]. In PI4KA-related disorder, multiple steps in the autophagic process appear to be dysregulated, leading to alterations of lipid synthesis, protein secretion, UPR and ultimately ER stress. This is supported by decreased levelsof BANF1 [163, 164] and SPCS3[165] proteins and upregulation of CEBPG

[160] King ZT, Butler MT, Hockenberry MA, et al. Coro1B and Coro1C regulate lamellipodia dynamics and cell motility by tuning branched actin turnover. J Cell Biol. 2021;221(8):e202111126. https:// doi. org/ 10. 1083/ jcb. 20211 1126.

[138] Ziyad S, Riordan JD, Cavanaugh AM, et al. A forward genetic screen targeting the endothelium reveals a regulatory role for the lipid kinase Pi4ka in myelo- and erythropoiesis. Cell Rep. 2018;22(5):1211–24. https:// doi. org/ 10. 1016/j. celrep. 2018. 01. 017.

[161] Kunii Y, Matsumoto J, Izumi R, et al. Evidence for altered phosphoinositide signaling-associated molecules in the postmortem prefrontal cortex of patients with schizophrenia. Int J Mol Sci. 2021;22:8280. https:// doi. org/ 10. 3390/ ijms2 21582 80.

[161] Saettini F, Guerra F, Fazio G, et al. Antibody deficiency in patients with biallelic KARS1 mutations. J Clin Immunol. 2023. https:// doi. org/ 10. 1007/ s10875- 023- 01584-7.

[162] He C, Klionsky DJ. Regulation mechanisms and signaling pathways of autophagy. Annu Rev Genet. 2009;43:67–93. https:// doi. org/ 10. 1146/ annur ev- genet- 102808- 114910.

[163] Sears RM, Roux KJ. Diverse cellular functions of barrier-to-autointegration factor and its roles in disease. J Cell Sci. 2020;133(16):jcs246546. https://doi.org/10.1242/jcs.246546

[164] Kobayashi S, Koujin T, Kojidani T, et al. BAF is a cytosolic DNA sensor that leads to exogenous DNA avoiding autophagy. Proc Natl Acad Sci U S A. 2015;112(22):7027–32. https://doi.org/10.1073/pnas.1501235112

[165]Liaci AM, Steigenberger B, Telles de Souza PC, et al. Structure of the human signal peptidase complex reveals the determinants for signal peptide cleavage. Mol Cell. 2021;81(19):3934-3948.e11 https://doi.org/10.1016/j.molcel.2021.07.031](https://doi.org/10.1016/j.molcel.2021.07.031).

[166], SERP1 [167] and XBP1 splicing [168] mRNA, indicative of autophagy activation and ER stress [169,170]. UPR and ER stress have been similarly elicited in a PIK3CD gain-of-function mutation mouse model [171], although resulting in decreased autophagy. mTOR hyperactivation physiologically inhibits autophagy and leads to increased protein synthesis. Nonetheless, in case of accumulation of misfolded proteins, increased autophagy attempts to alleviate the ER stress. mTOR-independent regulation of autophagy may occur also by means of PI4P, PI(4,5)P2 and PIP kinases at various stages [172]. The depletion of free inositol and myo-inositol-1,4,5 phosphate (IP3) stimulates autophagy [163, 173]. The upregulation of RAB8B,

[166] Huggins CJ, Mayekar MK, Martin N, et al. C/EBPγ is a critical regulator of cellular stress response networks through heterodimerization with ATF4. Mol Cell Biol. 2015;36(5):693–713. https://doi.org/10.1128/MCB.00911-15

[167] Hori O, Miyazaki M, Tamatani T, et al. Deletion of SERP1/RAMP4, a component of the endoplasmic reticulum (ER) translocation sites, leads to ER stress. Mol Cell Biol. 2006;26(11):4257–67. https://doi.org/10.1128/MCB.02055-05

[168] Yoshida H, Matsui T, Yamamoto A, Okada T, Mori K. XBP1 mRNA is induced by ATF6 and spliced by IRE1 in response to ER stress to produce a highly active transcription factor. Cell. 2001;107(7):881–91. https://doi.org/10.1016/s0092-8674(01)00611-0

[169] Chipurupalli S, Samavedam U, Robinson N. Crosstalk between ER stress, autophagy and inflammation. Front Med (Lausanne). 2021;8:758311. https://doi.org/10.3389/fmed.2021.758311

[170] Yorimitsu T, Nair U, Yang Z, Klionsky DJ. Endoplasmic reticulum stress triggers autophagy. J Biol Chem. 2006;281(40):30299–304. https://doi.org/10.1074/jbc.M607007200

[171] Al Qureshah F, Sagadiev S, Thouvenel CD, et al. Activated PI3Kδ signals compromise plasma cell survival via limiting autophagy and increasing ER stress. J Exp Med. 2021;218(12):e20211035. https://doi.org/10.1084/jem.20211035

[172] Baba T, Balla T. Emerging roles of phosphatidylinositol 4-phosphate and phosphatidylinositol 4,5-bisphosphate as regulators of multiple steps in autophagy. J Biochem. 2020;168(4):329–36. https://doi.org/10.1093/jb/mvaa089

[163]Sears RM, Roux KJ. Diverse cellular functions of barrier-to-autointegration factor and its roles in disease. J Cell Sci. 2020;133(16):jcs246546. https://doi.org/10.1242/jcs.246546

[173] Sarkar S, Rubinsztein DC. Inositol and IP3 levels regulate autophagy: biology and therapeutic speculations. Autophagy. 2006;2(2):132–4. https://doi.org/10.4161/auto.2387

[130]Ao X, Zou L, Wu Y. Regulation of autophagy by the Rab GTPase network. Cell Death Differ. 2014;21(3):348–58. https:// doi. org/ 10. 1038/ cdd. 2013

[131]Xu J, Gu J, Pei W, et al. The role of lysosomal membrane proteins in autophagy and related diseases. FEBS J. 2023. 10. 1111/ febs. 16820.

LAMP3 and TRIB3 mRNA [130,131,174,175], along with the downregulation of RAB24 [176] and increased LC3, suggest impaired autophagosome–lysosome fusion and degradation processes with accumulation of misfolded proteins and cellular stress [171]. PI4KA plays a pervasive role in cellular processes and signalling. PI4KA mRNA is overexpressed in hepatocellular carcinoma and results in increased proliferation [177]. Biallelic PI4KA mutations lead to decreased proliferation and resistance to drugs targeting the G2/M phase [134,135,136.]. PI4KAmut LCL were highly resistant to dexamethasone, which accumulates in mitochondria and promotes metabolic reprogramming. Steroid resistance can be sustained by activation of PI3K/AKT/mTOR signalling pathway [178]. PI4KAmut LCL were found to be sensitive to BET inhibitor JQ1, an immunomodulatory compound that

[174] Tanaka T, Warner BM, Michael DG, Nakamura H, Odani T, Yin H, Atsumi T, Noguchi M, Chiorini JA. LAMP3 inhibits autophagy and contributes to cell death by lysosomal membrane permeabilization. Autophagy. 2022;18(7):1629–47. https://doi.org/10.1080/15548627.2021.1995150

[175] Bednarczyk M, Zmarzły N, Grabarek B, et al. Genes involved in the regulation of different types of autophagy and their participation in cancer pathogenesis. Oncotarget. 2018;9(76):34413–28. https://doi.org/10.18632/oncotarget.26126

[176] Ylä-Anttila P, Eskelinen EL. Roles for RAB24 in autophagy and disease. Small GTPases. 2018;9(1–2):57–65. https://doi.org/10.1080/21541248.2017.1317699

[171] Al Qureshah F, Sagadiev S, Thouvenel CD, et al. Activated PI3Kδ signals compromise plasma cell survival via limiting autophagy and increasing ER stress. J Exp Med. 2021;218(12):e20211035. https://doi.org/10.1084/jem.20211035

[177] Igboudo A, Nault JC, Dubois-Pot-Schneider H, et al. Overexpression of phosphatidylinositol 4-kinase type IIIα is associated with undifferentiated status and poor prognosis of human hepatocellular carcinoma. BMC Cancer. 2014;14:7. https://doi.org/10.1186/1471-2407-14-7

[134] Li G, Xu D, Sun J, et al. Paclitaxel inhibits proliferation and invasion and promotes apoptosis of breast cancer cells by blocking activation of the PI3K/AKT signaling pathway. Adv Clin Exp Med. 2020;29(11):1337–45. https:// doi. org/ 10. 17219/ acem/127681

[135]Nakayama S, Torikoshi Y, Takahashi T, et al. Prediction of paclitaxel sensitivity by CDK1 and CDK2 activity in human breast cancer cells. Breast Cancer Res. 2009;11(1):R12. https://doi. org/ 10. 1186/ bcr22 31

[136]Ghelli Luserna Di Rorà A, Iacobucci I, Imbrogno E, et al. Prexasertib, a Chk1/Chk2 inhibitor, increases the effectiveness of conventional therapy in B-/T- cell progenitor acute lymphoblastic leukemia. Oncotarget. 2016; 7(33):53377–53391. https://doi. org/ 10. 18632/ oncot arget. 10535

[178] Olivas-Aguirre M, Pérez-Chávez J, Torres-López L, et al. Dexamethasone-induced fatty acid oxidation and autophagy/mitophagy are essential for T-ALL glucocorticoid resistance. Cancers (Basel). 2023;15(2):445. https://doi.org/10.3390/cancers15020445

increases apoptosis and reduces lymphoproliferation and antibody production [179]. In the setting of PI4KA-related disease, clinicians should be aware of these findings. The major limitation of our study is represented by the sole use of LCL in the experimental plan. Given the rarity of the condition, we were not able to obtain samples to validate our results in primary B cells and to investigate other sources of immune cells. It cannot be excluded that, although patients do not manifest a typical T-cell deficiency phenotype (i.e., severe viral or fungal infections) and the T-cell compartment is fairly intact with no defect in T-cell proliferation, T-cell intrinsic/B-cell extrinsic defects may also contribute to the immune dysregulation. It should also be considered that the early onset of neurological symptoms could significantly affect, at least in part, the rate of infections (i.e., due to microaspiration) or the immune-hematological abnormalities (i.e., due to anti-epileptic drugs).

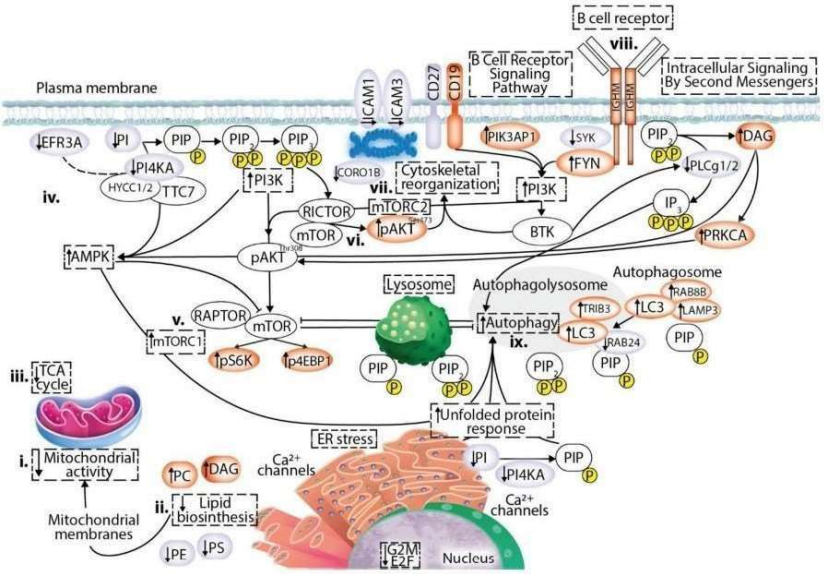

Fig. 7 Schematic representation of the consequences of biallelic PI4KA mutations in B lymphocytes. Impaired mitochondrial activity **(i)** resulting from dysregulated lipid biosynthesis **(ii)** and TCA regulation **(iii).** At the plasma membrane, downregulation of EFR3A results in altered anchoring of the PI4KA complex **(iv)**. Hyperactivation of mTORC1 **(v)** and mTORC2 **(vi)** pathways with deranged actin organization (vii). Dysregulation of B cell receptor and signaling pathways **(viii)**. Increased endoplasmic reticulum stress, unfolded protein response and autophagy **(ix).** Downregulated or upregulated transcripts, proteins, lipids or metabolites are depicted in light grey or red, respectively. Dotted rectangles indicate pathways

[179] Kong IY, Rimes JS, Light A, et al. Temporal analysis of Brd4 displacement in the control of B cell survival, proliferation, and differentiation. Cell Rep. 2020;33(3):108290. https://doi.org/10.1016/j.celrep.2020.108290

2.6 Conclusions

PI4KA-related disorder is a syndromic inborn error of immunity (IEI) characterized by neurological, gastrointestinal, and immunological manifestations, including B-cell lymphopenia and hypogammaglobulinemia. Biallelic *PI4KA* mutations disrupt lipid production, which in turn alters B cell metabolism, leading to mitochondrial dysfunction, ER stress, hyperactivation of the PI3K/mTOR pathway, increased autophagy, and disorganized cytoskeleton structure.

2.7 Supplementary: Material and Methods

Study Participants

This study was approved by the institutional review boards/ethic committee of Comitato Etico Brianza (Monza, Italy; GENPAT-PID). All study participants or their parents provided written informed consent. Recruitment of patients, genetic investigations (either whole-exome sequencing or whole-genome sequencing) and central nervous system phenotype have been previously described [7,103]. P1 to P10 refer to patients reported by Verdura et al.[7] while P11-P13 are patients 1-X1, 3-2:2 and 4-2:3 as reported by Salter et al.[103] Affected individuals were investigated according to routine clinical standards for the diagnosis of neurological disease, MIA, IBD and immunological disorders.

EBV-Immortalized Lymphoblastoid Cell Line Production

EBV-immortalized lymphoblastoid cell lines (LCLs) were generated from peripheral blood mononuclear cells (PBMC) of 3 subjects with biallelic *PI4KA* mutations (P1 carrying p.Pro876SerfsTer36/p.Glu1152Lys, P8 p.Asp1854Asn/p.Asp1854Asn and P10 p.Val1556Met/p.Thr1720Ile) and 4 control subjects (HD) by using a previously published protocol. [180]

---

[7] Verdura E, Rodríguez-Palmero A, Vélez-Santamaria V, Planas-Serra L, de la Calle I, Raspall-Chaure M, et al. Biallelic PI4KA variants cause a novel neurodevelopmental syndrome with hypomyelinating leukodystrophy. Brain. (2021) . 144:2659–69. doi: 10.1093/brain/awab124

[103]Salter CG, Cai Y, Lo B, et al. Biallelic PI4KA variants cause neurological, intestinal and immunological disease. Brain. 2021;144(12):3597-3610. doi:10.1093/brain/awab313

[180] Sie L, Loong S, Tan EK. Utility of lymphoblastoid cell lines. J Neurosci Res. 2009 Jul;87(9):1953-9. doi: 10.1002/jnr.22000. PMID: 19224581.

	PI4KA status	Age	Gender
P1	p.Pro876SerfsTer36/p.Glu1152Lys	6	Female
P8	p.Asp1854Asn/p.Asp1854Asn	5	Male
P10	Val1556Met/p.Thr1720Ile	18	Male
HD1	WT	8	Female
HD2	WT	9	Male
HD3	WT	39	Male
HD4	WT	42	Male
HD5	WT	6	Male

Whole Transcriptome Analysis (Rna-Seq) By Next-Generation Sequencing Of EBV-LCLs

Whole-transcriptome RNA-sequencing (RNA-Seq) analysis was performed on LCLs (P1, P8, P10 and HD1-HD4) by next-generation sequencing, using the Universal RNA-Seq kit (NuGen, Tecan). The Universal RNA-Seq is an end-to-end solution for strand-specific RNA-Seq library construction, using 300 ng amounts of total RNA obtained from LCLs. The workflow consists of double-stranded cDNA generation using a mixture of random priming, optional fragmentation of double-stranded cDNA, end repair, adaptor ligation, strand selection, targeted transcript depletion with AnyDeplete (Tecan) for globin genes, and PCR amplification to produce the final library. The yields of final libraries were assessed by Qubit 4.0 fluorimeter, and their sizes were assessed by Agilent Bioanalyzer. The libraries were analyzed by paired-end sequencing on NextSeq550 Illumina platform, 2×75, on a High Output v2.5 150-cycle cartridge. FASTQ files are available in the ArrayExpress database (www.ebi.ac.uk/arrayexpress) under accession numbers E-MTAB-13729. Raw FASTQ sequences were quality-tested with FastQC(https://www.bioinformatics.babraham.ac.uk/projects/

fastqc/) and aligned against the GRCh38/hg38 reference human genome with the splice-aware aligner Star v2.7.9 (https://github.com/alexdobin/STAR; commit ID f4fa8e8), using the quantMode GeneCounts parameter for read count generation. Binary alignment files were subsequently indexed with Samtools [181]. The Bioconductor package DESeq2 v1.30 [182] was used to perform differential gene expression analysis. Sorted, indexed BAM alignment files were used for manual data inspection using the Integrative Genomics Viewer [183]. GSEAs were performed with GSEA software v4.2.1 (https://www.gsea-msigdb.org/gsea/downloads.jsp) using a gene set permutation scheme with 1,000 random permutations. GSEA was applied on global protein-coding gene expression profiles: significant gene sets were selected based on nominal P value less than 0.05 and FDR less than 0.25.

Proteome Analysis

Cell lysis and trypsin digestion

Proteome analysis was performed on LCLs (P1, P8, P10 and HD1-HD3). Cells have been lysed by three freeze/thaw cycles and then by 10 cycles of sonication (30 seconds on/30 seconds off) of the sample which was previously resuspended in RapiGestTM SF Surfactant (Waters Corporation, Milford, MA, USA) at the final concentration of 1%. Each sample was processed starting from 10^6 cells and in a biological triplicate. Protein digestion was performed as already reported with few modifications [184]. Briefly, samples were diluted with ammonium bicarbonate (NH_4HCO_3, Sigma-Aldrich, ≥99.0%, Darmstadt, Germany) buffer solution at 50 mM to reach a concentration of 0.1% RapiGestTM SF Surfactant. The proteins were reduced by adding DL-Dithiothreitol (DTT) (Sigma-Aldrich, St. Louis, MO, USA, ≥99.5%) at a final concentration of 20 mM and incubated for 45 min at 56 °C; carbamidomethylation reaction was carried

[181] Li H. A statistical framework for SNP calling, mutation discovery, association mapping and population genetical parameter estimation from sequencing data. Bioinformatics. 2011;27(21):2987–2993.
[182] Love MI, et al. Moderated estimation of fold change and dispersion for RNA-seq data with DESeq2. Genome Biol. 2014;15(12):550.
[183] Robinson JT, et al. Integrative genomics viewer. Nat Biotechnol. 2011;29(1):24–26.
[184] Pagani L, Chinello C, Risca G, et al. Plasma Proteomic Variables Related to COVID-19 Severity: An Untargeted nLC-MS/MS Investigation. Int J Mol Sci. 2023;24(4):3570. Published 2023 Feb 10. doi:10.3390/ijms24043570

out by 30 mM iodoacetamide (IAA) (Sigma-Aldrich, St. Louis, MO, USA) (room temperature for 30 min).
Trypsin (trypsin from the porcine pancreas, Sigma-Aldrich, St. Louis, MO, USA) was added to the sample for protein digestion at an estimated enzyme/protein ratio of 1:50 and incubated overnight at 37° C. The digestion was stopped by adding trifluoroacetic acid (TFA) (Honeywell, Seelze, Germany) at a final concentration of 0.5% to reach an acidic pH (<2). RapiGestTM SF Surfactant removal was operated by incubating the samples for 30 minutes at 37° C followed by a centrifugation at 13000 rpm for 10 min. The supernatant which contained the peptides was collected and the volume was reduced using a vacuum centrifugal evaporator (Hetovac, Savant). Finally, dried peptides were resuspended in 50 µL of 0.1% formic acid (FA) (Aldrich, St. Louis, MO, USA).
Samples were desalted and purified by using Ziptip™ µ-C18 Pipette Tips (Merck Millipore Ltd., Sigma-Aldrich, St. Louis, MO, USA). The peptides were eluted with a solution of 80% acetonitrile (ACN) (Honeywell, ≥99.9%, Offenbach, Germany) and 0.1% FA, dried using a vacuum centrifugal evaporator (Hetovac, Savant) and resuspended in 50 µL of 0.1% FA.

Mass spectrometry analysis

For each sample, 400 ng of peptides were injected in duplicate into Evosep One (Evosep Biosystems, Odense, Denmark) LC system coupled online with timsTOF fleXTM (Bruker Daltonics, Bremen, Germany) mass spectrometer. The samples were loaded into a disposable trap column, Evotip PureTM (Evosep Biosystems, Odense, Denmark) following the manufacturer's protocol. Desalted and concentrated peptides were separated into an analytical 8 cm column (PepSep C18, 8cm Performance column, particle size of 1.5µm and internal diameter of 150µm) at a temperature of 40° C. For the separation a gradient of solvent A (0.1 % FA) and solvent B (ACN (LC-MS grade - LiChrosolv®) + 0.1 % FA) was used with a gradient of 21 minutes (30 SPD). The eluted peptides were ionised using a nanoBoosterCaptiveSpray™ (Bruker Daltonics). The mass spectrometer was operated in DIA (Data Independent Acquisition)-PASEF (Parallel Accumulation-Serial Fragmentation) mode. Ions were scanned in positive mode, over a *m/z* 100-1700 and mobility range of 0.85-1.30 V·s/cm². Dry gas flow was 3.0 l/min at 180°C and capillary voltage was 1400 V. For tandem mass PASEF analysis, the cluster of mono-

charged ions was excluded to reduce the complexity of MS2 spectra using the following parameters: *m/z* 475-1000 Da and 0.85-1.27 V·s/cm², the estimated cycle time for each PASEF analysis was 0.95 seconds with a total of 8 cycles using DIA windows of 25 Da.
The mass spectrometer was calibrated for mass and ion mobility accuracy, using a mix of ten standards with a known mass (MMI-L Low Concentration Tuning Mix, Agilent Technologies, Santa Clara, CA, USA). For calibration on nano-source, three specific lock masses (622.0290 *m/z*, 922.0098 m/z and 1221.9906 *m/z*) have been applied on filter.

Data processing
Raw data were elaborated by using SpectronautTM (v.17, https://biognosys.com) following a library-free processing method. A human database (Swissprot, downloaded on 09.02.2023) was used. The parameters were set as follows: trypsin/P as the enzyme, carbamidomethyl (C) as the fixed modifications, acetylation (protein N-term) and oxidation (M) as the variable modifications, 1% FDR at precursor and protein levels.
Proteins were considered identified and quantified only if they had at least one and two significant peptides respectively. This selected protein dataset was formatted and used for the statistical analysis based on the MetaboAnalyst platform (www.metaboanalyst.ca). Only one biological replicate (PT1III) resulted outlier and not considered in the differential proteomic analysis to minimize the technical variability and to not bias the comparison between sample groups. Data were processed with univariate statistics methods (t-test), in order to generate volcano plots, boxplots and a hierarchically clustered heatmap.
Volcano plots were performed setting a fold-change (FC) threshold of 1.5 and a p-value ≤ 0.05, with Benjamini–Hochberg adjustment for multiple comparisons for differential expressed proteins. The hierarchical clustered analysis (HCA) was conducted by using default software settings. Data were autoscaled. Euclidean was used as a distance measure, and ward as a clustering method. Heatmap data visualisation showed the top 50 features.
Functional annotations were performed using STRING (https://string-db.org/, version 12.0, accessed on October, 5th, 2023).

Lipidome And Metabolome Analysis

Metabolites and lipids extraction from cell pellets

Lipidome and metabolome analysis was performed on LCLs (P1, P8, P10 and HD1-HD3). Polar metabolome and lipidome were extracted from cell pellet (10^6 cells per sample) using the following protocol. Briefly, cell pellets were quenched in 250 µl of cold (-20°C) 100% MeOH and mixed with a vortex for 30 seconds. After 20 minutes incubation in ice, samples were vortexed for 30 seconds before centrifugation at 800 g for 1 minute at 0°C and the supernatant was collected and transferred to a fresh tube. The same process was repeated two times in total. The cell pellet obtained after the second centrifugation was then mixed with 125 µl of ice-cold Milli-Q water, vortexed for 30 seconds and froze at -20°C for 20 minutes. Next, samples were thawed in ice and vortexed for 30 seconds before centrifugation at 15000g for 1 minute at 0°C. The obtained supernatant was then added to those collected in the previous steps, obtaining a pooled supernatant solution for each sample. Following, each pooled supernatant was split in two Eppendorf tubes (300 µl of supernatant for each tube) and vacuum dried. For each sample, one tube was then resuspended in 200 µl of a 50% acetonitrile: water solution and used for polar metabolome analysis, the second tube was then resuspended in 200 µl of 100% MeOH and used for the lipidomic analysis.

Polar metabolome analysis

Polar metabolome measurement was performed with an Agilent 6546 LC/Q-TOF. Chromatographic separation was achieved using an HILIC-Z InfinityLab Poroshell 120 column (2.1 x 150 mm, 2.7 µm, - Agilent).

All samples were analysed three times: once in positive ionization mode and twice in negative ionization mode using acidic and neutral chromatographic conditions QC pooled sample, obtained by mixing a small aliquot from each sample was used as quality control and acquired every five injections in full scan and in Auto MSMS data dependent acquisition (DDA), with Iterative modality, at the end of the sample list in triplicate. In positive and negative acidic conditions, Mobile Phase A was 100% of 10 mM ammonium formate, 0.1% formic acid and B was of acetonitrile: Mobile Phase A (95:5 v:v). For the neutral condition, Mobile Phase A was 100% of 10 mM ammonium formate, and B was of acetonitrile: Mobile Phase A (95:5 v:v).

The following elution gradient was used in all the conditions: 0 min 98%, 1 min 98% B, 12 min 60% B, 13 min 50% B, 14 min 5% B, 15 min 5% B, 15.5 min 98% B, and 20 min 98% B. In all conditions, the flow rate was 0.25 ml/min, the column temperature was 25°C. The injection volume was 2 µl for positive ion mode and 5 µl for negative ion mode. In ESI positive mode, the mass spectrometer operated at a resolving power of 40,000 over a full scan range of *m/z* 50–1000 at a scan rate of 2 spectra/s with the following settings: gas flow 6 L/min; gas temperature 225°C; nebulizer 40 psi; sheath gas temperature 225°C; sheath gas flow 10 L/min; capillary voltage 3000 V and fragmentor at 150 V. In ESI negative mode, the mass spectrometer operated at a resolving power of 40,000 over a full scan range of *m/z* 50–1000 at a scan rate of 2 spectra/s with the following settings: gas flow 12L/min; gas temperature 225°C; nebulizer 40 psi; sheath gas temperature 350°C; sheath gas flow 12 L/min; capillary voltage 3500 V and fragmentor at 150 V. Purine and hexakis (Agilent) were used as reference mass both in positive (*m/z*= 121.0508 and *m/z*=922.0097) and negative (*m/z*= 112.9855 and *m/z*= 966.0002) experiments and continuously infused at flow rate of 0.08 ml/min.Polar metabolites were annotated based on accurate mass, MS/MS, isotopic pattern and retention times against our *in-house* database and/or online databases, including HMDB and METLIN. A total of 122 annotated metabolites had a coefficient of variation (QC%) <30% in quality controls. The corresponding chromatographic peaks areas were annotated and extracted from each sample using Agilent Mass Hunter Quantitative Analysis software and then used for data analysis.

Lipidome analysis

The lipidome measurement was performed using an Agilent 6546 LC/Q-TOF. Chromatographic separation was achieved using an ACQUITY UPLC CSH C18 Column 1.7 µm, 2.1× 100 mm Column (Waters™). All samples were analysed both in positive and negative ionization mode using acidic and basic chromatographic conditions. All samples were analysed in full scan, both in negative and positive ionization mode. QC pooled sample, obtained by mixing a small aliquot from each sample was used as quality control and acquired every five injections in full scan and in Auto MSMS data dependent acquisition (DDA), with Iterative modality, at the end of the sample list in triplicate. In both positive and negative conditions mobile phase A was 10

mM ammonium formate:acetonitrile (40:60 v:v) with 0.1% formic acid and Mobile Phase B was isopropanol:Phase A (90:10 v:v). The following elution gradient was used: 0 min 99% A, 1 min 99% A, 1.10 min 60% A, 5 min 20% A, 11 min 20% A, 12 min 1% A, 18 min 1% A, 18.10 min 60% A, 20 min 99% A. The flow rate was 0.25ml/min the column temperature was 55°C. The injection volume was 2 µl for positive ion mode and 5 µl for negative ion mode. In ESI positive mode, the mass spectrometer operated at a resolving power of 40,000 over a full scan range of *m/z* 50–1700 at a scan rate of 2 spectra/s with the following settings: gas flow 10 L/min; gas temperature 200°C; nebulizer 50 psi; sheath gas temperature 300°C; sheath gas flow 12 L/min; capillary voltage 3500 V and fragmentor at 150 V. In ESI negative mode, the mass spectrometer operated at a resolving power of 40,000 over a full scan range of *m/z* 50–1700 at a scan rate of 2 spectra/s with the following settings: gas flow 10L/min; gas temperature 200°C; nebulizer 50 psi; sheath gas temperature 300°C; sheath gas flow 11L/min; capillary voltage 3000 V and fragmentor at 150 V. Purine and hexakis (Agilent) were used as reference mass both in positive (*m/z*= 121.0508 and *m/z*= 922.0097) and negative (*m/z*= 112.9855 and *m/z*= 966.0002) experiments and continuously infused at flow rate of 0.08 ml/min. Collision energy voltage was set at 40 eV both in positive and negative ion mode. The annotation parameters were ±5ppm for the mass score, an isotope cluster score higher than 80% and an MS/MS score higher or equal to 90% when matching our in-house database generated using Lipid Annotator (Agilent). A total of 174 lipids were annotated and had a CV% in quality controls < 30%. The corresponding chromatographic peaks areas were annotated and extracted from each sample using Agilent Mass Hunter Quantitative Analysis software and then used for data analysis.

Polar metabolome and lipidome data processing

Data analysis was performed using MetaboAnalyst (https://doi.org/10.3390/metabo10050186). The polar metabolome and the lipidome datasets were then normalized separately by the sum of the features and Log transformed. Volcano Plots were obtained using a fold change threshold of 1.5 and a p-value<0.05 after Benjamini-Hochberg test. Quantitative Enrichment Analysis (QEA) of polar metabolites was then performed using the metabolic pathway associated metabolite sets of KEGG human metabolic pathways. The top

25 enriched metabolic pathways were displayed as a dot plot. Further, the two normalized datasets were also combined and used to perform a hierarchical clustering. The similarity measure and clustering algorithm employed were the Euclidean distance and the Ward's linkage, respectively. The hierarchical clustering of the top 90 substantially different expressed lipids and metabolites in the PI4KA patients compared to healthy donors was then displayed as a heatmap based on the clustering result.

Biochemical analysis of integrated multi–omics data

The integration of proteomic, metabolomic and lipidomic data was conducted using biochemical information available through the KEGG (Kyoto Encyclopedia of Genes and Genomes) and the Lipid Maps databases. Supplemental Figure 3 summarizes the workflow of analyses for the systematic integration of biochemical information across –omics data. Biochemical pathways where proteins (metabolic enzymes) and metabolites differentially expressed converge, in patients compared to healthy controls, were identified.

Proteomics workflow

Proteomic analysis was carried out to identify proteins that are significantly upregulated and downregulated. The KEGG 'GENES' category was first used to conduct this search. The KEGG 'ENZYMES' code for metabolic enzymes was also obtained to aid in identifying proteins of interest in KEGG maps. Contextualization of proteomics data within KEGG maps was realized by identifying common pathways within which proteins (metabolic enzymes) and metabolites converge. The KEGG Metabolic Pathways Map was used to identify differentially regulated metabolic enzymes.

Metabolomics workflow

Metabolomic analysis was carried out to identify metabolites that are significantly upregulated and downregulated. Some significantly regulated metabolites in patients reached a 1.5-fold difference in expression level and above, compared to healthy controls; other metabolites were found below 1.5-fold while still being significantly different between patients and healthy controls. The KEGG Metabolic Pathways Map was used to conduct the pathway analysis. Metabolites were identified under the KEGG 'COMPOUND' category. Pathways within which

the metabolites of interest are involved were identified and integrated with proteomic and lipidomic data to identify common or connected pathways characterized by a differential regulation. To allow for a comprehensive analysis of differentially regulated metabolites, metabolic enzymes associated with the metabolites were investigated to identify common pathways impacted in disease. Metabolic enzymes were only considered in pathways that were also associated with the metabolite(s) of interest.

Lipidomics workflow

A similar approach used for analysing metabolomic data was taken to analyse lipidomics data, focusing on differentially regulated lipids. Lipidomic analysis identified lipids based on their carbon composition and bond saturation, hence attributing structural names. These chemical structure details were investigated using the Lipid MAPS database, to obtain the systematic name of the molecules of interest. The Lipid MAPS database was also used to identify metabolic enzymes associated with the differentially regulated lipids. Within this database, the category, main class and sub class of the lipids of interest were retrieved. This information was subsequently used in the KEGG 'Lipids' category to identify the specific differentially regulated lipids. The biochemical pathways within which the lipids appeared, or were associated with, were identified in the KEGG maps. These pathways were then integrated with proteomic and metabolomic data to identify common or connected pathways characterized by a differential metabolic regulation.

Confocal microscopy and image analysis

Mitochondrial abundance and membrane potential

LCLs from three patients (P1, P8, P10) and three HD (HD1, HD2 and HD5) were used. HD cells were treated with GSK-A1 100nM for 30 minutes. Cells were incubated for 30 minutes in culture condition (RPMI, 10% FBS) with 50nM MitoTrackerTM Red CMXRos (Thermo Fisher Scientific), 25nM MitoTrackerTM Green FM (Thermo Fisher Scientific), and subsequently nuclei were stained with Hoechst 33342 (Thermo Fisher Scientific). Cells were washed twice in PBS and mounted on glass slides with a 90% (v/v) glycerol/PBS solution.

Actin rearrangement

LCL cells derived from three patients and three HD (HD1, HD2 and HD5) were used. HD cells were treated with GSK-A1 100nM for 30 minutes. Cells were washed twice with PBS and then incubated for 10 minutes at room temperature in 4% paraformaldehyde in 0.12M sodium phosphate buffer, pH 7.4, then left in PBS overnight at 4 °C. Actin staining was performed for 2 hours at room temperature with Alexa Ffluor 594 phalloidin (Thermo Fisher Scientific) (1:400 dilution in GDB buffer [0.02M sodium phosphate buffer, pH 7.4, containing 0.45M NaCl, 0.2% (w/v) bovine gelatin]), followed by staining with Hoechst 33342 (Thermo Fisher Scientific), coverslips were mounted on glass slides with a 90% (v/v) glycerol/PBS solution.

Autophagy Protocol

LCL cells derived from three patients and three HD (HD1, HD2 and HD5) were used. HD cells were treated with GSK-A1 100 nM for 30 minutes. Cells were stimulated with chloroquine 10uM or vehicle in 10% FBS/RPMI for 3 hours at 37°C. Cells were washed twice with PBS, fixed for 10 minutes at room temperature in 1.6% paraformaldehyde and permeabilized with 90% ice-cold methanol overnight at -20°C. After two washes with PBS, cells were stained LC3A/B (#12741 Cell signaling), LC3B (#3868 Cell signaling) and acquired on a FACSaria™ flow cytometer (BD).

Images acquisition and analysis

Images were acquired using Zeiss LSM 710 confocal laser-scanning microscope (Zeiss) using a 63x, 1.4 N/A oil-immersion objective. Laser intensities and acquisition parameters were held constant throughout each experiment. Confocal microscopy fields were analyzed using specific homemade-designed macro with ImageJ (https://imagej.nih.gov/ij/) software.

In brief, we quantified the size of mitochondria by measuring the integrated density (ID) of the green signal, which was then normalized over the total number of nuclei analyzed. To assess mitochondrial activity, we measured the ID of the red signal and calculated the ratio with the green signal after applying a manual threshold. We collected data from a minimum of ten fields per sample, with at least 80 cells analyzed in each field.

For the analysis of the actin signal, we measured the distribution of positive active staining starting from the nuclear center of mass and normalized it relative to untreated HD cells. To evaluate the intensity of the LC3 signal, we measured the ID and normalized it relative to the HD cells cultured under untreated conditions. Similarly, data for these analyses were collected from a minimum of ten fields per experimental condition, with at least 80 cells analyzed in each field.
Statistical analysis and graphing were performed using GraphPad Prism6 (GraphPad Software, Inc.). We conducted statistical tests using Welch's t-test or one-way ANOVA, and the results were expressed as means ± SD.

Metabolic Profiling

LCL cells derived from three patients and three HD (HD1, HD2 and HD5) were used. HD cells were treated with GSK-A1 100 nM for 30 minutes. All respiratory profiles were performed using the XF96 extracellular flux analyzer (Seahorse Bioscience). Prior to respiration analysis, dead cells were removed with a magnetic dead cell–depletion kit (Miltenyi Biotec). A total of 2 × 10^5 cells in 180 µL of XF media (Seahorse Bioscience) were seeded onto XFe96 plates (102416-100, Agilent Technologies) and incubated at 37°C, in CO2 free incubator, for 1 hour. OCR and extracellular acidification rate were then evaluated using an XF96 extracellular flux analyzer (Seahorse Bioscience). To measure ATP-linked OCR, maximal respiration, and mitochondrial-dependent basal OCR and proton leak, 1.5 µmol/L oligomycin A, 1 µmol/L carbonyl cyanide-4-phenylhydrazone (FCCP), and 1 µmol/L antimycin A and 0.5 µmol/L rotenone were added, respectively.

Phosphoflow cytometry

EBV-LCLs from patients and three HD (HD1-HD3) were starved in X-VIVO medium and rested at 37°C for 1 hour. Thereafter cells were assessed for count and viability with trypan blue dye before phosphoflow testing. Cells rested unstimulated for 30 minutes at 37°C, fixed with 1.5% paraformaldehyde and permeabilized with 90% ice-cold methanol prior to staining with anti-phospho-protein-directed MoAbs such as pSTAT5 Alexa 488, p4EBP1 Alexa 488, pAkt473 Alexa 647, pS6 Alexa 647 (or isotype matched IgG). Cells were acquired on LSR Fortessa X-20 flow cytometer (BD). Data (at least 100,000 events per condition) were collected and analyzed using FacsDIVA

software. Phosphoprotein expression was established by the comparative use of isotype IgG correspondent to the phosphoprotein specific antibody. Basal level of each phosphoprotein was then calculated as Mean Fluorescence Intensity (MFI) fold change of the fluorescence distribution in unstimulated/isotype conditions. Statistical analysis and graphs were analyzed using GraphPad Prism6 (GraphPad Software, Inc.). Statistics was performed using a one-sample t-test and data were expressed as means ± SD.

EBV-transformed B-cell proliferation

LCLs, derived from 2 patients (P1 and P10) and 3 HD (HD1-HD3), after having been grown at exponential phase, were serum starved overnight and then assessed for count and viability with trypan blue dye before testing. Cells were washed twice with PBS and resuspended in 1 ml of pre-warmed Saline Solution. LCLs were stained with 15 uL CFSE, incubated for 10 minutes at room temperature in the dark, then stopped labelling by adding 8 ml of complete media (containing ≥10% serum). Samples were centrifuged for 5 minutes at 1400 rpm. CFSE labelled cells were seeded in triplicate in multi-well tissue culture plates and cultured in RPMI and 10% FBS for 24 hours. Cells were fixed with 1% w/v paraformaldehyde in a PBS solution and analyzed by cytometer (LSRFortessa™) at basal level (0h), 3 hours, 12 hours, 24 hours. Analysis was performed using a DIVA™ software (BD). For each time point, percentage of divided cells (PD) and division Index (DI), defined as the average number of divisions for all cells in the original population, were calculated using FlowJo software (version 10.5.3).

Ex vivo drug screening experiments

Ex vivo extended drug screenings were performed in patients (P1, P8 and P10) and HD (HD1-HD3) LCL as previously described. Briefly the DMSO dissolved compound library (MedChemExpress, NJ, USA) was dispensed with increasing concentrations of the inhibitors in 6 dilution steps (0.008 - 25 µM) using digital dispenser (D300e, Tecan, Mannedorf, Switzerland), which ensures precise and robotic compound application in randomized fashion. Differential responses were monitored with ATP-dependent CellTiter-Glo Luminescent cell viability kit (Promega, Madison, USA) after 72 h of inhibitor exposure using Microplate reader (Spark 10M, Tecan). Drug

sensitivity scores (DSS) for the inhibitors were determined as previously described.[185]

2.8 Supplementary: Figures and Text

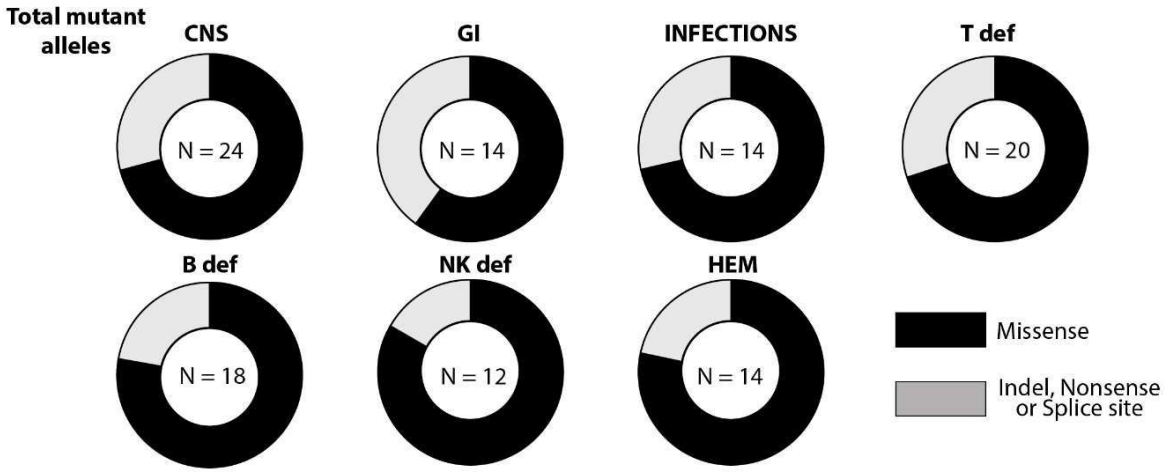

Supplemental Figure 1. Analysis of *PI4KA* variants by patient phenotype. Circle charts illustrating the types of mutations associated with each phenotype.

CNS = central nervous system manifestations. GI = gastrointestinal manifestations. GU = genito-urinary manifestations. HEM = hematological manifestations (anemia, monocytosis, neutropenia or thrombocytopenia). T def = decreased absolute number of T cells (CD3+, CD4+ or CD8+) or altered T cell subsets. B def = hypogammaglobulinemia, decreased absolute B-cell numbers or altered B-cell subsets. NK def = decreased absolute number of NK cells.

[185] Yadav B, Pemovska T, Szwajda A, Kulesskiy E, Kontro M, Karjalainen R, Majumder MM, Malani D, Murumägi A, Knowles J, Porkka K, Heckman C, Kallioniemi O, Wennerberg K, Aittokallio T. Quantitative scoring of differential drug sensitivity for individually optimized anticancer therapies. Sci Rep. 2014 Jun 5;4:5193. doi: 10.1038/srep05193.

Supplemental Figure 2. Whole RNA sequencing analysis: principal component analysis between PI4KA-deficient patients' LCL and healthy donors' LCL.

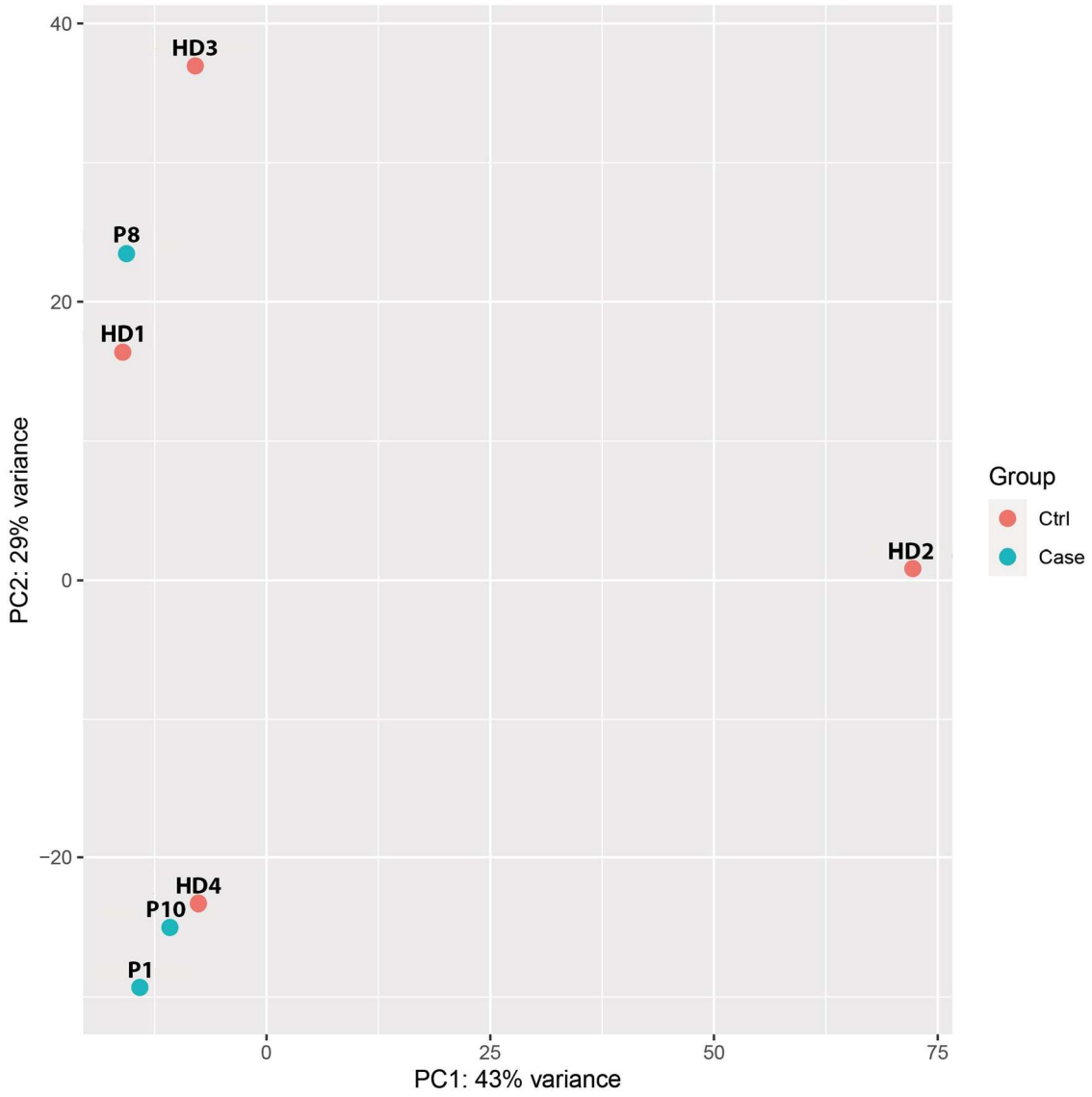

Supplemental Figure 3. Gene ontology enrichment analysis of the differentially expressed genes.

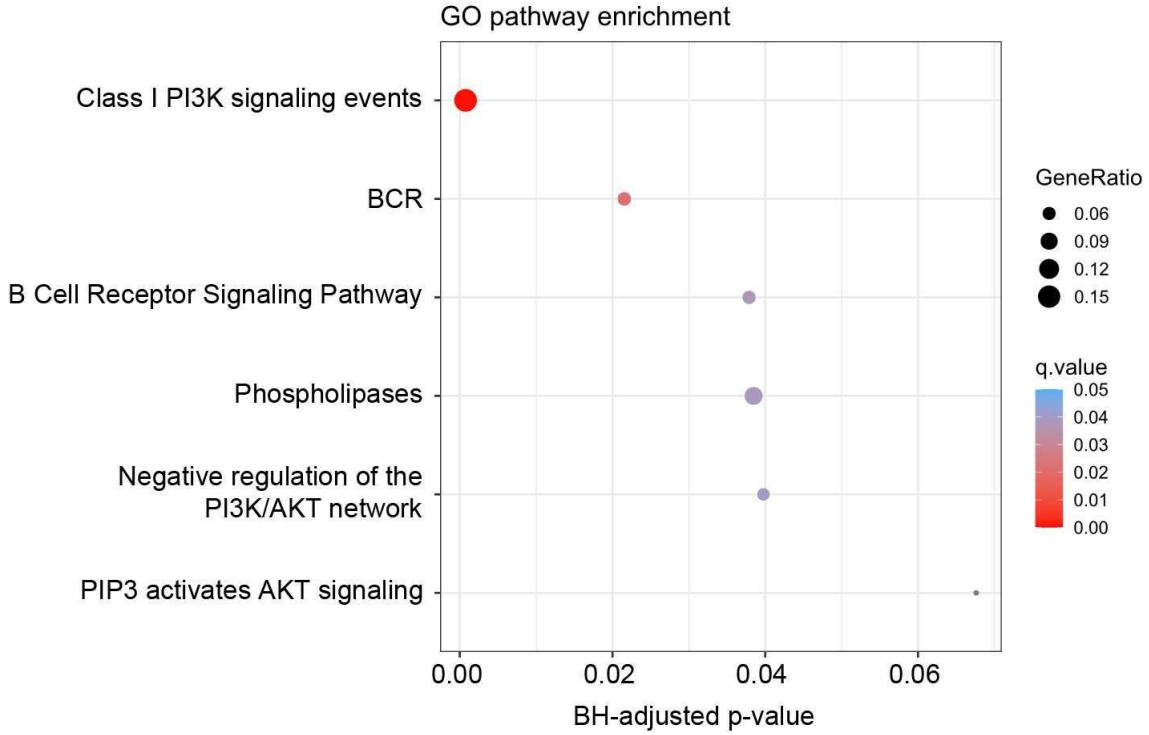

Supplemental Figure 4. Bioinformatic STRING analysis of the proteomic data from the label-free mass spectrometric study of PI4KA-related disorders. Bioinformatic analysis was carried out with the available STRING (http:// http://string-db.org/) database of known and predicted protein interactions that include direct physical and indirect functional protein ssociations.[186]

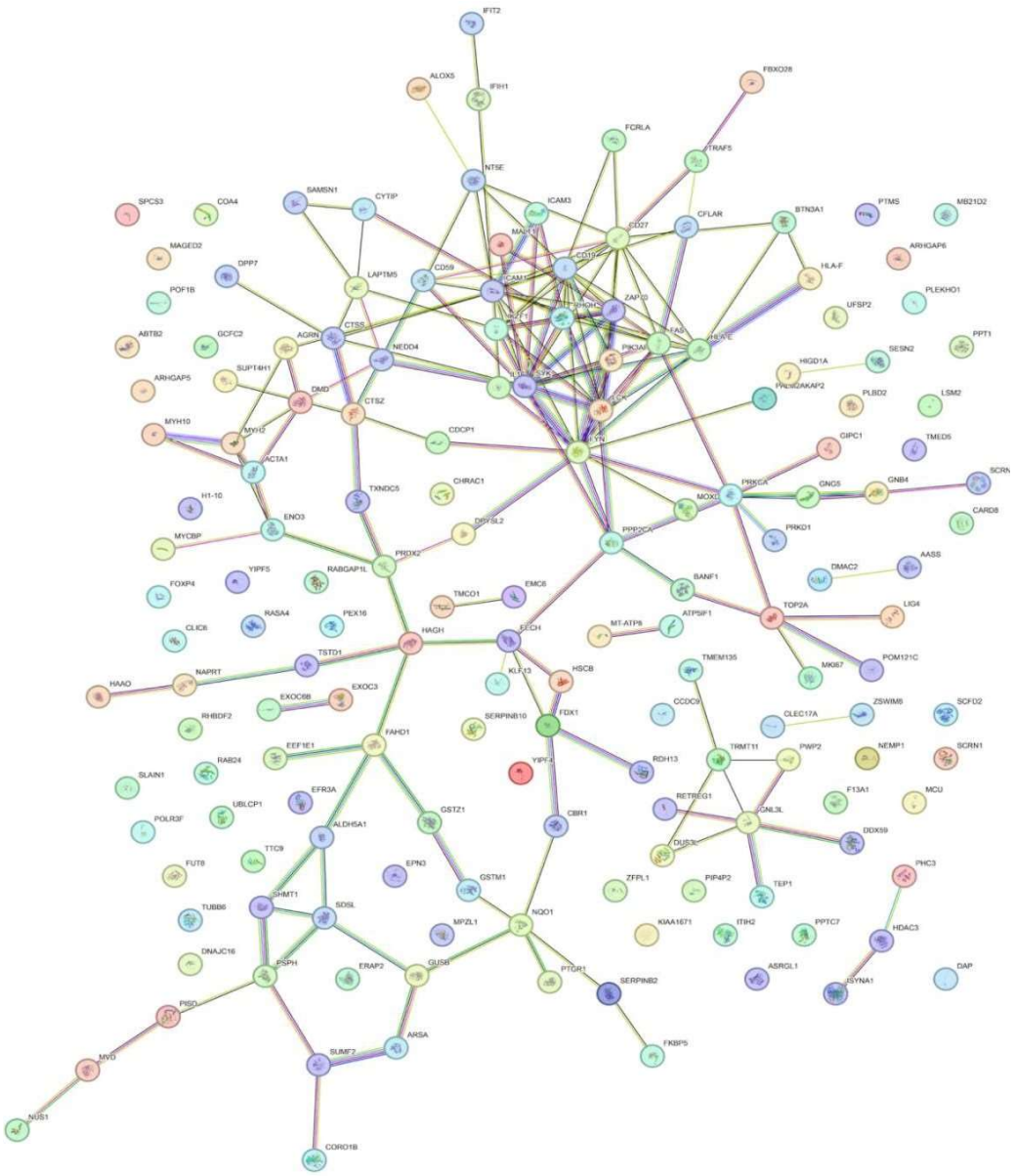

[186] Szklarczyk D, Franceschini A, Wyder S, Forslund K, Heller D, Huerta-Cepas J, Simonovic M, Roth A, Santos A, Tsafou KP, Kuhn M, Bork P, Jensen LJ, von Mering C. STRING v10: protein-protein interaction networks, integrated over the tree of life. Nucleic Acids Res. 2015 Jan;43(Database issue):D447-52. doi: 10.1093/nar/gku1003. Epub 2014 Oct 28. PMID: 25352553; PMCID: PMC4383874.

Supplemental Figure 5. Top 25 enriched metabolite sets. Enrichment analysis was performed with MetaboAnalyst.

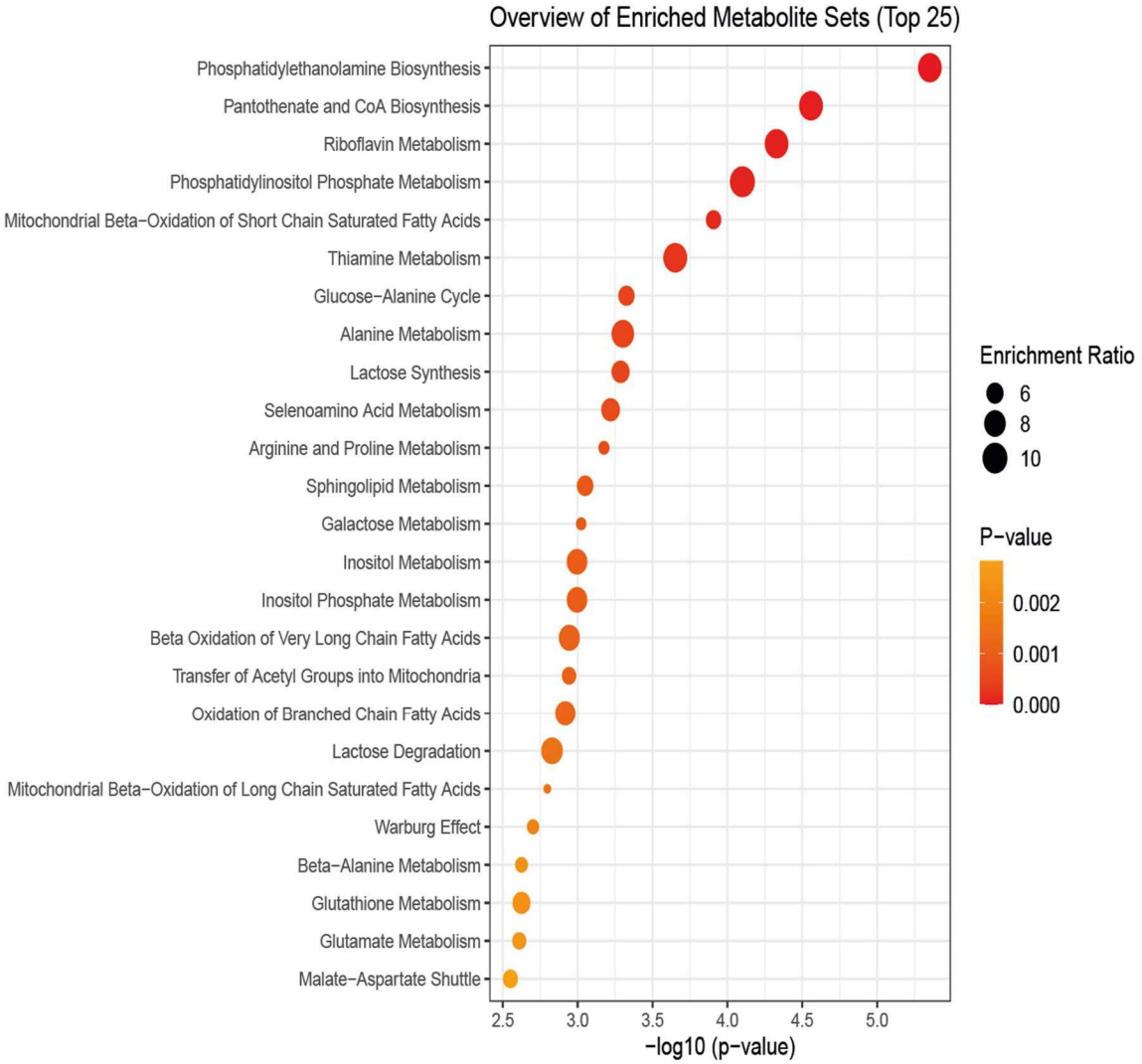

Supplemental Figure 6.

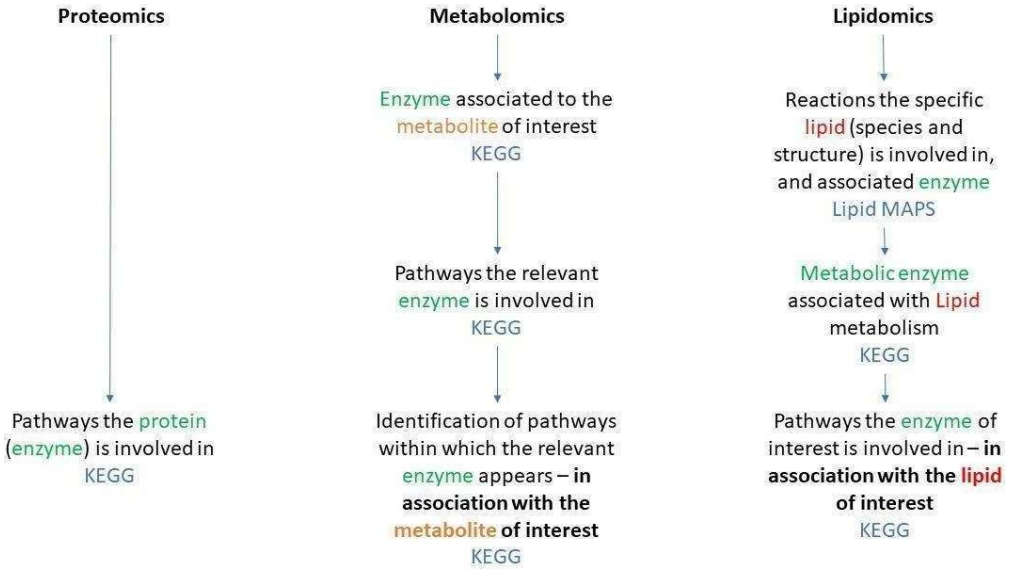

Supplemental Figure 7.

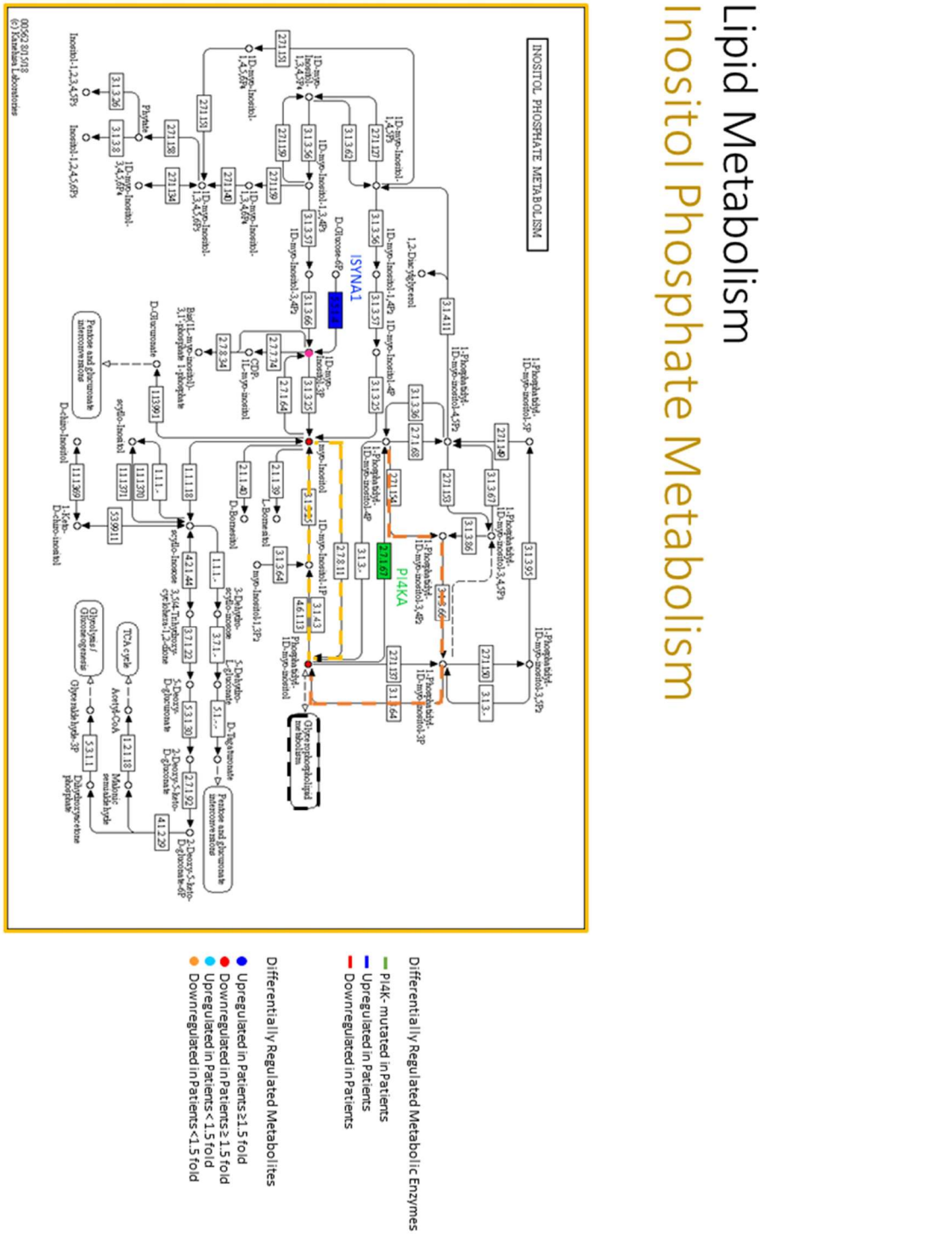

Supplemental Figure 8.

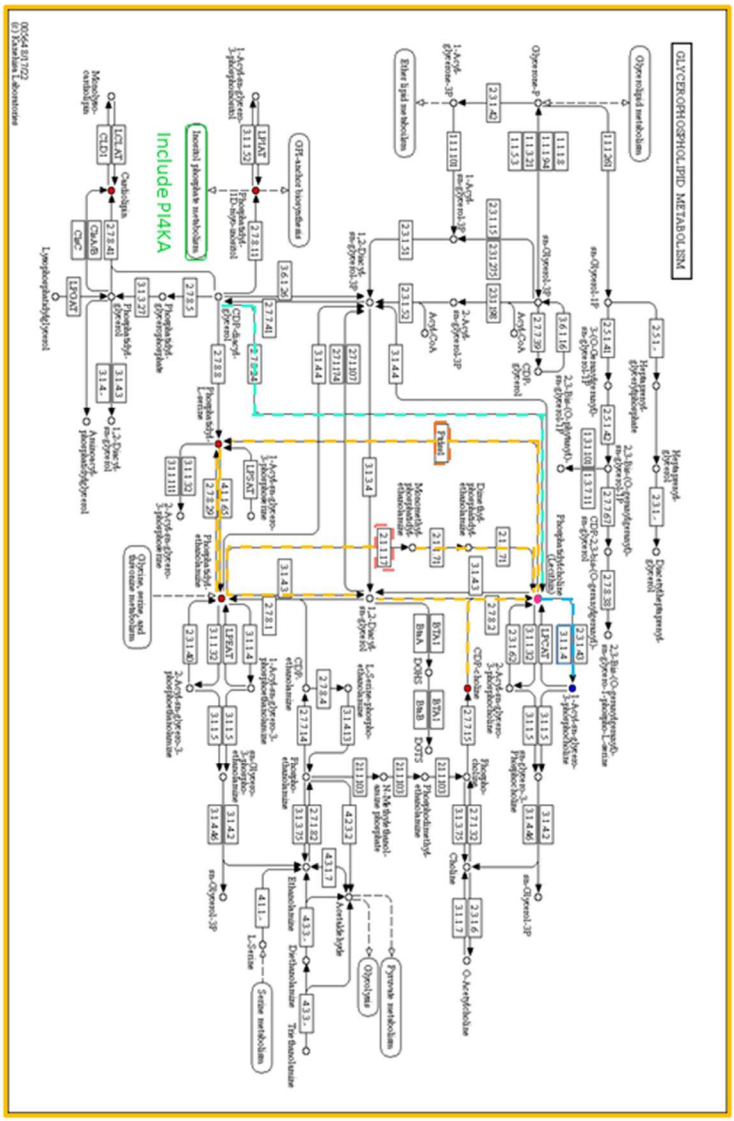

Supplemental Figure 9.

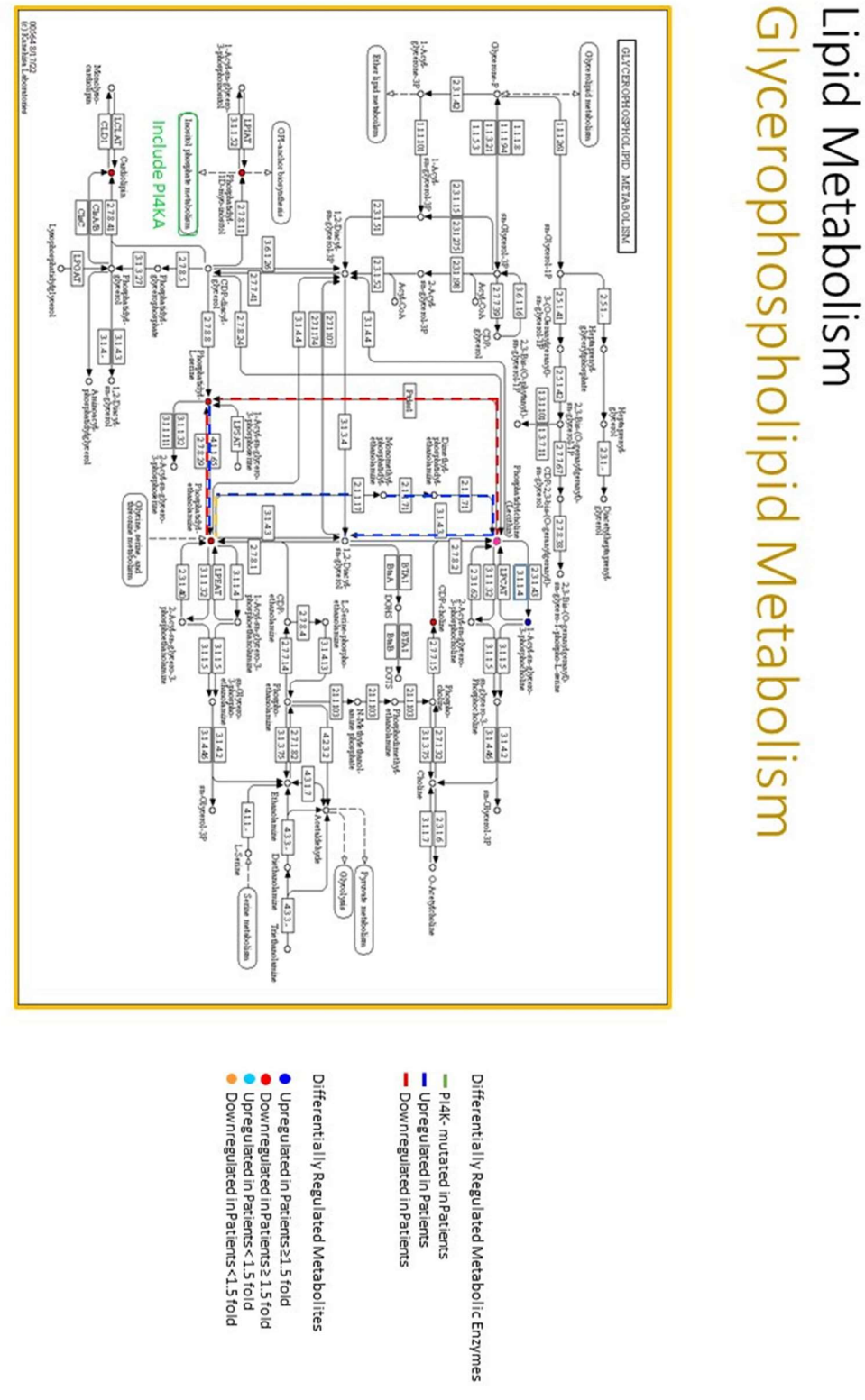

Supplemental Figure 10.

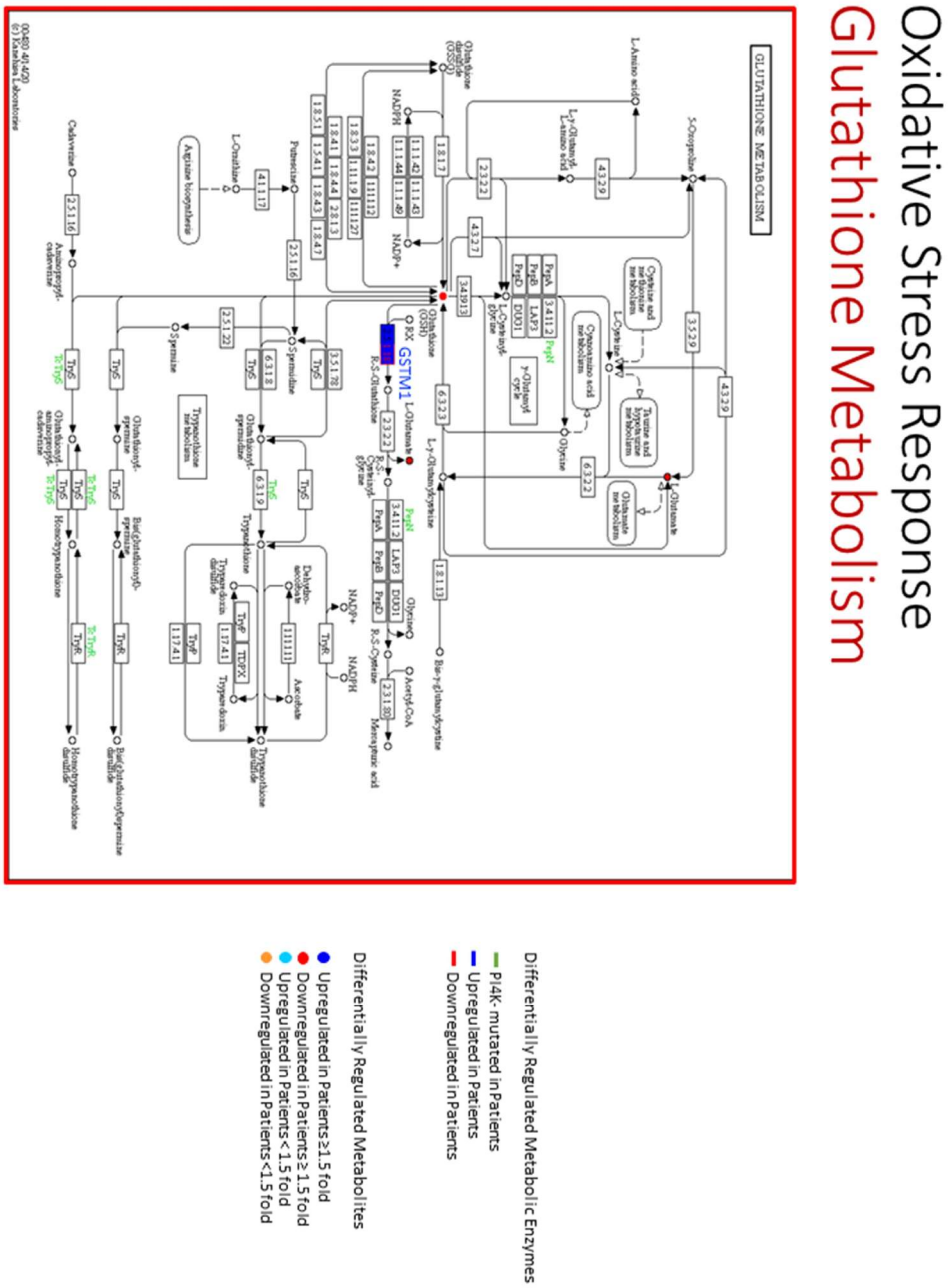

Supplemental Figure 11.

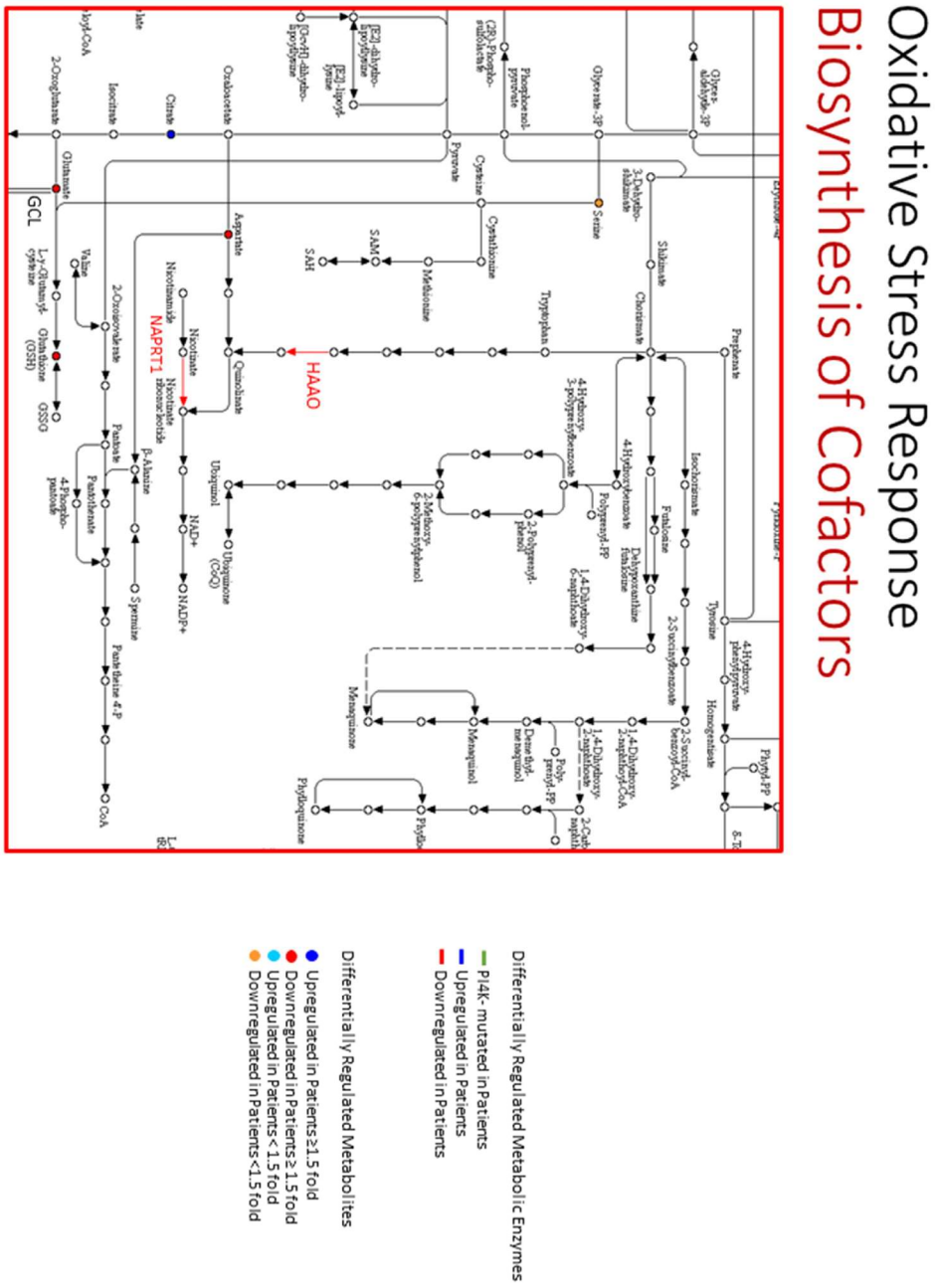

Supplemental Figure 12.

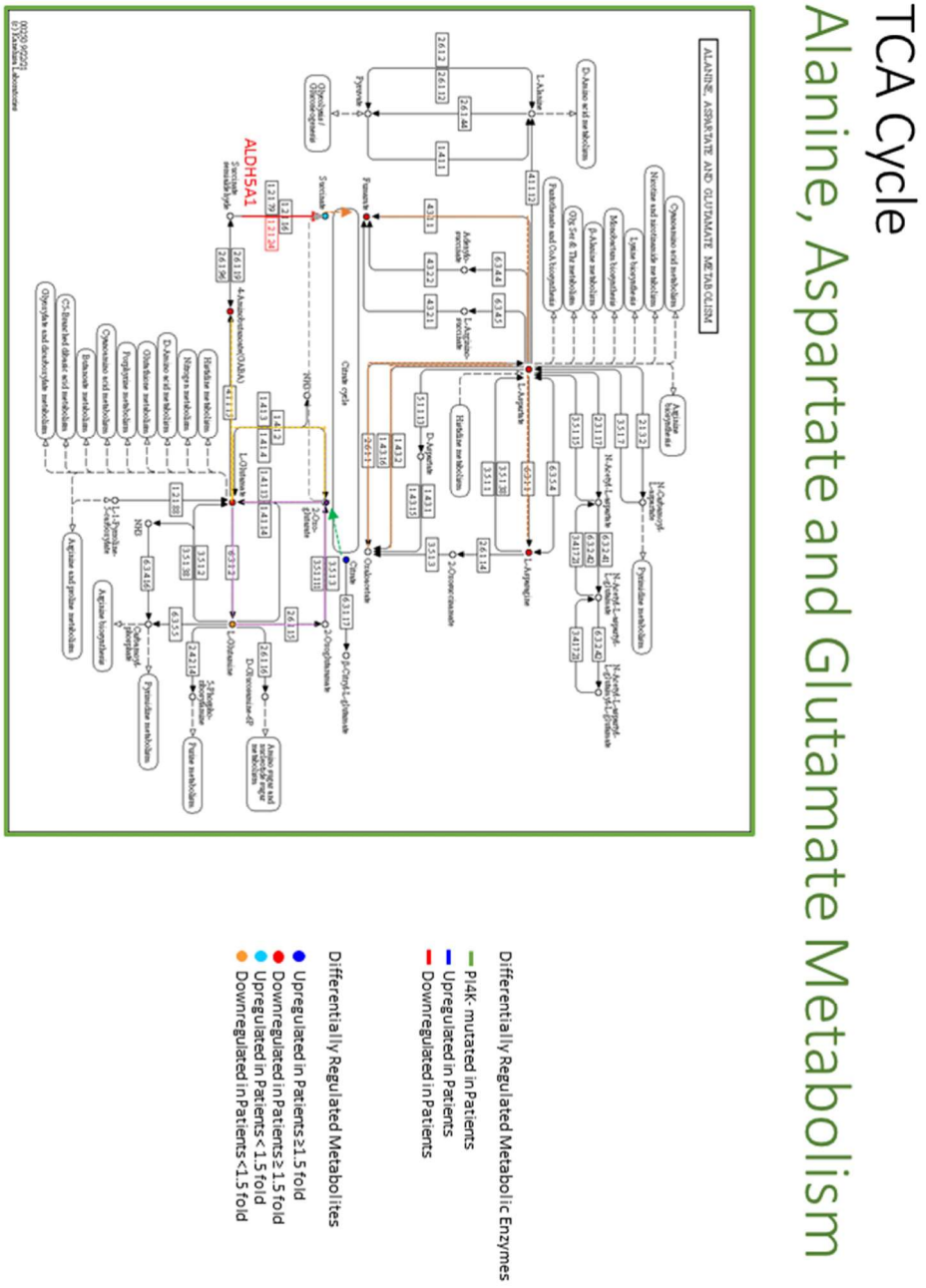

Supplemental Figure 13.

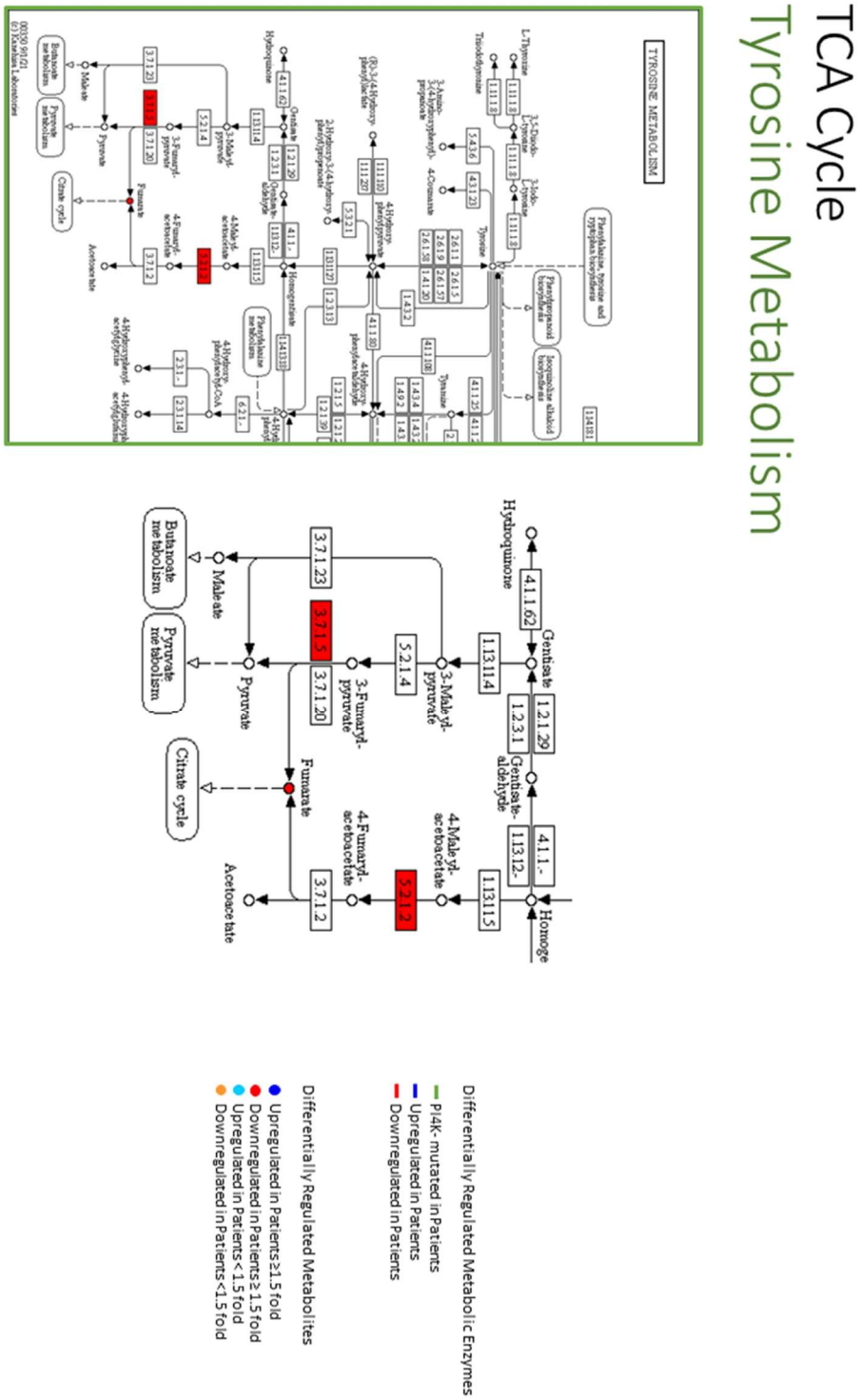

Supplemental Figure 14. Representative images of Mitotracker Red and Green signals in EBV-transformed B cells from one healthy control (upper panel) and one patient with biallelic *PI4KA* mutations (lower panel). Nuclei were stained with Hoechst 33342. Scale bar: 20µm.

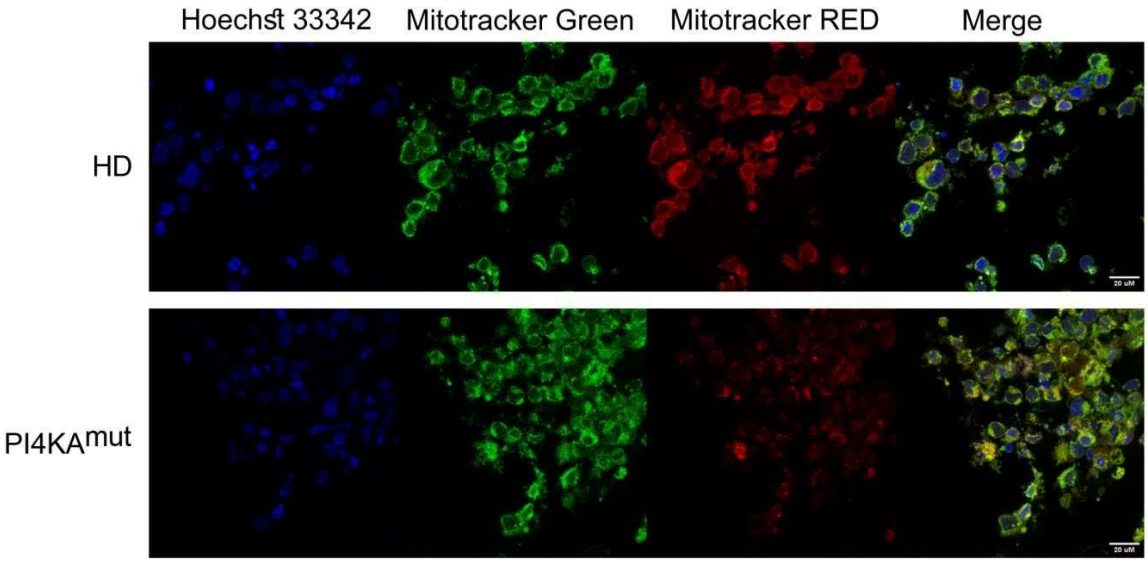

Supplemental Figure 15. Quantification of mitochondrial function analyzing basal respiration, extracellular acidification rate, ATP production, maximal respiration and spare respiratory capacity in individual patients.

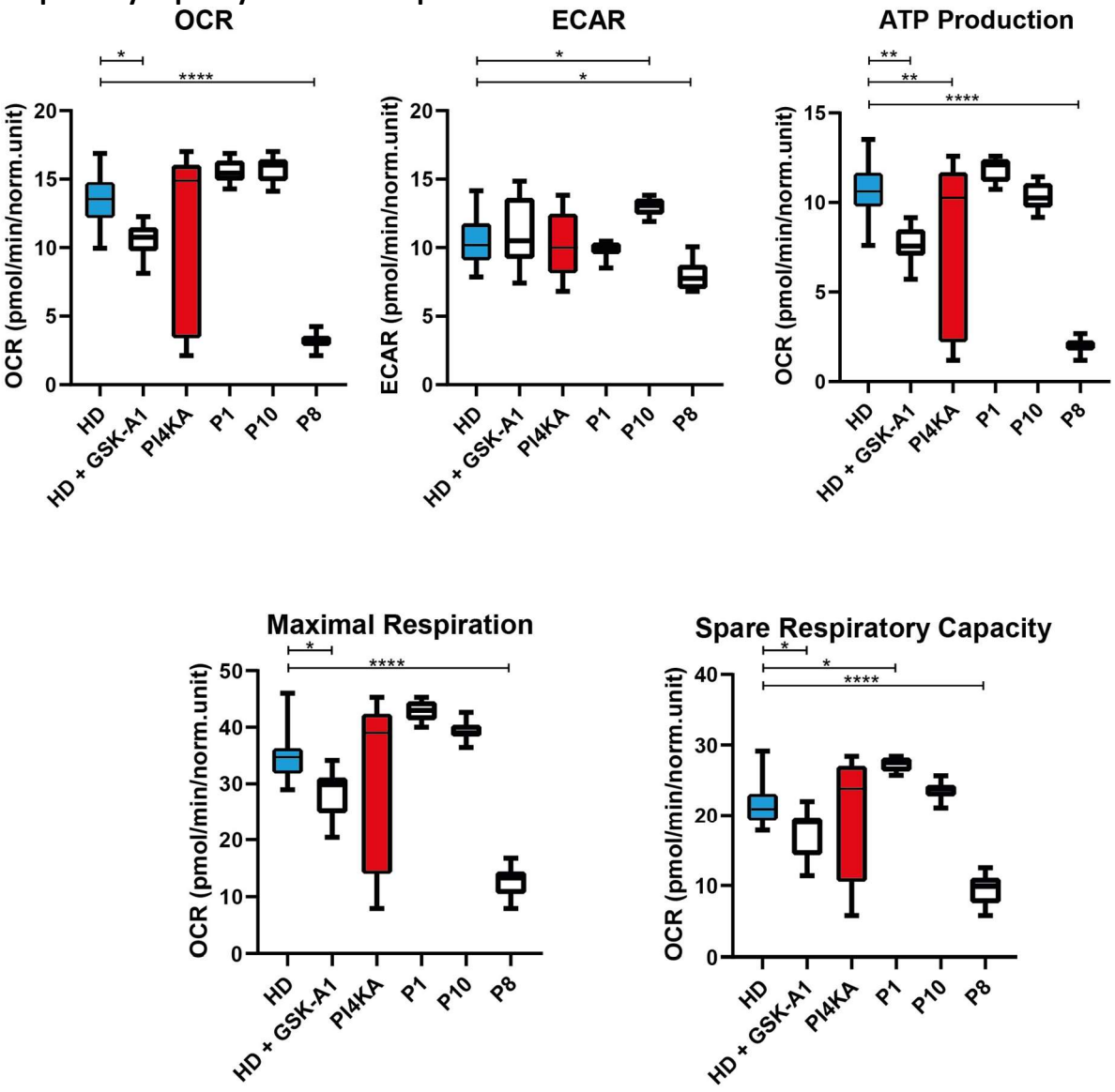

Supplemental Figure 16. Representative images of actin distribution in PI4KA-mutated EBV-transformed B cells from one healthy control (left) and one patient with biallelic *PI4KA* mutations (right).

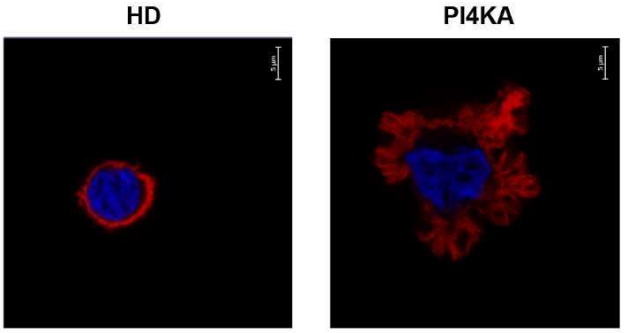

Supplemental Figure 17. pSTAT5 (A) and apoptotic rates after treatment with staurosporine (B) in individual patients.

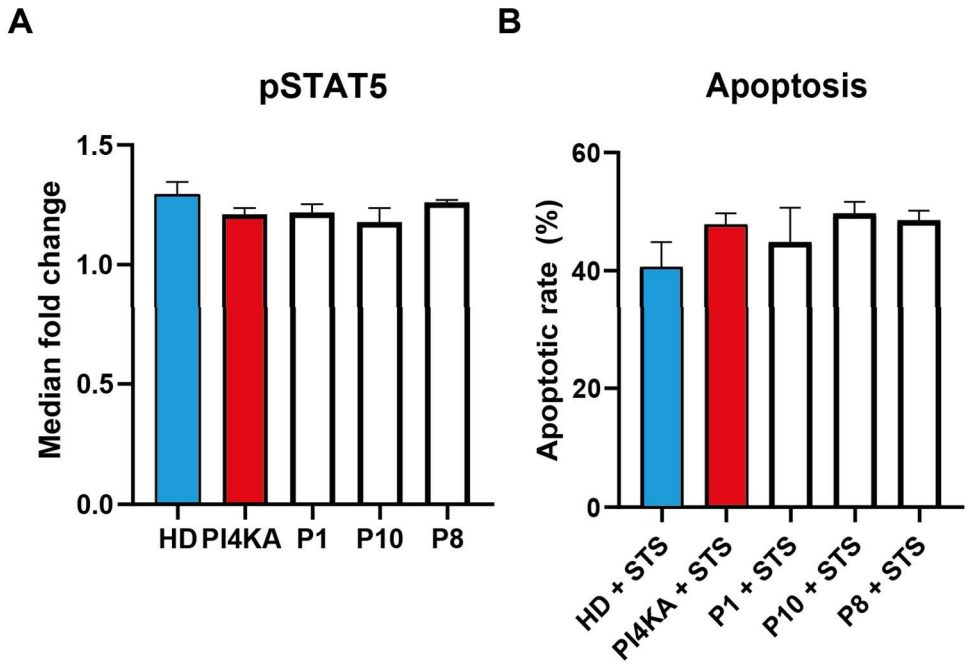

Supplemental text

Integration of multi–omics data indicates failure of mitochondrial function in patients with biallelic *PI4KA* mutations

In patients with biallelic *PI4KA* mutations, lipid metabolism, glutathione metabolism, biosynthesis of cofactors, pathways contributing to the regulation of TCA cycle, and amino acid metabolism were affected as compared to healthy controls. Here the detailed explanation of molecular mechanisms that integrate the specific (sub-)metabolic pathways are presented.

1) Lipid Metabolism

***1a) Inositol Phosphate Metabolism* (Supplemental Figure 5)**

- PI4KA in a unidirectional reaction consumes phosphatidyl-1D-myo-inositol (PI), phosphorylates it to produce 1-phosphatidyl-1D-myo-inositol 4-phosphate (PIP). PIP, amongst other reactions, is metabolized by the enzyme phosphatidylinositol-4-phosphate 3 kinase (PIK3C2; 2.7.1.154) to produce 1-phosphatidyl-1D-myo-inositol 3,4-biphosphate (PIP_2). PIP_2 is dephosphorylated by the enzyme inositol polyphosphate-4-phosphatase (INPP4; 3.1.3.66) to form 1-phosphatidyl-1D-myo-inositol-3-phosphate, which is metabolized, through a positive feedback loop, to replenish phosphatidyl-1D-myo-inositol, by the enzyme myotubularin (MTM1; 3.1.3.64). Phosphatidyl-1D-myo-inositol is largely regulated through the Glycerophospholipid metabolism, which includes many differentially regulated lipids as suggested by the lipidomic analysis.
- Low levels of phosphatidyl-1D-myo-inositol are mirrored by the relatively low concentration of myo-inositol. The two substrates are linked via the enzyme CDP-diacylglycerol-inositol-3-phosphatidyltransferase (CDIPT; 2.7.8.11), through which myo-inositol is metabolized to phosphatidyl-1D-myo-inositol in a unidirectional reaction. This would suggest that myo-inositol is initially downregulated in patients and consequently, phosphatidyl-1D-myo-inositol is reduced.
- The only other component of the Inositol Phosphate Metabolism that has been suggested to be differentially regulated is the enzyme myo-inositol-1-phosphate synthase (INO1/ISYNA1; 5.5.1.4), which is upregulated in patients compared to healthy controls. This enzyme facilitates the conversion of D-glucose-6-phosphate to 1D-myo-inositol-3-phosphate in a unidirectional reaction. ISYNA1 may be upregulated to compensate for the reduced myo-inositol, utilizing D-glucose-6-phosphate to replenish myo-inositol, through the direct reaction catalysed by the enzyme myo-inositol-1,4-monophosphatase (IMPA; 3.1.3.25).

***1b) Glycerophospholipid Metabolism* (Supplemental Figure 6)**

- Phosphatidyl-1D-myo-inositol is reduced in patients, and this downregulation affects the Glycerophospholipid metabolism. In addition to phosphatidyl-1D-myo-inositol, other compounds including cardiolipin, phosphatidyl-L-serine, phosphatidyl-ethanolamine and CDP-choline are also significantly downregulated in patients compared to healthy controls. The only compound that is significantly upregulated in

patients is 1-acyl-sn-glycero-3-phosphocholine. No metabolic enzymes were found to be differentially regulated in the disease state in this metabolic pathway.

- The downregulated lipids phosphatidyl-1D-myo-inositol, phosphatidyl-L-serine and cardiolipin have a common substrate CDP-diacyl-glycerol. Although CDP-diacyl-glycerol has not been found to be significantly different between patients and healthy controls, it may be possible that as a precursor for other lipids it is not sufficiently replenished, hence contributing to the reduced availability of its products.
- CDP-diacyl-glycerol is also a substrate of phosphatidylcholine (lecithin) through the enzyme phosphatidylcholine synthase (pcs; 2.7.8.24). Phosphatidylcholine is not differentially regulated between patient and healthy controls; however, it is a substrate for the production of 1-acyl-sn-glycero-3-phosphocholine, which is significantly upregulated in patients. It may be speculated that the phosphatidylcholine synthase enzymatic activity may be upregulated, redirecting the CDP-diacyl-glycerol to phosphatidylcholine synthesis and, subsequently, to 1-acyl-sn-glycero-3-phosphocholine production. However, it might be not highly feasible that five other reactions that are shown to consume CPD-diacyl-glycerol would be actively downregulated to support this metabolic route. Indeed, no significant differential protein expression can be observed in any metabolic enzymes facilitating relevant reactions.
- The reduced level of phosphatidyl-L-serine is mirrored in the low availability of phosphatidyl-ethanolamine. The most direct route of reactions between these two compounds include the conversion of phosphatidyl-L-serine to phosphatidylethanolamine by the enzyme phosphatidylserine decarboxylase (psd/PISD; 4.1.1.65), and the conversion of phosphatidyl-ethanolamine to L-1-phosphatidylserine and ethanolamine by the enzyme phosphatidylserine synthase 2 (PTDSS1; 2.7.8.29). Other routes of phosphatidyl-L-serine synthesis, such as Ptdss1, are likely to be downregulated in activity, rationalizing the low levels of the former.
- Due to the downregulation of phosphatidyl-L-serine, phosphatidyl-ethanolamine and CDP-choline, it is also unlikely that the pathways consuming these substrates for phosphatidylcholine replenishment are activated in patients.
- The enzyme phospholipid methyltransferase (PEMT/PLMT; 2.1.1.71) is unlikely to be responsible for phosphocholine accumulation, due to the significantly low concentration of the substrates (phosphatidyl-ethanolamine and phosphatidyl-L-serine) feeding the reaction, with no apparent source of phospholipid availability (Supplemental Figure 7).

2) Oxidative Stress Response

***2a) Glutathione Metabolism* (Supplemental Figure 8)**

- L-glutamate and glutathione (GSH) are significantly downregulated in patients compared to healthy controls, whereas the enzyme glutathione s-transferase mu 1 (GSTM1; 2.5.1.18) is significantly upregulated. Glutathione transferases (GSTs) utilizes GSH to metabolize organic halide (RX) into halide (HX), producing R-S-glutathione as a by-product. R-S-glutathione is then metabolized by the enzyme gamma-

glutamyltransferase (GGT; 2.3.2.2) producing R-S-Cysteinyl-glycine and L-glutamate. Increasing GSTM1 may be a mechanism contributing to L-glutamate replenishment; however, it does not suffice to restore a healthy state as both GSH and L-glutamate are significantly low in patients.

***2b) Biosynthesis of Cofactors* (Supplemental Figure 9)**

- L-glutamate and glutathione (GSH) are significantly downregulated in patients compared to healthy controls. L-glutamate and cysteine are metabolized to synthesize GSH, through the enzyme L-glutamate:L-cysteine ligase (GCL; 6.3.2.2), via the intermediate L-y-glutamylcysteine. Therefore, low L-glutamate availability may contribute to reduced glutathione, thus impacting the regulation of the oxidative stress response.
- Nicotinate metabolism is also downregulated in patients via downregulation of the enzymes 3-hydroxyanthranilate-3,4-dioxygenase (HAAO; 1.13.11.6) and nicotinate phosphoribosyltransferase (NAPRT1; 6.3.4.21). The pathways involving these enzymes, along with low levels of Aspartate in patients may converge to contribute to reduced NADP+ synthesis, which impacts the oxidative phosphorylation chain.

3) TCA Cycle

***3a) Alanine, Aspartate and Glutamate Metabolism* (Supplemental Figure 10)**

- L-aspartate is metabolized to produce fumarate and oxaloacetate, which both feed into the TCA cycle. Upregulation of citrate, subsequent to oxaloacetate in the TCA cycle, and downregulation of fumarate suggest that conversion of L-aspartate to oxaloacetate may be upregulated through the enzymes L-amino-acid oxidase (1.4.3.2) and L-aspartate oxidase (NadB; 1.4.3.16). The conversion of L-aspartate to fumarate through the enzyme aspartate ammonia-lyase (4.3.1.1) is likely to be downregulated.
- 2-oxoglutarate (2-ketoglutarate) is also a metabolite participating in the TCA cycle, and is metabolized from both L-glutamate and citrate. L-glutamate, involved in the pathways of Glutathione Metabolism and in the Biosynthesis of Cofactors (see point 2), participates in the regulation of the TCA cycle; in fact, 2-oxoglutarate both participates as a substrate for producing L-glutamate as well as in a bidirectional reaction with L-glutamate. Low levels of L-glutamate, while citrate is high, suggest that the conversion of citrate to 2-oxoglutarate, or conversion of 2-oxoglutarate to L-glutamate is comprised in patients. Thus, subsequent TCA metabolites such as fumarate are also reduced in patients.
- L-glutamate further contributes to regulate the TCA cycle through its role in succinate synthesis. L-glutamate is a substrate for 4-aminobutanoate (GABA) synthesis, which is involved in a bidirectional reaction with succinate semialdehyde that is further metabolized to form succinate. Low L-glutamate levels are reflected in low 4-aminobutanoate in patients. Although succinate semialdehyde is unaffected in patients, the enzyme succinate-semialdehyde dehydrogenase (NAD+) (ALDH5A1; 1.2.1.24) metabolizing this substrate to succinate is significantly downregulated in patients. Succinate is the precursor for fumarate synthesis; although succinate is significantly upregulated (< 1.5 fold) in patients, fumarate is downregulated in

patients, suggesting that succinate levels are not sufficiently replenished subsequent to increased citrate formation. The multiple regulation of fumarate synthesis through various routes in the Alanine, Aspartate and Glutamate Metabolism contributes to an overall lower fumarate level in patients compared to healthy controls, thus exacerbating the disease state.

***3b) Tyrosine Metabolism* (Supplemental Figure 11)**

- Fumarate is significantly downregulated in patients compared to healthy controls. This occurs because of the downregulation of two enzymes: acylpyruvate hydrolase (FAHD1; 3.7.1.5), which consumes 3-fumarylpyruvate to produce pyruvate and a carboxylate, and maleylacetoacetate isomerase (GSTZ1; 5.2.1.2), which metabolizes 4-maleylacetoacetate to produce 4-fumarylacetoacetate. 4-fumarylacetoacetate, not reduced in patients, is further metabolized by fumarylacetoacetase (FAH; 3.7.1.2) to produce acetoacetate and fumarate. The multiple regulation of fumarate synthesis through various routes in the Tyrosine Metabolism contributes to an overall lower fumarate level in patients compared to healthy controls, thus exacerbating the disease state.

Supplemental Table 1. Comprehensive clinical and laboratory features in patients with PI4KA-related disorders.

	P1	P2	P3	P4	P5	P6	P7	P8	P9	P10	P11	P12	P13
Gender	F	M	F	F	M	M	F	M	M	M	M	F	F
Ethnicity	Caucasian	Caucasian	Caucasian	Caucasian	Caucasian	Asian/ Caucasian	Caucasian	Turkish	Caucasian	Latin American	Amish	Turkish	Indian
Consanguinity	No	No	No	No	No	No	No	Yes	No	No	Yes	Yes	No
Age													
Onset	Newborn	Newborn	1 year	1 year	Newborn	Newborn	4 months	Newborn	17 years	2 years	Newborn	Newborn	1.5 months
Immune Evaluation	6	6	13	19	8	9	11	5	40	18	18 days	13	7
Variant													
c.DNA	c.2624dup C c.3454G>A	c.5773G>C c.5773G>C	c.3884A>G c.6122T>C	c.3592G>A c.6156_6159delGACA	c.1852C>T c.4990G>A	c.5116+1>A c.5960A>G	c.1414A>C c.355C>T	c.5560G>A c.5560G>A	c.5459_5461delAAG c.6156_6159delGACA	c.4666G>A c.5159C>T	c.4867T>G; c.4867T>G;	c.5560G>A c.5560G>A	c.5774G>A; c.6065delG
Protein	P876SfsTer36/ E1152K	G1925R/ G1925R	H1295R/ M2041T	A1198T/ T2053SfsTer4	R618Ter/ D1664N	p.?/ N1987S	S472R/ R119W	D1854N/ D1854N	E1820del/ T2053SfsTer4	V1556M/ T1720I	Y1623D/ Y1623D	D1854N/ D1854N	G1925E/ R2022Qfs Ter36
CNS symptoms	ST, ataxia, epilepsy, Dystonia, ChA, hyperexcitability, nystagmus	Hypotonia, epilepsy, Axonal sensory neuropathy, nystagmus	SP, ataxia, epilepsy, tremor, nystagmus	ST, ataxia, epilepsy, tremor, nystagmus	SP, ataxia	ST, ataxia, epilepsy	ST, ataxia, Stereotypic movements, ocular dyspraxia	ST, epilepsy, dystonia	SP	SP	-	Epileptic encephalopathy	progressive spastic diplegia

MRI findings	Diffuse HM, WM atrophy, VM, thin CC, BH, CH	Diffuse HM, WM atrophy, VM, thin CC	Diffuse HM, dysplastic thin CC, CA with calcifications	Diffuse HM, thin CC, BA, cerebral, CA	Delayed myelination, dysplastic CC, CA, VM	Delayed myelination, dysplastic CC, BA, CA	Delayed myelination, external hydrocephalus, CA	Bilateral perisylvian polymicrogyria	Arachnoid cyst of the posterior fossa, CSCA	CSCA	MIA	Immature gyral pattern, CH, CA after status epilepticus, Diffuse T2-elevation of WM signal in the entire supratentorial WM, thin CC	Profound HM, Myelin present in the posterior limbs of the internal capsules, lateral thalami, and within the CC and brainstem
GI symptoms	-	-	GERD	-	Constipation	-	GERD	GERD	Crohn disease	-	-	-	Colitis, Rectovaginal fistula
GU symptoms	-	BC	-	-	-	-	-	BC	-	-	-	-	-

Other										
Subclinical hypothyroidism	-	Atrial septal defect	-	JIA	-	-	-	-	Optic atrophy, convergent strabismus, hearing loss, Follicular non-Hodgkin lymphoma, Chronic lung disease; hypothyroidism, interstitial lung emphysema and bronchiectasis	-
Recurrent URTI (ear) and LRTI (bronchitis and pneumonia)	Recurrent URTI (ear) and LRTI (bronchitis); pneumococcal bacteremia	Recurrent URTI (rhinopharyngitis, otitis) and LRTI (bronchitis, pneumonia); GI infections, parotitis	Pneumonia requiring ICU-admission	Recurrent skin and GI infections	No	No	URTI and LRTI requiring ICU	No	No	No	Recurrent GI infections
Infections										
NO	NO	IgRT	NO	IgRT, methotrexate, diclofenac, Autologous stem cell transplantation	NO	NO	IgRT	Mercaptopurine	NO	Rituximab for NHL	IgRT, Adalimumab
Treatment										

Anemia	No	Neonatal anemia	Yes, normocitic	No	No	No	Yes, normocitic and two episodes of anemia requiring RBC transfusions	No	No	No	Yes, iron deficiency anemia	Yes, iron deficiency anemia		
Monocytosis	No	Yes	Yes	No	No	No	Yes	No	No	No	No	Yes		
Neutropenia	Mild, chronic	No	No	No	No	Mild, intermittent	No	No	Normal	No	Severe, intermittent	No		
Platelets	Normal	Mild thrombocytosis (477000)	Normal	Normal	Normal	Mild thrombocytopenia	Normal	Normal	Normal	Normal	Normal	Normal		
IgG subclasses														
IgG1, mg/dl	NA	<160 mg/dl,	NA	478	IgRT ongoing	NA	522	196	486,	NA	NA	NA		
IgG2	NA	71,9	NA	138	IgRT ongoing	NA	237	74	249	NA	NA	NA		
IgG3	NA	19,4	NA	31	IgRT ongoing	NA	38	115	34	NA	NA	NA		
IgG4	NA	< 6	NA	20	IgRT ongoing	NA	36.7	<3	21	NA	NA	NA		
Vaccine responses	NA	NA	NA (under IgRT)	NA	Normal to tetanus and diphteria	Absent to Pneumo23, Mumps and Hib	Normal to HBV	NA	NA	NA	NA	NA		

T-cell proliferation	NA	Normal to PHA, aCD3, aCD3±IL2, PM+ionomicina, ConA, PWM	Normal to PHA, aCD3	NA	Reduced to aCD3±CD28, PHA	Normal to PHA, aCD3	NA	Normal to PHA, aCD3±IL2	NA	NA	Normal to PWM and PHA	NA	Normal to aCD3±CD28
T-cell subtypes *	NA	↑naive CD4+ and CD8+, ↓ effmem CD4+	↑naive CD4+, ↓effmem CD8+	NA	NA	↑naive CD4+, CD4+ and CD8+ central memory	Normal	↑naive CD8+, ↓effmem and term diff CD8+	NA	NA	Normal naive CD4+	Low naive CD4+, ↑ senescent CD57+ CD8+ T cells	↑CD4+ naïve, ↑CD8+ TEMRA, ↓CD8+ central memory
B cell subsets	NA	↑transitional, ↓unswitched and smB	↑transitional	NA	normal naive and smB	↑IgD+IgM+ CD27+	↑unswitched, ↓switched	↑transitional, ↓unswitched and switched	NA	NA	NA	Low naive, ↑transitional and CD21 low B cells	↑transitional

ANA = antinuclear antibodies. BA = brainstem atrophy. BC = bilateral cryptorchidism. BH =brainstem hypoplasia. CA = cerebellar atrophy. ChA = choreoathetosis. CC = corpus callosum. CH = cerebellar hypoplasia. CNS = central nervous system. CSCA = cervical spinal cord atrophy. F = female. GERD = gastroesophageal reflux disease. GI = gastrointestinal. GU = genitourinary. HM = hypomyelination. ICU = intensive care unit. IgRT = immunoglobulin replacement therapy. JIA = Juvenile idiopathic arthritis. LRTI = lower respiratory tract infections. M = male. MIA = multiple intestinal atresia. MRI = Magnetic resonance imaging. NA = not available. RF= Rheumatoid factors. SP = Spastic paraparesis. ST = Spastic tetraparesis. tTG = Anti-Tissue Transglutaminase Antibody. URTI = upper respiratory tract infections. VM = Ventriculomegaly. WM = white matter.

Detailed T and B cells subsets in the investigated patients.
CENTMEM = central memory. EFFMEM = effector memory. RTE = recent thymic emigrants. TEMRA = Terminally differentiated effector memory. Treg = regulatory T cells.

P2	%	Aged-matched normal values, %	Absolute count	Aged-matched normal values, absolute count
CD3+	81.49	59-83	1.53	1.38-2.78
CD3+CD4+	49.79	28-47	0.91	0.66-1.6
RTE (CD4+ CD27+ CD31+ CD45RA+ CCR7+)	65	45-70		
NAIVE (CD3+CD4+CD45RA+CCR7+)	80.06	32-68		
CENTMEM (CD3+CD4+CD45RA-CCR7+)	12.9	10-24		
TEMRA (CD3+CD4+CD45RA+CCR7-)	0.73	4-16		
EFFMEM (CD3+CD4+CD45RA-CCR7-)	6.31	9-32		
Treg (CD4+CD25+hCD127-CD45RO+CCR4+)	1.18	1-3		
CD8+ CD3+	30.67	18.00-33.00	0.56	0.45 - 1.05
NAIVE (CD3+CD8+CD45RA+CCR7+)	64.94	24-62		
CENTMEM (CD3+CD8+CD45RA-CCR7+)	1.16	2-12		
TEMRA (CD3+CD8+CD45RA+CCR7-)	7.34	7-26		
EFFMEM (CD3+CD8+CD45RA-CCR7-)	26.55	18-55		
CD19+	2.7	9-22	0.05	0.23 - 0.78
Transitional (CD24hCD38h)	92.56	9-24		
Naive IgD+CD27-	71.34	58-85		

Unswitch memory CD19+IgD+CD27+	3.61	5-16		
Switched memory CD19+IgD-CD27+	1.06	5-19		
CD19+CD21low	1.38	2-9		
CD19+ Plasmablasts	20	4-17		
CD56+CD16+CD3-	14.4	6-20	0.28	0.18 - 0.53

P3	**%**	**Aged-matched normal values, %**	**Absolute count**	**Aged-matched normal values, absolute count**
CD3+	92	62.6-80.4	1.61	0.65-2.33
CD4+	68	35.6-51.5	1.19	610-1.45
RTE (CD4+CD45RA+CD31+)	65			
Naive (CD4+CD45RA+)	71	40.9-65.7		
Memory (CD4+CD45RO+)	28	25.1-52.1		
Treg (CD4+CD25+CD127low)	3			
CD8+	24	19-29	0.41	0.28-0.75
Naive (CD8+CD45RA+CD31+)	66	52-68		
CENTMEM (CD8+CD45RA+CCR7+)	6			
TEMRA (CD8+CD45RA+CCR7-)	19	16-28		
EFFMEM (CD8+CD45RA-CCR7-)	8	11-20		
CD19+	4	6.5-24	0.069	0.19-0.63

Transitional (CD19+CD24hiCD38hi)	14	3.9-7.8		
Naive (CD19+CD27-IgD+)	84	61.6-87.4		
CD19+CD21lowCD38low	2	<10		
Unswitched (CD19+CD27+IgD+)	3	2.6-13.4		
Switched (CD19+CD27+IgD-)	9	4-21.2		
Plasmablasts (CD19+IgM-IgD-CD27hiCD38hi)	<1			

P5	**%**	**Aged-matched normal values, %**	**Absolute count**	**Aged-matched normal values, absolute count**
CD3+	93.6	55.3-87.7	1.99	0.651-2.804
CD3+CD4+	58.4	27.9-55.8	1.244	0.37-1.336
RTE (CD3+CD4+CD31+CD45RA)	40.3	2.6-25.3	0.858	0.047-0.527
Naive (CD3+CD4+CD62L+CD45RA+)	52.7	6.2-26.9	1.123	0.087-0.796
Naive (CD3+CD4+CD45RA+CCR7+)	53.1	6.7-35.0	1.132	0.102-0.987
CENTMEM (CD3+CD4+CD62L+CD45RA-)	1.2	9.1-28.6	0.0026	0.166-0.544
EFFMEM (CD3+CD4+CD62L-CD45RA-)	0.9	3.7-12.9	0.019	0.080-0.262
TEMRA (CD3+CD4+CD3CD62L-CD45RA+)	3.5	0.1-5.5	0.075	0.001-0.132
CD3+CD8+	30.9	13.6-46.2	0.658	0.185-1.024
Naive (CD3+CD8+CD62L+CD45RA+)	24.6	2.3-18.2	0.524	0.037-0.484
CENTMEM (CD3+CD8+CD62L+CD45RA-)	0.1	1.2-7.6	0.002	0.019-0.175

EFFMEM (CD3+CD8+CD62L-CD45RA-)	0.1	2.0-12.4	0.002	0.047-0.383
TEMRA (CD3+CD8+CD62L-CD45RA+)	6.1	0.9-13.6	0.130	0.017-0.274
CD19+	1.3	3.8-18.0	0.028	0.079-0.399
CD20+	1.3	3.8-18.0	0.028	0.079-0.399
Transitional (CD19+CD24hiCD38hi)	32.2	1.2-10.9	0.009	0.003-0.026
Naive (CD20+CD27-)	88	78.6-95.8		
Unswitched (CD20+CD27+IgM+)	5.7	0.3-2.5	0.002	0.006-0.065
Switched (CD20+CD27+IgM-)	6.3	0.3-2.2	0.002	0.006-0.049

P6	**%**	**Aged-matched normal values, %**	**Absolute count**	**Aged-matched normal values, absolute count**
CD3+	87	55-78	1.701	0.700-4.200
CD3+CD4+	47	37-53	0.670	0.497-2.267
Naive (CD4+CD45RA+)	76	21-75	0.509	0.135-0. 893
Memory (CD4+CD45RO+)	23	11-44	0.154	0.056-0.411
CENTMEM (CD4+CD62L+CD27+CD45RO+)	20	5-28	0.134	0.023-0.288
EFFMEM (CD4+CD62L-CD27-CD45RO+)	0.6	0.3-4.0	0.004	0.002-0.027
CD8+	38	19-34	0.603	0.243-1.303
Naive (CD8+CD45RA+)	79	23-88	0.476	0.083-0.653
Memory (CD8+CD45RO+)	21	2-26	0.127	0.010-0.142

CENTMEME (CD8+CD62L+CD27+CD45RO+)	16	0-14	0.096	0-0.079
EFFMEM (CD8+CD62L-CD27-CD45RO+)	1	0-3	0.006	0-0.015
CD19+	5	10-31	0.098	0.200-1.600
Naïve (CD19+CD27-)	22	48-95		
Transitional (CD38++CD24++CD10+)	7.2	0.6-9.0		
Switched (CD19+CD27+IgG+(of CD19+CD27+)	8.1	10.0-80.0		
Plasmablasts (CD19+ CD24-CD38+++)	23.0	0.0-4.0		

P7	**%**	**aged-matched normal values**
CD4+		
RTE (CD4+CD45RA+CD31+ of CD4+CD45RA+)	76.1	50.7-78.9
Naive (CD4+CD45RA+)	67.2	49.3-72.0
Memory (CD4+CD45R0+)	41.4	24.5-44.4
CENTMEM (CD4+ CD62L+ CD45R0+)	27.7	
EFFMEM (CD4+CD62L-CD45R0+)	12.6	
TEMRA (CD4+CD62L-CD45R0-)	0.2	
CD8+		
Naive (CD8+CD27+CD28+)	79.0	62.3-86.3

Early EFFMEM (CD8+CD27+CD28-)	14.3	3.0-18.0
Late EFFMEM (CD8+CD27-CD28-)	6.0	1.0-41.0
CD19+		
Transitional (IgM++CD38++)	7.7	1.4-13.0
Naïve (IgD+IgM+CD27-)	60.7	51.3-82.5
Unswitched (IgD+IgM+CD27+)	21.41	4.6-18.2
Switched (IgD-IgM-D27+) of CD19+ B cells Class switched memory B cells	5.35	8.7-25.6
CD21lowCD38-	0.9	2.9-13.2
Plasmablasts (IgM-/(+)CD38+++)	1.2	0.6-6.5

P8	**%**	**Aged-matched normal values, %**	**Absolute count**	**Aged-matched normal values, absolute count**
CD3+	90.4	56.0-78.9	1.046	1.464-4.509
CD3+CD4+	57.1	29.4-55.7	0.660	0.744-2.765
Naïve (CD45RA+CCR7+)	78.3	49.2-85.8		
RTE (CD45RA+CCR7+CD31+)	68.2	36.2-71.8	0.450	0.339-1.533
CENTMEM (CD45RA-CCR7+)	17.1	9.6-31.9		
EFFMEM (CD45RA-CCR7-)	3.6	2.8-16.9		
TERMDIFF (CD45RA+CCR7-)	1	0.7-4.8		

CD3+CD8+	32.4	11.6-32.4	0.375	0.442–1.553
Naïve (CD45RA+CCR7+)	89.8	22.8-79.9		
CENTMEM (CD45RA-CCR7+)	3.9	0.9-11.3		
EFFMEM (CD45RA-CCR7-)	2.7	4.3-31.4		
TERMDIFF (CD45RA+CCR7-)	3.6	6.8-52.7		
CD19+	7	10.7-34.9	0.081	0.363-1.743
Transitional (CD38++CD10+)	43.9	10.6-42.6		
Naive (IgD+IgM+CD27-)	42.9	34.2-65.5		
CD19++CD27low	1.2	1.5-9.8		
Switched (IgM-IgD-CD27+)	0.4	1.5-14.2		
Unswitched (IgM+IgD+CD27+)	1.5	2.9-15.3		
TERMDIFF (CD38++CD27+CD20)	9.0	0.37-15.3		

P11	**%**	**Aged-matched normal values, %**	**Absolute count**	**Aged-matched normal values, absolute count**
CD3+			0.237	2.500-5.500
CD4+	90	35-64	0.208	1.600-4.000
Naive (CD4+CD45RA+)	57	64-95		
Memory (CD4+CD45RA+CD62L+)	72	61-94		
CD8+			0.005	0.560-1.700

CD19+			0.067	0.300-2.000

P12	**%**	**Aged-matched normal values, %**	**Absolute count**	**Aged-matched normal values, absolute count**
CD3+	94.42	56-84	1.056	1.0-2.2
CD4+	61.77	55-62	0.653	0.53-1.3
Naïve (CD4+/CD45RA+)	3.26	33-66	0.021	0.23-0.77
Memory (CD4+/CD45RO+)	95.33	18-38	0.622	0.24-0.7
CD27+CD28+	87.94	37-97	0.43	0.004-5.8
CD8+	31.88	32-42	0.337	0.33-0.92
CD27+CD28+	57.78	20-95	28.01	0.009-0.065
senescent CD57+ CD8+	40.52	13-18	0.136	0.081-0.157
CD19+	2.44	6-23	0.027	0.110-0.570
Transitional (IgM++CD38++)	42.40	1-25		
Naïve IgD+CD27-	17.14	49-100		
IgD+CD27+ IgM-memory of B cells	3.78	2-28		
IgD-CD27+ memory of B cells	2.52	1-43		
IgA+CD27+ memory B cells	0.44			
IgA+CD27- atypical IgG+ memory B cells	0.82			
IgG+CD27+ memory B cells	0.46			

IgG+CD27- atypical IgG+ memory B cells	2.08			
IgM+/-CD38++ plasmablasts of B cells	1.28			
CD21-CD38- of B cells	30.46	1-11		
IgD-IgM+CD27+ of B cells (IgM only)	1.57	0.5-7		

P13		**aged-matched normal values**
CD4+		
naive (CCR7+CD45RA+)	73.1	47.4
CM (CCR7+CD45RA-)	11.2	22.4
EM (CCR7-CD45RA-	11.5	22.8
TEMRA (CCR7-CD45RA+)	4.14	7.43
CD8+		
naive (CCR7+CD45RA+)	44.0	27.9
CM (CCR7+CD45RA-)	1.24	3.04
EM (CCR7-CD45RA-	14.9	17.3
TEMRA (CCR7-CD45RA+)	39.9	51.8
CD19+		

IgM hi CD38 hi (transitional)	11.9	
IgD+CD27- (naïve)	83.4	
IgD+CD27+ non-switched	4.0	
IgD-CD27+ (class-switched)	8.0	

Supplemental Table 2. Selected deregulated gene sets in PI4KA-related disorders.

GSEA			
Name	***NES***	***FDRq***	
Immunologic			
GSE12845 Naive versus pre germinal center tonsil B cell UP	1.99	2.61E-04	
GSE13411 Naive B cell versus plasma cell UP	1,77	9.48E-04	
GSE12366 Naive versus memory B cell UP	1.70	0.001	
GSE22886 Naive versus IgG IgA memory B cell UP	1.59	0.003	
Hallmark			
Hallmark E2F targets	-2.02	0	
Hallmark unfolded protein response	1.59	0.01	
Hallmark hypoxia	1.57	0.009	
Hallmark G2M checkpoint	-1.55	0.022	
Hallmark apoptosis	1.39	0.049	
Hallmark protein secretion	1.37	0.052	
Hallmark MTORC1 signaling	1.32	0.062	
Curated up			
Rhein all glucocorticoid therapy UP	2.03	0.005	
Reactome ATF4 activates genes in response to endoplasmic reticulum stress	1.79	0.037	
WP MAPK signaling pathway	1.78	0.037	
WP sphingolipid metabolism integrated pathway	1.68	0.065	
PID MTOR 4 pathway	1.75	0.044	
Biocarta ceramide pathway	1.64	0.079	
WP glucocorticoid receptor pathway	1.55	0.113	

Reactome late endosomal microautophagy	1.38	0.190	
Reactome autophagy	1.33	0.220	
Kegg regulation of autophagy	1.33	0.221	
Curated down			
WP oxidative phosphorylation	-1.68	0.078	
WP electron transport chain oxphos system in mitochondria	-1.66	0.086	
Reactome respiratory electron transport ATP synthesis by chemiosmotic coupling and heat production by uncoupling proteins	-1.66	0.087	
Reactome fatty acids	-1.61	0.123	
Reactome complex I biogenesis	-1.58	0.147	
CPDB			***p value***
Pathway			
Class I PI3K signaling events			1.75E-06
BCR			0.0003
Phospholipase D signaling pathway - Homo sapiens (human)			0.0007
B Cell Receptor Signaling Pathway			0.0018
Phospholipases			0.002
PIP3 activates AKT signaling			0.008
Protein complex			
CD20-LCK-FYN-p75/80 complex			0.0005
Phospholipase C gamma:PKC			0.0005
GO results			

B cell activation			0.0002
Cell motility			0.0008
Phosphatidylinositol-mediated signaling			0.0033
CT pathway		***FDRq***	***p value***
Glutamate biosynthesis II		1.51E-05	1.18E-08
Glutamate degradation X		1.51E-05	1.18E-08
Aspartate biosynthesis		1.25E-04	2.43E-07
Glutamate degradation II		1.25E-04	2.43E-07
Alanine, aspartate and glutamate metabolism		9.55E-04	6.98E-06
Arginine biosynthesis IV		1.03E-03	1.01E-05
Glycerophospholipid catabolism		4.62E-03	1.21E-04
Asparagine biosynthesis I		4.71E-03	1.31E-04
Glutathione-mediated detoxification I		4.82E-03	1.47E-04
Aspartate degradation II		7.59E-03	2.90E-04

Supplemental Table 3. Selected dysregulated pathways and significant differentially expressed proteins.

	p-adj	Upregulated proteins	Downregulated proteins
Reactome			
Immune System R-HSA-168256	0.00162	CD19, FYN, PIK3AP1, ZAP70	CTSS, HLA-F, ICAM1, ICAM3, IFIH1, IFIT2, LCK, MALT1, NEDD4, PPP2CA, SYK
Antigen Activates B Cell Receptor Leading To Second Messenger Generation R-HSA-983695	0.01206	FYN, PIK3AP1, CD19, IGHM	SYK
Adaptive Immune System R-HSA-1280218	0.01209	CD19, ERAP2, FYN, IGHM, PIK3AP1, TUBB6, ZAP70	BTN3A1, CTSS, HLA-E, HLA-F, ICAM1, ICAM3, LCK, MALT1, NEDD4, PPP2CA, SYK
Infectious Disease R-HSA-5663205	0.02551	FYN, IGHM, NT5E, TUBB6	AGRN, BANF1, FUT8, GNB4, GNG5, HDAC3, HLA-E, HLA-F, IFIH1, LCK, LIG4, MYH2, POM121C, RHBDF2, SUPT4H1, SYK
CTLA4 Inhibitory Signaling R-HSA-389513	0.03317	FYN	LCK, PPP2CA
Metabolism Of Amino Acids And Derivatives R-HSA-71291	0.04073	-	AASS, ASRGL1, EEF1E1, GSTZ1, HAAO, NQO1, PSPH, SDSL, SHMT1, TSTD1
Intracellular Signaling By Second Messengers R-HSA-9006925	0.04073	FYN, PIK3AP1, CD19, IGHM	SYK
KEGG			
NF-kappa B signaling pathway	0.00260	ZAP70	LCK, MALT1, SYK, TRAF5
Lysosome	0.02816	-	ARSA, CTSS, CTSZ, GUSB, PPT1, LAPTM5
WikiPathways			

Lysosome	0.02816	-	ARSA, CTSS, CTSZ, GUSB, PPT1, LAPTM5
WikiPathways			
B Cell Receptor Signaling Pathway WP23	0.01749	CD19, FYN, PIK3AP1	LCK, MALT1, SYK
IL-18 signaling pathway WP4754	0.03109	PRKCA	CFLAR, FAS, LCK
NRF2-ARE regulation WP4357	0.03109	FYN	NQO1
Serine Metabolism WP4688	0.03653	-	PSPH, SHMT1
Corum			
CD20-LCK-LYN-FYN-p75/80 complex, (Raji human B cell line) (human)	0.01625	FYN	LCK
Emerin regulatory complex (human)	0.04906	-	BANF1, HDAC3
Emerin complex 25 (human)	0.04906		

Supplemental Table 4. Comparative cellular viability of PI4KA^{mut} and control B lymphoblastoid cell lines (CTR-B-LCSs), measured by ATP-Glo based luminescent based assay after exposure of the depicted drugs. The p-values are calculated with the one-way Anova test related to PI4KA^{mut} group.

Drug name	Drug class	PI4KA^{mut} mean	HD mean	P value
Dexamethasone	GC/GCR complex	38.67	60.93	0.003
Ibrutinib	BTK inhibitors	2.557	17.17	0.052
Trametinib	MEK	3.359	25.31	0.004
PD184352	MEK	4.951	19.97	0.046
Mirdametinib	MEK	0	18.1	0.016
Teniposide	Topoisomerase inhibitors	58.77	74.82	0.033
Alisertib	Aurora Kinase A	22.06	39.04	0.024
MI-463	Mennin Inhibitor	10.71	32.05	0.005
MI-503	Mennin Inhibitor	13.99	41.21	0.0003
AT9283	JAK	27.71	45.18	0.02
JQ1	BET bromodomain	35.06	19.87	0.043
Paclitaxel	Antimicrotubule	69.02	90.46	0.004
Floxuridine	Antimetabolite agents	3.491	21	0.02
Talazoparib	PARPi	31.59	54.72	0.002
S63845	MCL inhibitor	12.25	36.86	0.001
Prexasertib	CHK inhibitor	74.23	93.23	0.012

CHAPTER 3

CONCLUSIONS, FUTURE PERSPECTIVES AND ADDITIONAL PUBBLICATIONS

3.1 Conclusions and Future Perspectives

The present doctoral work significantly advances our understanding of how multi-omics approaches can unravel the molecular complexity of B cell–related immunodeficiencies and metabolic dysfunctions. By integrating multi-layered datasets across transcriptomics, proteomics, lipidomics, and metabolomics, this research establishes a comprehensive framework for exploring the intersection between immune signaling, metabolism, and genetic variation. Focusing on PI4KA-related disorder as a paradigmatic example of a syndromic inborn error of immunity, this thesis provides novel mechanistic insights into how lipid signaling, mitochondrial function, and immune regulation converge to maintain homeostasis in B cells, and how their perturbation results in disease.

A central achievement of this work lies in the elucidation of the molecular consequences of biallelic *PI4KA* mutations. Through the integration of multiple omic layers, it has been demonstrated that PI4KA deficiency profoundly alters phosphoinositide metabolism, thereby impairing the structural and signaling integrity of cellular membranes. This disruption leads to downstream mitochondrial dysfunction, endoplasmic reticulum stress, and aberrant activation of the PI3K/mTOR signaling cascade. The cumulative effect of these alterations compromises B cell differentiation, impairs antibody secretion, and disrupts metabolic plasticity, ultimately causing B cell lymphopenia and hypogammaglobulinemia. From a mechanistic standpoint, the data presented here delineate PI4KA as a pivotal metabolic checkpoint, coordinating lipid synthesis, organelle function, and signaling fidelity, and position phosphoinositide metabolism as a critical interface between energy homeostasis and immune regulation.

Beyond the specific insights into PI4KA-related disease, this thesis demonstrates the transformative potential of multi-omics approaches in immunology. The simultaneous exploration of transcripts, proteins, lipids, and metabolites enables the reconstruction of biological networks with unprecedented resolution, revealing both direct and compensatory pathways that underlie disease phenotypes. The integrative computational pipeline developed and applied in this work represents not only a methodological advancement but also a conceptual framework for the study of complex diseases where single-omic analyses fail to capture the full biological context. In this sense, the thesis contributes to the growing field of systems immunology and underscores the value of data integration in achieving precision diagnosis and targeted therapeutic design.

The findings of this doctoral research carry several implications for both basic and translational science. From a biological perspective, they highlight the essential role of lipid metabolism in B cell homeostasis, showing that even subtle perturbations in phosphoinositide dynamics can ripple through cellular networks to affect mitochondrial energy production and immune cell fate decisions. From a clinical perspective, they expand the phenotypic spectrum of PI4KA-related syndromes by defining a distinct immunological signature characterized by combined defects in B cell metabolism, signaling, and differentiation. These insights open new avenues for diagnostic refinement, biomarker discovery, and therapeutic innovation in rare immunometabolic diseases.

Looking forward, several promising lines of investigation emerge from this work. Experimental modeling of PI4KA deficiency represents an immediate priority. Conditional or tissue-specific Pi4ka knockout models could recapitulate distinct aspects of the human phenotype, while patient-derived induced pluripotent stem cells (iPSCs) differentiated into B cells or organoids could allow mechanistic dissection of tissue-specific effects. Such models would help clarify the temporal and spatial dynamics of lipid metabolic disruption and its systemic repercussions on the immune and nervous systems.

In parallel, functional rescue studies are needed to assess the therapeutic reversibility of PI4KA-associated metabolic defects. Approaches could include gene therapy vectors restoring PI4KA expression, small-molecule modulators targeting lipid kinases

or phosphatases, or nutritional and lipid supplementation strategies aimed at restoring phosphoinositide balance. The success of such interventions would not only validate the causal role of PI4KA dysfunction but also lay the groundwork for personalized therapeutic strategies in syndromic immunodeficiencies.

At the systems level, future research should leverage single-cell multi-omics technologies to resolve the cellular heterogeneity that bulk analyses cannot capture. Single-cell transcriptomics and proteomics, coupled with spatial metabolomics and advanced imaging, will make it possible to identify compensatory metabolic circuits, intercellular signaling dependencies, and distinct B cell subpopulations with differential susceptibility to metabolic stress. Integrating these high-dimensional datasets through computational modeling of metabolic fluxes—particularly genome-scale models encompassing phosphoinositide turnover, mitochondrial respiration, and redox balance—could yield predictive simulations of disease progression and therapeutic response.

Furthermore, translational applications should focus on identifying diagnostic biomarkers and metabolic signatures associated with PI4KA deficiency. Specific lipid species, mitochondrial metabolites, or protein phosphorylation patterns may serve as measurable correlates of disease severity or treatment efficacy. The integration of such molecular signatures into clinical pipelines could facilitate early diagnosis, patient stratification, and the monitoring of therapeutic interventions. Beyond PI4KA-related conditions, this integrative framework can be adapted to other immune and hematological disorders characterized by metabolic imbalance, such as common variable immunodeficiency or B cell malignancies.

Finally, the conceptual advances achieved through this thesis extend beyond immunology. They underscore the broader relevance of multi-omics integration for systems medicine, in which complex diseases are understood not as isolated genetic defects but as network-level perturbations affecting interconnected pathways. By linking lipid biochemistry, mitochondrial dynamics, and immune cell signaling into a unified framework, this research contributes to the establishment of a truly interdisciplinary field of immunometabolic systems biology.

In conclusion, this doctoral research bridges molecular immunology, metabolism, and computational biology, providing a detailed and integrative picture of how metabolic and signaling perturbations shape immune cell function. The findings presented here not only elucidate the pathophysiology of PI4KA-related disorders but also establish methodological and conceptual foundations for future studies in precision immunology. By demonstrating the analytical and translational potential of multi-omics approaches, this thesis paves the way toward predictive, systems-level models of immune dysfunction and offers a path forward for the development of targeted, mechanism-based therapies for rare and complex immunometabolic diseases.

3.2 Additional publications

1. Saettini F, Guerra F, Fazio G, Bugarin C, McMillan HJ, Ohtake A, Ardissone A, Itoh M, Giglio S, Cappuccio G, Giardino G, Romano R, Quadri M, Gasperini S, Moratto D, Chiarini M, Akira I, Fukuhara Y, Hayakawa I, Okazaki Y, Mauri M, Piazza R, Cazzaniga G, Biondi A. Antibody Deficiency in Patients with Biallelic KARS1 Mutations. J Clin Immunol. 2023 Nov;43(8):2115-2125. doi: 10.1007/s10875-023-01584-7. Epub 2023 Sep 28. Erratum in: J Clin Immunol. 2023 Nov;43(8):2126. doi: 10.1007/s10875-023-01600-w. PMID: 37770806.

2. Roncareggi S, Girardi K, Fioredda F, Pedace L, Arcuri L, Badolato R, Bonanomi S, Borlenghi E, Cirillo E, Coliva T, Consonni F, Conti F, Farruggia P, Gambineri E, Guerra F, Locatelli F, Mancuso G, Marzollo A, Masetti R, Micalizzi C, Onofrillo D, Piccini M, Pignata C, Raddi MG, Santini V, Vendemini F, Biondi A, Saettini F. A Nationwide Study of GATA2 Deficiency in Italy Reveals Novel Symptoms and Genotype-phenotype Association. J Clin Immunol. 2023 Nov;43(8):2192-2207. doi: 10.1007/s10875-023-01583-8. Epub 2023 Oct 14. PMID: 37837580.

3. Vendemini F, Roncareggi S, L'Imperio V, Guerra F, Mottadelli F, Chiarini M, Maglia O, Sala S, Fazio G, Piazza R, Bonanomi S, Biondi A, Saettini F. Bone Marrow CD8 + Abundance Inversely Correlates with Progressive Marrow Fibrosis and Myelodysplastic Evolution in GATA2 Deficiency: Case Report. J Clin Immunol. 2025

Feb 20;45(1):77. doi: 10.1007/s10875-025-01871-5. PMID: 39976744; PMCID: PMC11842526.

4. Guerra F, Gasperini S, Bonanomi S, et al. Finding balance between mature and immature neutrophils: The effects of empagliflozin in GSD-Ib. EJHaem. 2023;4(2):551-554. Published 2023 Jan 29. doi:10.1002/jha2.649

5. Saettini F, Coliva TA, Vendemini F, et al. Abnormal B-Cell Maturation and Increased Transitional B Cells in CBL Syndrome. Front Pediatr. 2022;10:935951. Published 2022 Jul 28. doi:10.3389/fped.2022.935951

6. Di Majo BE, Guerra F, Mauri M, et al. The novel XIAP Lys396Ter variant alters mitochondrial membrane potential and endoplasmic reticulum intensity in monocytes of two XIAP-deficient patients. Pediatr Hematol Oncol. 2025;42(5):287-295. doi:10.1080/08880018.2025.2521122